Studies on Condition Assessment of Dry-Type Insulation in High Voltage System

Thesis Submitted by

Subhajit Maur

Doctor of Philosophy
(Engineering)

Electrical Engineering Department
Faculty Council of Engineering & Technology
Jadavpur University
Kolkata, India

2024

Jadavpur University
Kolkata – 700032, India

INDEX NO. 105/21-22/E

1. **Title of the Thesis :**

   Studies on Condition Assessment of Dry-Type Insulation in High Voltage System

2. **Name, Designation & Institution of the Supervisor :**

Dr. Biswendu Chatterjee
Professor,
Electrical Engineering Department,
Jadavpur University

1. List of Journal Publications :

- **S. Maur**, S. Dalai and B. Chatterjee, "Sensing the Polarization and Depolarization Current of Solid Dielectrics Used in High-Voltage Applications", ***IEEE Sensors Letters***, Vol. 3, No. 9, pp. 1-4, 2019. DOI: 10.1109/LSENS.2019.2935672.

- **S. Maur**, N. Haque, P. Preetha, B. Chakraborty, S. Dalai and B. Chatterjee, "Investigations on the effect of ageing on charge de-trapping processes of epoxy–alumina nanocomposites based on isothermal relaxation current measurements", ***IET Nanodielectrics***, Vol. 3, No. 4, pp. 116-123, 2020. DOI: 10.1049/iet-nde.2020.0020.

- **S. Maur**, S. Chatterjee, N. Haque, P. Preetha, S. Dalai and B. Chatterjee, "Sensing the Thermal Aging of Epoxy Alumina Nano-Composites Using Electric Modulus", ***IEEE Sensors Journal***, Vol. 21, No. 10, pp. 12236-12244, 2021. DOI: 10.1109/JSEN.2021.3065447.

- **S. Maur**, B. Chakraborty, A. K. Pradhan, S. Dalai and B. Chatterjee, "A Novel Approach to Estimate Electrothermal Aging of Epoxy–Alumina Nanocomposites Using Dielectric Relaxation Current Analysis", ***IEEE Transactions on Dielectrics and Electrical Insulation***, Vol. 30, No. 1, pp. 41-48, 2023. DOI: 10.1109/TDEI.2022.3227885.

- **S. Maur**, B. Chakraborty, A. K. Pradhan, S. Dalai and B. Chatterjee, "Relaxation Frequency Distribution Based Approach toward Moisture Estimation of 11kV XLPE Cable Insulation", ***IEEE Transactions on Dielectrics and Electrical Insulation***, Vol. 31, No. 6, pp. 3261-3268, 2024. DOI: 10.1109/TDEI.2024.3355367.

2. List of Patents :

Nil

3. List of Presentations in National/International Conferences :

- **S. Maur**, B. Chakraborty, S. Dalai and B. Chatterjee, "Investigation on Effects of Thermal Ageing on LDPE Based on Polarization and Depolarization Currents", Proceedings of ***2020 IEEE 1st International Conference for Convergence in Engineering (ICCE)***, Kolkata, India, pp. 200-204, 2020. DOI: 10.1109/ICCE50343.2020.9290689.

- **S. Maur**, S. Dalai and B. Chatterjee, "Studies on Ageing Status of Epoxy Nano-Composites for Dry-Type Insulation using Electric Modulus", Proceedings of ***2020 IEEE Applied Signal Processing Conference (ASPCON)***, Kolkata, India, pp. 354-358, 2020. DOI: 10.1109/ASPCON49795.2020.9276 716.

- **S. Maur**, B. Chakraborty, A. K. Pradhan, S. Dalai and B. Chatterjee, "An Approach for Aging State Estimation of Epoxy- Alumina Nano-Composites based High Voltage Dry-Type Insulation using Debye Model Parameters", Proceedings of ***2022 IEEE Calcutta Conference (CALCON)***, Kolkata, India, pp. 327-331, 2022. DOI: 10.1109/CALCON56258.202 2.10060148.

- **S. Maur**, B. Chakraborty, A. K. Pradhan, S. Dalai and B. Chatterjee, "Estimation of Thermal Aging of Epoxy-Alumina Nano-Composites for Dry-Type High Voltage Insulation Using Dielectric Modulus", Proceedings of ***2022 IEEE 6th International Conference on Condition Assessment Techniques in Electrical Systems (IEEE CATCON 2022)***, Durgapur, India, pp. 298-302, 2022. DOI: 10.1109/CATCON 56237.2022.10077705.

Statement of Originality

I, **Subhajit Maur** registered on **30th July, 2021** do hereby declare that this thesis entitled "***Studies on Condition Assessment of Dry-Type Insulation in High Voltage System***" contains literature survey and original research work done by the undersigned candidate as part of Doctoral studies.

All information in this thesis have been obtained and presented in accordance with existing academic rules and ethical conduct. I declare that, as required by these rules and conduct, I have fully cited and referred all materials and results that are not original to this work.

I also declare that I have checked this thesis as per the "Policy on Anti Plagiarism, Jadavpur University, 2019", and the level of similarity as checked by iThenticate software is **2 %**.

Subhajit Maur

(Signature of Candidate)

Date : 30.10.2024

Certified by Supervisor:

BChatterjee

(Signature with date, seal)

30 OCT 2024

Dr. Biswendu Chatterjee
Professor
Electrical Engineering Department
Jadavpur University
Kolkata-700032

Certificate from the Supervisor

This is to certify that the thesis entitled "***Studies on Condition Assessment of Dry-Type Insulation in High Voltage System***" submitted by **Shri Subhajit Maur**, who got his name registered on **30th July, 2021** for the award of Ph. D. (Engg.) degree of Jadavpur University is absolutely based upon his own work under the supervision of **Prof. Biswendu Chatterjee** and that neither his thesis nor any part of the thesis has been submitted for any degree/diploma or any other academic award anywhere before.

BChatterjee

Signature of the Supervisor
and date with Office Seal

30 OCT 2024

Dr. Biswendu Chatterjee
Professor
Electrical Engineering Department
Jadavpur University
Kolkata-700032

Acknowledgment

The author expresses his sincere appreciation and deep gratitude to his esteemed guide Prof. Biswendu Chatterjee for his invaluable guidance in carrying out the thesis work. The author was allowed to enjoy all the necessary freedom during his work and at the same time the intense supervision by the mentor led the work towards perfection. His moral support, caring personality, untiring endeavor, unparalleled firmness of knowledge and vision, perpetual encouragement and precious advice made the daunting task possible for the author.

The author expresses his deep sense of appreciation to the Head of the Department of Electrical Engineering, Jadavpur University for his kind accordance in providing necessary departmental facilities for implementation of this work. The author also acknowledges the financial support provided by DST, Government of India (Grant no EMR/2016/005246) and AICTE through AICTE Doctoral Fellowship (ADF 2020-21).

It is the author's pleasure to acknowledge his respected teachers Prof. Sovan Dalai, Dr. Arpan Kumar Pradhan, Prof. Sivaji Chakravorti, Prof. Debangshu Dey, Prof. Kesab Bhattacharya, and Prof. Debasis Sarkar for their advice and encouragement in completing the research work.

The author also wants to acknowledge contributions of Mr. Biswajit Chakraborty, Dr. Nasirul Haque, Dr. Soumya Chatterjee, and Dr. P. Preetha in the course of the research work.

The author is thankful to his colleagues Dr. Suhas Deb, Mr. Rakesh Das, Mr. Sandipan Kumar Paul and Mr. Soumyadeep Maity, Mr. Pradipta Ghosh, Dr. Arup Kumr Das and Dr. Kaushik Sit for providing support in various ways for carrying out the work.

The author would like to express his heart-felt gratitude to all his family members and relatives for their never-ending support and encouragement during the course of the thesis work.

The author also extends thanks to all the members of the High Tension Laboratory of Electrical Engineering Department, Jadavpur University for making it possible to work in a homely atmosphere. Last but not least, the author remains indebted to all the resources that he was fortunate to have during the work.

Subhajit Maiz.
30.10.2024

Dedicated to
My Family
and
Teachers

List of Symbols and Abbreviations

Symbol	Description
∞	Infinity
A	Cross-sectional area of the electrode
A_g	Amplitude of the exponential decay function for g^{th} dipolar group
A_p	Proportionality constant
B^*_{eq}	Critical value of B_c for thermal ageing
B_c	Coefficient in Curie Von Schneidler's law
B_{eq}	Equilibrium constant of B_c for irreversible thermal aging.
$^{\circ}C$	Degree centigrade
C'	Real part of complex capacitance
C''	Imaginary part of complex capacitance
C_0	Geometric capacitance
C_g	Energy Storage element of g^{th} dipolar group
c_{m1}	Concentration of unaged moieties in thermal ageing reaction
c_{m2}	Concentration of aged moieties in thermal ageing reaction
D	Flux density
d	Distance between two electrode
$E(t)$	Electric Field at t^{th} instant
e_n	probability of de-trapping of an electron per unit time from a trap level to energy E
E_t	Trap depth
$f(t)$	Monotonically decreasing dielectric response function
$f_0(E)$	Initial occupancy of electrons
f_p	Relaxation peak frequency
$\overline{F}(\omega)$	Fourier transform of the dielectric response function $f(t)$
G_{EF}	Gibbs free energy
G_{EF1}	Gibbs free energy of unaged state
G_{EF2}	Gibbs free energy of aged state
h	Planck's constant
$h(t)$	Monotonically increasing function
$i(t)$	Response current
$I_d(t)$	Depolarization current
$i_d(t)$	Depolarization current
$I_{de\text{-}trap}(t)$	Detrapping current at t^{th} instant

$I_{df}(t)$	Current due to dipolar relaxation at t^{th} instant for voltage stress of U_f
$I_{dipol}(t)$	Current due to dipolar relaxation at t^{th} instant
$i_p(t)$	Polarization current
$i_p(t)$	Polarization current
$I_r(t)$	Relaxation current at t^{th} instant
$i_r(t)$	Dipolar relaxation current
$J(t)$	Total current density
k	Boltzmann's constant
l	Depth of the electron injection
M^*	Complex electric modulus
M'	Real part of complex electric modulus
M''	Imaginary part of complex electric modulus
M_p	Peak amplitude of relaxation frequency distribution function
$N(E)$	Energy distribution of traps throughout the energy gap
N_t	Trap density
n_t'	Rate of release (de-trapping) of charge carriers
$\wp(t)$	Polarization at t^{th} instant
$\wp_{0total}$	Total polarization in the dielectric under equilibrium condition
$\wp_\infty$	Instantaneous polarization
$\wp_S$	Static polarization
$\wp_{total}$	Total polarization at any time instant t
q	Electron charge
$Q(t)$	Total Charge Density at t^{th} instant
$Q_0(t)$	Static Charge Density at t^{th} instant
$Q_{de\text{-}trap}$	De-trapped charge
$r(t)$	Dielectric relaxation function
$r(v)$	Distribution density function
$R(v)$	Total summation of the individual relaxation function of each dipole group having distinct relaxation frequency
R_g	Energy dissipating element of g^{th} dipolar group
r_s	Radius
R_{se}	Series resistance
R_{sh}	Shunt resistance
s	Laplace operator
t	time
T	Absolute Temperature

t_0	Time at when charging process starts
$tan\delta$	Dissipation factor
t_c	Charging time
t_{ch}	Specific charging time
t_{dp}	Duration of depolarization
t_f	Total measurement time of detrapping current
t_p	Duration of polarization
t_r	Effective relaxation time constant of the dielectric material
T_{th}	Threshold temperature for thermal ageing
$U(t)$	Charging voltage at t^{th} instant
$u(t)$	Unit step function
U_0	Step DC voltage
$V(t)$	Excitation Voltage
V_{dc}	DC voltage
v_i	Insulation volume
V_r	Recovery voltage
$V_{r(peak)}$	Peak recovery voltage
v_w	Injected water volume
W_{em}	Electromechanical energy stored due to space charge
Y	Young's Modulus
β	Relaxation time distribution parameter varying from 0 to 1
β_t	Electrostriction coefficient
$\delta(t)$	Dirac delta function
ΔG_{EF}	Energy difference
ε^*	Complex permittivity
ε'	Real part of complex permittivity
ε''	Imaginary part of complex permittivity
ε_0	Permittivity of free space or vacuum
ε_r	Relative permittivity
ε_s	Relative permittivity at near infinite frequency
λ	Integration constant
ρ	Volume density
σ_0	DC conductivity
σ_{eff}	Effective conductivity
τ	Relaxation time
τ_{aging}	Rate of thermal ageing reaction in polymer
τ_{ar}	Apparent relaxation time

τ_{deep}	Retention time of charges after being captured by deep traps
τ_{DM}	Debye Model relaxation time constant
τ_{dtp}	Time between two trapping events into deep traps
τ_g	Time constant of g^{th} dipolar group
τ_M	Electric modulus relaxation time constant
τ_p	Relaxation time constant
υ	Attempt to escape frequency
$\chi(t)$	Dielectric susceptibility at t^{th} instant
χ'	Real part of complex susceptibility
χ''	Imaginary part of complex susceptibility
χ_∞	Material's susceptibility at $t = 0$
χ_s	Material's susceptibility at $t \gg 0$
v_w	Injected water volume
ω	Angular frequency

ADC	Analog to Digital Converter
BDV	Breakdown Voltage
C-C	Cole-Cole
CDM	Conventional Debye Model
DAQ	Data Acquisition
DBM	Debye Model
DC	Direct Current
DP	Degree of Polymerization
DRC	Dielectric Relaxation Current
DRF	Dielectric Response Function
DSC	Differential Scanning Calorimetry
DSO	Digital Storage Oscilloscope
EDX	Energy Dispersive X-Ray
EpA	Epoxy Alumina
EPDM	Ethylene-Propylene-Diene Copolymer
EPNC	Epoxy Nano-Composite
FDS	Frequency Domain Spectroscopy
FTIR	Fourier-Transform Infrared Spectroscopy
GC-MS	Gas Chromatography-Mass Spectrometry
GND	Ground
H-N	Havriliak-Negami
HV	High Voltage

HVDC	High Voltage Direct Current
IDAX	Insulation Diagnostic Analysers
IR	Insulation Resistance
IRC	Isothermal Relaxation Current
ISPD	Isothermal Surface Potential Decay
KWW	Kohlrausch-Williams-Watts
LDPE	Low Density Polyethylene
LIBS	Laser Induced Breakdown Spectroscopy
LIMM	Laser Intensity Modulation Method
LPC	Long Polymeric Chain
LV	Low Voltage
m.c.	Moisture Content
MDM	Modified Debye Model
OIP	Oil Impregnated Paper
OP AMP	Operational Amplifier
PDC	Polarization And Depolarization Current
PEA	Pulse Electro Acoustic
PI	Polarization Index
PWP	Pressure Wave Propagation
RFD	Relaxation Frequency Distribution
RMSE	Root Mean Square Error
RPF	Relaxation Peak Frequency
RS	Raman Spectroscopy
RV	Recovery Voltage
RVM	Return Voltage Measurement
SEM	Scanning Electron Microscopy
SPC	Short Polymeric Chain
SPD	Surface Potential Decay
TCA	Thermal Conductivity Analysis
TDS	Time Domain Spectroscopy
TEM	Transmission Electron Microscopy
TGA	Thermo-Gravimetric Analysis
WCA	Water Contact Angle
XLPE	Cross-Link Polyethylene
XPS	X-ray Photoelectron Spectroscopy

Contents

Chapter 4: **Condition Assessment of Dry-Type Insulation Using Electric Modulus**

Chapter 5: **Condition Assessment of Dry-Type Insulation Using Dielectric Relaxation Current Analysis**

List of Figures

List of Tables

Chapter 1

Condition Assessment of Dry-Type Insulation

1.1 Introduction

In high voltage systems, the reliability and performance of electrical equipment are among the most critical requirements for any power system network. The insulation system plays a vital role in ensuring the safe operation of these systems by preventing electrical breakdowns and maintaining the continuity of power supply. However, insulation materials are susceptible to degradation over time, and if this degradation is not detected and addressed promptly, it can lead to catastrophic failures [1-5]. High voltage equipment such as power transformers, rotating machines, and switchgear are very costly, making it impractical to always have spare units available for backup. As a result, these expensive assets are prioritized for extended life expectancy to enhance the reliability of the power system network. Therefore, condition monitoring of power equipment in high voltage systems is essential to identify potential faults, predict failures, prevent downtime, ensure safety, and maintain power continuity [6-8].

Based on current industry trends, the application of dry type equipment (such as dry-type transformer) is continuously increasing. A situation will arrive when the installed dry type equipment will become older or aged. Consequently, the equipment will become non-functional and as a result of this, the associated power system will fail until and unless a new replacement is available. It is always beneficial to adapt a condition based maintenance scheme rather than replacement of costly, pivotal power equipment after failure [3-4]. Dry type equipment (e.g. transformer) are practically maintenance free over their oil-type counterpart. Moreover, combustible property of oil is unsafe. But, due to combined cause of electrical, mechanical, thermal and environmental effect, type insulation undergoes ageing. As a result of this ageing, the dry type insulation system also deteriorates like oil impregnated paper (OIP) of oil immersed equipment. Several researchers developed theoretical explanation on ageing of the dry type equipment which can be useful for further research [9-11].

1.2 Conventional Oil-Paper Insulation in High Voltage Power Equipment

The insulation system of high voltage power equipment, such as power transformers, relies on a combination of mineral oil and paper, collectively known as composite oil-paper insulation. Mineral oil, sourced from crude petroleum through fractional distillation, serves the dual purpose of providing both insulation and cooling within the transformer. This oil, characterized by its composition of alkanes, naphthalenes, and aromatic hydrocarbons, initially exhibits a dielectric strength of approximately 30 kVrms, which can escalate to 60 kVrms after post-treatment. Additionally, the oil's flash point is 140°C, with a pour point of -6°C, ensuring stability across a wide range of temperatures. It also maintains minimum volume resistivity and a dielectric dissipation factor at 90°C [12-13].

However, despite these advantageous properties, mineral oil is not without its vulnerabilities. The oil's hygroscopic nature makes it susceptible to moisture ingress, particularly during transportation, storage, and refilling. This moisture can significantly alter the oil's dielectric properties over time, leading to potential degradation of the insulation system. Such alterations not only affect the oil's ability to insulate but also accelerate its ageing process, further compromising the overall reliability of the power equipment. To understand these vulnerabilities better, it is essential to explore how these changes occur under different conditions and the impact they have on the performance of the insulation system. At elevated temperatures, mineral oil undergoes thermal degradation, leading to the formation of various by-products that impact its insulating properties. The rate of oil degradation approximately doubles with every 8°C-10°C increase in temperature. The decomposition of mineral oil at high temperatures results in the formation of several by-products, including moisture (water), carbon monoxide (CO), carbon dioxide (CO_2), ethylene (C_2H_4), acids, and sludge [13-16]. These acids are low molecular weight having polar carboxylic acids (R-COOH) and phenol (C_6H_5OH) which are formed due to oxidation of mineral oil. These acids can damage insulation and decompose metals in contact with the oil [13, 16]. In case of sludge, it contains various polar chemical compounds such as alcohols (-OH), aldehydes (-CHO), and ketones (RCR') are generated during the oil oxidation process, increasing the oil's conductivity and decreasing its dielectric strength. Oxidative ageing of mineral oil also leads to the formation of highly reactive peroxide groups (R-O-O-R) by breaking the hydrocarbon chain of the oil insulation. These groups accelerate the oxidation

mechanism, contributing to further degradation of the oil insulation [17]. In addition, Moisture is detrimental to the insulation of mineral oil, whether it may be in a free or bonded state. It is generated inside transformers due to the thermal degradation of mineral oil and cellulosic paper. Additionally, moisture can seep into transformers via breathers or oil-drain valves in moisture-rich environments. While moisture migration from paper to oil occurs at very high temperatures, the solubility of moisture in mineral oil also increases with temperature. However, at lower temperatures, excess moisture present in the oil can migrate back to the paper, leaving the mineral oil saturated with moisture. This excess moisture can lead to partial discharges, flashovers, or even short circuits due to insulation failure [13, 16].

In addition to oil, the paper insulation is the integral part of transformer insulation. It provides mechanical support, encases copper conductors to separate high voltage (HV) and low voltage (LV) windings. The paper insulation is consisting of 90% cellulose derived from wood pulp processed via the Kraft-Chemical method. Paper insulation gains mechanical strength from its lengthy polymeric chains. The chemical formula $(C_6H_{10}O_5)_n$ signifies cellulose's polymerization degree (DP), indicative of mechanical resilience [12, 16-17]. The volume resistivity of the paper is in the range of 10^{15}-10^{17} Ω·cm and *tanδ* at power frequency is varying from 3% to 4% [13]. This paper offers cost-effective electrical as well as mechanical insulation. However, its porous nature renders it hygroscopic, requiring impregnation with mineral oil to restrict moisture absorption and increase dielectric strength by displacing air pockets. Nevertheless, even after impregnation, the paper can absorb moisture from the surrounding oil, significantly impairing its dielectric properties. Additionally, paper insulation exhibits high moisture affinity and reacts vigorously in the presence of oxygen, with thermal instability at elevated temperatures [16].

Similar to mineral oil, the cellulosic paper insulation undergoes a gradual deterioration process attributed to thermal, oxidative, and hydrolytic influences. This degradation primarily entails depolymerisation of cellulose, instigated by the fragmentation of higher molecular weight cellulosic chains. Consequently, the mechanical and dielectric resilience of the paper insulation diminishes, discernible through a substantial decline in its Degree of Polymerization (DP) value. Initially, the DP value ranges from 1200 to 1300 (at post-processing), but with degradation, it reduces significantly to approximately 200-300 [13, 16]. Consequently, the tensile strength of the paper insulation wanes, rendering it brittle, potentially leading to detachment from the copper conductor—an indication of advanced ageing. It is yet to be mentioned here that, thermal degradation of paper insulation ensues from

chemical reactions catalysed by oxygen and moisture, where moisture playing a predominant role in hydrolysis. The insulation's lifespan diminishes by almost 50% with every 6°C-8°C increase in the temperature rise within the hot spot temperature range of 80°C to 100°C. Elevated temperatures expedite the shortening of polymeric chains, fostering mechanical failure incapable of withstanding the internal mechanical stresses during through-fault conditions. At exceedingly high temperatures, the glycosidic linkage of cellulose molecules undergoes cleavage, liberating CO_2, CO, hydrogen (H_2), moisture, and traces of methane (CH_4) [13, 16]. Furthermore, thermal degradation yields aldehydes (-CHO) and carboxyl (R-COOH) groups. Oxygen exacerbates the insulation's degradation by accelerating oxidation, facilitating the rupture of polymeric chains and rapid depolymerisation [. Oxidative depolymerisation produces hydrogen peroxide (H_2O_2) and other reactive peroxide (R-O-O-R) groups. Moreover, oxygen oxidizes hydroxyl (–OH) groups into carboxyl (R-COOH) and carbonyl (C=O) groups, further catalyzing insulation degradation. Positive metal ions (Fe^{+}/Fe^{2+}/Cu^{2+}/Cu^{3+}) also act as oxidation catalysts [13, 16-19]. In addition, moisture significantly influences cellulosic insulation degradation [2]. Despite using relatively dry-Kraft paper during transformer manufacturing, residual moisture remains due to ineffective factory drying processes. Initially, new transformers contain minimal moisture, but operational use can increase moisture content to 3-4% or more. Moisture induces hydrolysis, rupturing glycosidic chains and accelerating chain scission [2]. Wet cellulose degradation intensifies at higher temperatures, prompting cautious operation of heavily wet transformers at reduced loads to prolong their lifespan.

1.3 Limitation of Conventional Oil-Paper Type Insulation

The conventional oil-paper insulation system has been widely used in high voltage power equipment, such as transformers and bushings, for many decades. While this system has proven effective in providing both electrical and thermal insulation, it is not without its limitations. As modern power systems continue to evolve, the demands placed on insulation systems have increased, making it essential to understand these limitations in greater detail. Identifying these constraints is crucial not only for improving existing technologies but also for exploring and adopting alternative insulation solutions that better meet current and future needs.

One of the primary limitations of the conventional oil-paper insulation system is its susceptibility to ageing and degradation over time. The paper

insulation, a critical component, undergoes significant chemical and physical changes due to moisture absorption, oxidation, and thermal stress. These factors cause the paper to become brittle, leading to a loss of dielectric strength and an increased risk of insulation failure. Additionally, the mineral oil used in this system can deteriorate due to oxidation, hydrolysis, and contamination, further compromising the insulation's overall performance [2, 16]. These ageing processes not only reduce the effectiveness of the insulation but also increase maintenance costs and the risk of catastrophic equipment failures.

To overcome these limitations, researchers and engineers have been exploring alternative insulation solutions (i.e. dry-type insulation) for high voltage power equipment.

1.4 Importance of Dry-Type Insulation

Dry-type insulation has gained significant importance in the field of power equipment due to its numerous advantages over conventional oil-paper insulation systems. This modern insulation technology offers several benefits, including improved safety, reduced environmental impact, enhanced performance, and greater versatility. As the demands on power equipment continue to evolve, the development of next-generation dry-type insulation further pushes the boundaries of what insulation technology can achieve, promising even more significant advancements [3-4, 20].

To better understand the critical role that dry-type insulation plays in the power equipment industry, it is essential to explore its key advantages in detail. These advantages not only highlight the superiority of dry-type insulation over traditional systems but also underscore its growing relevance in modern applications.

1.4.1 Advantages of Dry-Type Insulation in Power Equipment

- **Enhanced Safety:** One of the most significant benefits of dry-type insulation is its ability to eliminate the need for flammable oil, thereby significantly reducing the risk of fire and explosion hazards. With the absence of oil, the likelihood of leaks, spills, and associated environmental pollution is also eliminated. This greatly enhances the overall safety of power equipment installations, making dry-type insulation particularly suitable for sensitive environments such as

hospitals, data centers, and industrial facilities where fire safety is of utmost importance [4].

- **Environmental Friendly**: Dry-type insulation systems are environmental friendly compared to oil-paper insulation. They do not contain hazardous oils, eliminating the risk of oil spills and the associated environmental contamination. Additionally, dry-type insulation does not emit harmful gases or contribute to greenhouse gas emissions. The absence of oil in dry-type insulation reduces the overall carbon footprint, aligning with global efforts to reduce environmental impact and promote sustainability [21-23].
- **Versatility and Compact Design:** Dry-type insulation systems offer greater flexibility and adaptability in terms of installation and equipment design. They can be designed in various shapes and sizes, allowing for more compact and space-efficient designs. The versatility of dry-type insulation makes it suitable for a wide range of power equipment applications, including transformers, switchgear, and cables [24-25].
- **Reduced Maintenance:** Dry-type insulation systems require minimal maintenance compared to conventional oil-paper insulation systems. The absence of oil eliminates the need for regular oil sampling, testing, and filtering processes. This results in cost savings, reduced downtime, and increased availability of power equipment. The reduced maintenance requirements make dry-type insulation particularly attractive for applications where access to equipment for maintenance is challenging or costly [24-30].

1.4.2 Next-Generation Dry-Type Insulation

The importance of dry-type insulation is further amplified by the development of next-generation insulation technologies. Researchers and engineers are continuously exploring innovative materials and designs to enhance the performance and capabilities of dry-type insulation [20, 30-31]. Some of the key advancements in next-generation dry-type insulation include:

- **Solid Insulation Materials:** Next-generation dry-type insulation systems explore the use of solid insulation materials, such as epoxy resins, silicone rubber, composite materials etc. These materials offer enhanced mechanical strength, improved thermal stability, and excellent electrical insulation properties. Solid insulation eliminates the need for liquid dielectrics, providing maintenance-free operation and eliminating

the risk of leakage. It also allows for more compact designs and increased flexibility in equipment installation [30].

- **Nanocomposite Insulation:** Incorporating nano-materials (such as nanoparticles) into the insulation matrix enhances its electrical, thermal, and mechanical properties. Nanocomposite insulation offers improved dielectric strength, reduced thermal conductivity, enhanced resistance to partial discharges, increased resistance to ageing etc. These advancements enable the development of more compact and efficient power equipment with higher voltage ratings and improved insulation performance [32-35]. In the quest for more advanced and efficient insulation materials for dry-type applications, epoxy-based nano-composites have emerged as a promising next-generation solution. The addition of nanoparticles, such as silicon dioxide, alumina etc. to the epoxy matrix enhances the insulation performance by reducing the occurrence of partial discharges. These nanoparticles act as barriers and traps for electrical discharges, preventing their propagation and minimizing the risk of insulation breakdown [36-37]. The dispersed nanoparticles also improve the homogeneity of the insulation material, reducing the chances of defects (or weak points) that could lead to premature failure [37-38]. The enhanced dielectric strength of epoxy-based nano-composites makes them suitable for high voltage applications, where reliable insulation performance is crucial. Furthermore, epoxy-based nanocomposites exhibit improved thermal conductivity compared to conventional epoxy resins. The nanoparticles, such as boron nitride or aluminum nitride, have high thermal conductivity, which facilitates efficient heat dissipation. This property is particularly important in high power-density applications, as it helps to maintain lower operating temperatures and prevent thermal stress on the insulation material [37]. By effectively dissipating heat, epoxy-based nanocomposites can extend the lifespan of power equipment and improve overall system reliability. Mechanical strength is another critical aspect of insulation materials, and epoxy-based nanocomposites offer enhanced mechanical properties. The incorporation of nanoparticles reinforces the epoxy matrix, resulting in improved tensile strength, flexural strength, and impact resistance. This enhanced mechanical strength ensures the durability and integrity of the insulation material, making it more resistant to mechanical stresses and vibrations [37]. It also allows for the design of compact and lightweight power equipment without compromising structural integrity.

To further optimize the performance of epoxy-based nanocomposites, researchers have been investigating various parameters, including nanoparticle type, concentration, dispersion, and processing techniques. For instance, the choice of nanoparticles greatly influences the final properties of the nanocomposite. Different types of nanoparticles offer unique advantages and can be tailored to specific requirements. Additionally, the concentration and dispersion of nanoparticles within the epoxy matrix impact the overall performance of the insulation material. Effective dispersion techniques, such as ultra-sonication or high-shear mixing, are employed to achieve uniform distribution and prevent agglomeration of nanoparticles [37]. Researchers have also explored surface modification techniques to enhance the compatibility between the nanoparticles and the epoxy resin, improving the interfacial adhesion and overall performance of the nanocomposite [35-39].

- **Dry-Air Insulation:** Dry-air insulation systems replace the traditional insulating oil with dry air as the dielectric medium. This approach eliminates the environmental concerns associated with oil-based insulation systems. Dry-air insulation offers comparable dielectric performance to oil but with improved thermal properties. It enables more efficient heat dissipation, leading to lower operating temperatures and reduced energy consumption. Dry-air insulation is gaining attention as a sustainable and eco-friendly solution for high voltage power equipment [40].

1.5 Degradation of Dry-Type Insulation System

Ensuring the longevity and reliability of high voltage power equipment hinges significantly on the condition of its insulation systems. Dry-type insulation, widely used due to its advantages over conventional oil-paper systems, is not immune to degradation. Understanding the factors that contribute to the degradation of dry-type insulation is crucial for enhancing design, maintenance practices, and overall system reliability. The primary factors influencing the degradation of dry-type insulation systems include thermal stress, mechanical stress, environmental conditions, and electrical stress [37, 39-43]. Figure 1.1 shows the four factors influencing the ageing of the insulation system [43].

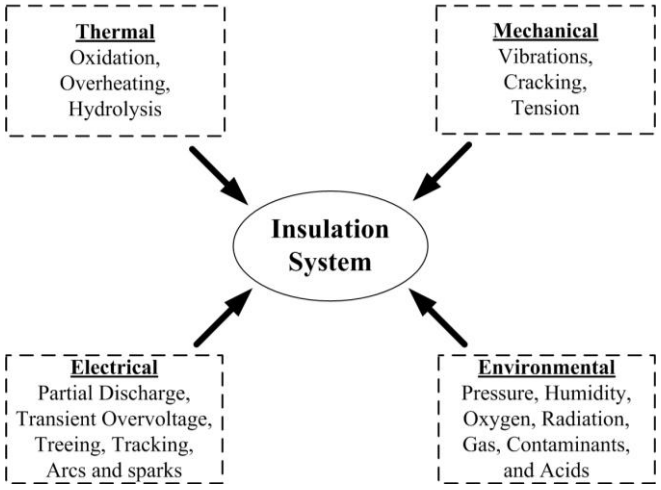

Figure 1.1: Four factors influencing the ageing of the insulation system.

1.5.1 Thermal Stress

One of the foremost contributors to insulation degradation is thermal stress. When operating temperatures exceed the design limits, the insulation materials undergo accelerated ageing. Elevated temperatures can induce chemical and physical changes in the insulation, reducing its dielectric strength and mechanical integrity. Prolonged exposure to high temperatures not only shortens the insulation's effective lifespan but also increases the susceptibility to thermal breakdowns [30, 32-34]. Therefore, effective thermal management is essential to mitigate these effects and ensure the insulation system's durability.

1.5.2 Mechanical Stress

In addition to thermal factors, mechanical stress plays a critical role in the degradation process. Vibrations, mechanical shocks, and improper handling during installation and maintenance can cause physical damage to the insulation materials. Such mechanical disturbances may lead to micro-cracks, abrasions, or complete dislodgment of insulation components, compromising their protective capabilities. Addressing mechanical stress through careful handling and robust installation practices is vital to maintaining the integrity of dry-type insulation systems [37, 41].

1.5.3 Electrical Stress

Electrical stress, encompassing overvoltages, lightning strikes, and switching surges, is another pivotal factor contributing to insulation degradation. These electrical disturbances can induce partial discharges within the insulation material. Partial discharges are localized dielectric breakdowns that, over time, can erode the insulation, leading to an increased risk of complete electrical failure. Continuous exposure to electrical stress without adequate mitigation can significantly reduce the insulation's reliability and lifespan [32, 37, 39]. Effective electrical stress management, including surge protection and proper insulation design, is essential to prevent such degradation.

1.5.4 Environmental Conditions

The surrounding environment significantly impacts the condition of dry-type insulation. Factors such as humidity, pollution, and exposure to chemicals can degrade insulation properties over time. Moisture ingress, in particular, can be detrimental as it affects the dielectric properties and can lead to the formation of conductive paths, increasing the risk of electrical faults. Additionally, pollutants and corrosive chemicals present in the environment can cause chemical reactions that deteriorate the insulation materials [37, 41]. Implementing appropriate environmental controls and protective measures is necessary to minimize these adverse effects.

In summary, the degradation of dry-type insulation systems is a multifaceted issue influenced by thermal, mechanical, environmental, and electrical factors. A comprehensive understanding of these degradation mechanisms is essential for developing strategies to enhance insulation performance, extend its service life, and ensure the reliability of high voltage power equipment. Addressing these factors through improved design, regular maintenance, and environmental controls can lead to more robust and durable insulation systems [37-41].

1.6 Condition Assessment of Dry-Type Insulation

Condition assessment of dry-type insulation is an essential process for ensuring the reliability, safety, and performance of high voltage systems. Given the critical role that insulation plays in maintaining the operational integrity of electrical equipment, particularly in high-stress environments,

regular and thorough assessments are necessary to prevent unforeseen failures and extend the lifespan of these systems. Dry-type insulation materials, such as epoxy-based composites, have become widely used in various electrical applications due to their excellent thermal, mechanical, and dielectric properties [3, 32, 35]. These materials offer several advantages over traditional insulation systems, including reduced fire risk and environmental impact. However, like all insulation materials, dry-type insulation is subject to ageing and environmental stresses that can degrade its performance over time. Factors such as thermal cycling, electrical stress, mechanical wear, and exposure to moisture or contaminants can lead to a gradual decline in the insulation's effectiveness [37, 43].

Conducting a comprehensive condition assessment enables early detection of insulation deterioration, allowing for timely maintenance or replacement. This proactive approach is crucial for preventing costly failures, minimizing downtime, and ensuring the continued reliability of high voltage systems [2]. By identifying potential issues before they lead to catastrophic failures, condition assessment helps maintain system integrity and extends the operational life of electrical equipment.

Moreover, the unique properties of dry-type insulation necessitate specific assessment techniques tailored to its material characteristics. Understanding the precise ageing mechanisms and stress factors that affect dry-type insulation is key to developing accurate diagnostic methods. These methods can include thermal analysis, dielectric testing, and mechanical evaluation, all of which contribute to a holistic understanding of the insulation's condition.

In summary, the condition assessment of dry-type insulation is not only a preventive measure but a critical component of high voltage system management. By implementing regular and targeted assessments, operators can ensure that their systems remain safe, reliable, and efficient throughout their operational life.

1.7 Methods for Condition Assessment of Dry-Type Insulation

To accurately assess the condition of dry-type insulation materials, various methods are employed, each providing unique insights into the insulation's health and performance. These assessment methods can be broadly categorized into four main areas: physical, chemical, thermal, and electrical property analysis. Together, these analyses offer a comprehensive view of the insulation's condition, enabling engineers to determine the extent of

degradation, diagnose potential failure modes, and predict the remaining service life of the insulation system.

1.7.1 Analysis of Physical Properties

The physical properties of dry-type insulation, such as mechanical strength, surface roughness, and interfacial characteristics, are critical indicators of the material's structural integrity. These properties directly influence the insulation's ability to withstand mechanical stresses and environmental conditions. Techniques like scanning electron microscopy (SEM), water contact angle (WCA) measurement, and transmission electron microscopy (TEM) are commonly used to assess these physical properties [37, 45-51]. By analyzing these aspects, engineers can identify degradation mechanisms such as cracking, delamination, and surface erosion, which may compromise the insulation's performance over time [37, 45-51]. In this context, different condition assessment techniques (or, methods) for physical properties analysis and its findings have been tabulated in Table 1.1.

Table 1.1: Condition assessment techniques for physical properties analysis.

Investigative Methods	Condition Assessment Properties	References
TEM	Interfacial Characteristics, Agglomeration Degree, Internal Structure	[45, 46, 47]
SEM	Interfacial Zone, Surface Defects, Dispersion, Agglomeration Degree	[37, 46, 48]
WCA	Surface Energy, Surface Roughness, Hydrophobicity, Surface Morphology	[49-51]

1.7.2 Analysis of Chemical Properties

In addition to physical characteristics, the chemical composition of the insulation material plays a vital role in its overall performance and longevity. Chemical analysis techniques, such as Fourier-transform infrared spectroscopy (FTIR), gas chromatography-mass spectrometry (GC-MS) Energy Dispersive X-Ray (EDX), X-ray Photoelectron Spectroscopy (XPS), Raman Spectroscopy (RS), and Laser Induced Breakdown Spectroscopy (LIBS) allow for the identification of chemical changes that occur during ageing and exposure to environmental stresses [48, 52-56]. These methods provide insights into the chemical stability of the insulation, the presence of

contaminants, and the formation of degradation by-products, all of which can significantly impact the material's effectiveness [37, 48, 52-63]. In this context, different condition assessment techniques (or, methods) for chemical properties analysis and its findings have been tabulated in Table 1.2.

Table 1.2: Condition assessment techniques for chemical properties analysis.

Investigative Methods	Condition Assessment Properties	References
FTIR	Molecules Identification, Functional Groups Detection	[48, 52-54]
GC-MS	Chemical Components of Decomposed Gases, Severity of Partial Over-Fault using the Decomposed Gases Concentration	[37, 55]
EDX	Chemical Composition	[37, 56]
XPS	Chemical States of the Surface Elements, Binding State of the Elements, Elemental Composition	[37, 57]
XRD	Crystallographic Structure, Defects Identification, Crystallite Size, Micro-Stains, Structural Heterogeneity, Alignment of Nanoparticles	[58, 59]
RS	Functional Group Identification, Modification in Chemical Bonds, Electrical Treeing Characteristics	[60, 61]
LIBS	Insulation Surface Elements (Major & Trace), Atomic Structure, Isotopic Ratio	[62, 63]

1.7.3 Analysis of Thermal Properties

The thermal properties of insulation materials, including thermal conductivity, specific heat capacity, and thermal stability, are crucial for ensuring that the insulation can effectively manage the heat generated during operation. Thermal analysis methods, such as differential scanning calorimetry (DSC) and thermo-gravimetric analysis (TGA), thermal conductivity analysis (TCA) help evaluate these properties, providing essential data on how the insulation responds to temperature variations and thermal stresses. This information is vital for predicting thermal ageing and ensuring that the insulation can perform reliably under varying thermal conditions [37, 48, 57, 64-68]. In this regard, different condition assessment techniques for thermal properties analysis and its findings have been tabulated in Table 1.3.

Table 1.3: Condition assessment techniques for thermal properties analysis.

Investigative Methods	Condition Assessment Properties	References
TGA	Thermal Stability, Identification of Volatile Components inside Insulation, Decomposition Temperature	[37, 48, 57, 64]
TCA	Thermal Diffusivity, Thermal Conductivity, Specific Heat Capacity	[37, 65, 66]
DSC	Specific Heat Capacity, Glass Transition Temperature (*Tg*), Crystallization Temperature, Melting Point, Thermal Stability, Degree of Cross-Linking, Curing Process, Oxidation Behavior	[67, 68]

1.7.4 Analysis of Electrical Properties

The electrical properties of dry-type insulation, such as dielectric strength, insulation resistance, and dielectric loss, are fundamental to its ability to function effectively in high voltage environments. Electrical property analysis includes methods like dielectric spectroscopy, polarization and depolarization current (PDC) measurement, frequency domain spectroscopy (FDS) measurement, and breakdown voltage (BDV) testing. These techniques help assess the insulation's ability to resist electrical stress, detect the presence of partial discharges, and identify any degradation in the insulation's electrical performance over time [1, 2, 7, 13, 16, 37]. In addition, the information about the space charge, trap charge, and surface charge characteristics can be evaluated using different advanced methods such as surface potential decay (SPD) method, laser intensity modulation method (LIMM), pressure wave propagation (PWP) method, pulse electro-acoustic (PEA) method, etc. [71-76]. In this regard, different condition assessment techniques for electrical properties analysis and their findings have been tabulated in Table 1.4.

By integrating the results from these various analyses, a comprehensive understanding of the insulation's condition can be achieved. This holistic approach to condition assessment enables more accurate predictions of the insulation's remaining life, allowing for better planning of maintenance and replacement activities, ultimately ensuring the reliability and safety of high voltage systems.

Table 1.4: Condition assessment techniques for electrical properties analysis.

Investigative Methods	Condition Assessment Properties	References
BDV	Breakdown Strength	[37, 69, 70]
SPD	Characterization of Surface Charge, Trap Characteristics (Shallow and Deep Traps)	[71, 72]
LIMM	Space Charge Characteristics	[73]
PWP	Space Charge Distribution	[74]
PEA	Space Charge Distribution	[75, 76]
PDC	Polarization Current, Depolarization Current, Conduction Current, DC Conductivity, Detrapping Current, Charge Trapping Characteristics	[1, 2, 7, 17, 37, 77, 78]
FDS	Complex Capacitance, Dielectric Constant (ε') and Dielectric Loss (ε''), Dissipation Factor ($tan\delta$), Electric Modulus, *etc.*	[1, 2, 13, 16, 37, 79, 80]

1.8 Dielectric Response Measurement of Dry-Type Insulation

Dielectric response measurement is a powerful non-invasive technique used for the condition monitoring of electrical insulation systems. It provides valuable information about the insulation's dielectric properties, such as complex capacitance, dissipation factor ($tan\delta$), conductivity, space charge/ trap charge, insulation resistance, polarization index etc. which are critical indicators of insulation health and degradation.

In the process of dielectric response measurement, the AC or DC voltage excitation is applied on the test insulation and the resulting current and voltage waveforms are recorded. From these recorded voltage and current signals, it is possible to extract valuable information about the insulation's reliability, ageing, and moisture content etc. The commonly used techniques for dielectric response measurement is two types, i) time domain spectroscopy (TDS) analysis and ii) frequency domain spectroscopy (FDS) analysis [1, 2]. In TDS, there are two popular methods which are polarization and depolarization current (PDC) measurement and return voltage measurement (RVM). According to several research performances on real life assessment of insulation condition, the PDC is preferred as more reliable over RVM [2]. In FDS, where the insulation is subjected to a sinusoidal

voltage signal at different frequencies, and the resulting current and voltage responses are measured and analyzed [1, 2, 13, 16]. In FDS, the complex capacitance (or, complex permittivity) and dissipation factor (*tanδ*) are two important parameters obtained from dielectric response measurement. The real part of the complex capacitance reflects the storage ability of electric charge in the insulation and the imaginary part of the complex capacitance represents the dielectric loss component inside the dielectrics material. Both of the part of complex capacitance are influenced by factors such as ageing of insulation, temperature, moisture content, and the presence of contaminants etc. Changes in capacitance can indicate variations in the insulation's dielectric constant and electrical properties, providing insights into insulation ageing and degradation processes [2]. Besides, the dielectric dissipation factor (*tanδ*) is the ratio of imaginary part and real part of complex capacitance, which reflects the amount of energy loss in the insulation. High *tanδ* values can indicate the presence of insulation defects or degradation, highlighting potential areas of concern for further investigation [2].

Dielectric spectroscopy techniques rely on the fundamental interaction between an applied electric field and the dipole groups within the insulating material. For an isotropic and homogeneous dielectric material, the relationship between the polarization vector $\wp(t)$ and the electric field $E(t)$ is described by equation (1.1).

$$\wp(t) = \chi(t)\varepsilon_0 E(t) \tag{1.1}$$

Here, $\chi(t)$ represents the electric susceptibility of the material, and ε_0 denotes the permittivity of free space. On a macroscopic level, insulating materials can be regarded as isotropic, linear, and homogeneous [1, 2]. Consequently, the dielectric flux density $D(t)$ within the material can be described using the properties of the insulating material, as given in equation (1.2) [16, 81-82].

$$D(t) = \varepsilon_0 E(t) + \wp(t) = \varepsilon_0 \big(1 + \chi(t)\big) E(t) \tag{1.2}$$

The polarization vector $\wp(t)$ reflects the cumulative effect of various mechanisms, including polarization processes that occur over different timescales. These range from very rapid processes, such as electronic polarization, to slower ones like dipolar polarization. Consequently, when a constant DC voltage V_{dc} is applied to a dielectric material that is initially free of charge at $t = t_0$, the resulting polarization vector $\wp(t)$ exhibits a gradually increasing profile, as illustrated in Figure 1.2 [1].

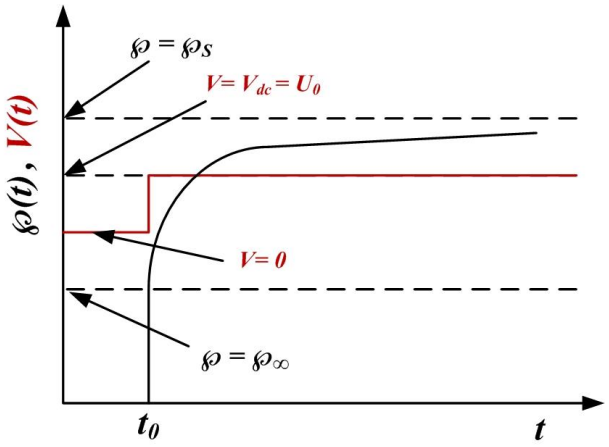

Figure 1.2: Time-dependent behavior of polarization under the influence of a constant voltage V_{dc} (= U_0) starting at $t = t_0$.

In Figure 1.2, $\wp_\infty$ represents the polarization resulting from fast mechanisms, while $\wp_S$ denotes the total saturated polarization of the material (at infinite time i.e. $t \rightarrow \infty$). As seen in Figure 1.2, the polarization process can be described by the expression provided in equation (1.3).

$$\wp(t) = \wp_\infty \delta(t - t_0) + (\wp_S - \wp_\infty) h(t - t_0) \tag{1.3}$$

In equation (1.3), $\delta(t-t_0)$ denotes the Dirac delta function and $h(t-t_0)$ is a monotonically increasing function with time [1, 2]. By applying equation (1.2), the total polarization resulting from any electric field ($E(t)$) can be reformulated as shown in equation (1.4).

$$\wp(t) = \varepsilon_0 \left[\chi_\infty + (\chi_S - \chi_\infty) h(t - t_0)\right] E(t) \tag{1.4}$$

In equation (1.4), χ_∞ and χ_S represent the material's susceptibility at $t = 0$ and $t \gg 0$, respectively. The total polarization of the material can also be expressed in terms of relative permittivity, as shown in equation (1.5) [16, 82-83].

$$\wp(t) = \varepsilon_0 \left[\left(\varepsilon_\infty - 1\right) + (\varepsilon_S - \varepsilon_\infty) h(t - t_0)\right] E(t) \tag{1.5}$$

It is important to note that equation (1.5) can be generalized to derive the total polarization process for any given electric field *E(t)*. The formula for the total polarization process with an arbitrary electric field profile *E(t)* is provided in equation (1.6).

$$\wp(t) = \varepsilon_0(\varepsilon_\infty - 1)E(t) + \varepsilon_0 \int_{-\infty}^{\infty} f(t-\tau)E(\tau)d\tau \tag{1.6}$$

In equation (1.6), the dielectric response function is represented by the monotonic decreasing function *f(t)*. The total current density *J(t)* that flows through the material in response to the applied electric field *E(t)* is given by the expression in equation (1.7).

$$J(t) = \sigma_0 E(t) + \frac{\partial D(t)}{\partial t} = \sigma_0 E(t) + \varepsilon_0 \frac{\partial E(t)}{\partial t} + \frac{\partial \wp(t)}{\partial t} \tag{1.7}$$

In equation (1.7), σ_0 and ε_0 represent the DC conductivity of the dielectric medium and the permittivity of free space, respectively. In a homogeneous material, the electric field strength, *E(t)* is considered to be induced by an applied excitation voltage, *V(t)*. As a result, the total current, *i(t)*, flowing through a dielectric medium with a geometric capacitance C_0 (calculated as the measured capacitance at or near the power frequency divided by the relative permittivity) can be represented as follows [84].

$$i(t) = C_0 \left[\underbrace{\frac{\sigma_0}{\varepsilon_0} V(t)}_{1st-Part} + \overbrace{\varepsilon_\infty \frac{\partial V(t)}{\partial t}}^{2nd-Part} + \underbrace{\frac{d}{dt} \int_{-\infty}^{t} f(t-\tau)V(\tau)d\tau}_{3rd-Part} \right] \tag{1.8}$$

In equation (1.8), 1st-Part represents the conduction current passing through the dielectric material, while 2nd-Part and 3rd-Part correspond to the displacement and polarization currents, respectively. It is important to note that equation (1.8) applies to both a single dielectric material and configurations involving multiple dielectric materials arranged in series or parallel. Additionally, equation (1.8) indicates that the excitation voltage, *V(t)*, can either be constant or time-varying. Based on the characteristics of the excitation voltage, dielectric spectroscopy can be categorized into two types: i) time-domain spectroscopy and ii) frequency-domain spectroscopy.

1.8.1 Time Domain Dielectric Response Measurement

In Time Domain Spectroscopy (TDS), a constant voltage is applied to the insulation under test, and the resulting dielectric response current is recorded. Upon applying the steady voltage, the dipoles within the insulation align with the electric field, resulting in a polarization current [1, 2, 7, 84-86]. During this polarization process, energy is stored in the dielectric material due to the alignment of the dipoles. When the applied field is removed by short-circuiting, this stored energy is released, causing an equivalent current to flow in the opposite direction. Various dielectric properties of the insulating material are assessed based on these dielectric phenomena. In the category of TDS measurement, the polarization and depolarization current measurement and return voltage measurement are two popular methods.

1.8.1.1 Polarization and Depolarization Current Measurement

In PDC measurement, a constant DC voltage is applied to the insulation being examined [2, 84-86]. This voltage causes the dipoles within the insulation material to align with the electric field, thereby initiating the polarization process [1]. The schematic of PDC measurement circuit arrangement has been shown in Figure 1.3. During polarization, a monotonically decreasing current, denoted as $i_P(t)$, flows through the insulating material (refer to Figure 1.3). The polarization process is considered complete when all dipoles are aligned with the field, at this stage, the polarization current decreases to zero, leaving only the conduction current to flow through the dielectric medium. The conduction current's magnitude depends on the insulation resistance of the dielectric material.
In depolarization current measurement, the excitation voltage is removed, and the insulation is short-circuited. This causes the dipoles to revert to their original alignment, releasing the stored polarization energy, which generates a depolarization current ($i_d(t)$) that decreases monotonically, flows in the opposite direction. The typical behavior of the polarization and depolarization currents is illustrated in Figure 1.4 [2].
In dry-type insulation or solid-dielectric media, such as polymeric insulation, the initial value of the PDC is influenced by the smaller chain polymeric groups, while the higher time constant dipoles in the long polymeric chain components of the insulation affect the latter part of the current [85]. Consequently, the dielectric properties of the dry-type insulation can be analysed by examining the polarization current. Additionally, the degradation of the dry-type insulation (due to ageing or other environmental factors)

tends to increase the PDC value over a longer time. Therefore, the condition of dry-type insulation can be evaluated using PDC measurements.

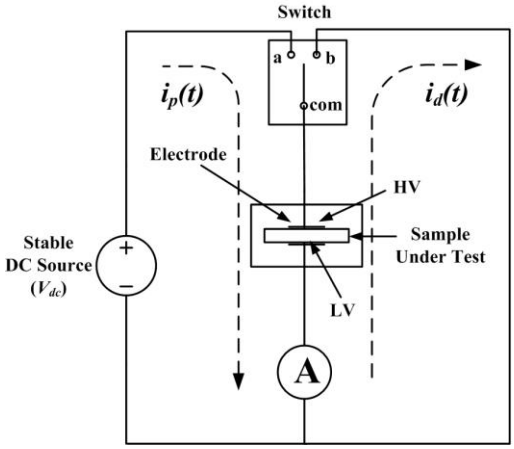

Figure 1.3: Schematic of PDC measurement circuit arrangement.

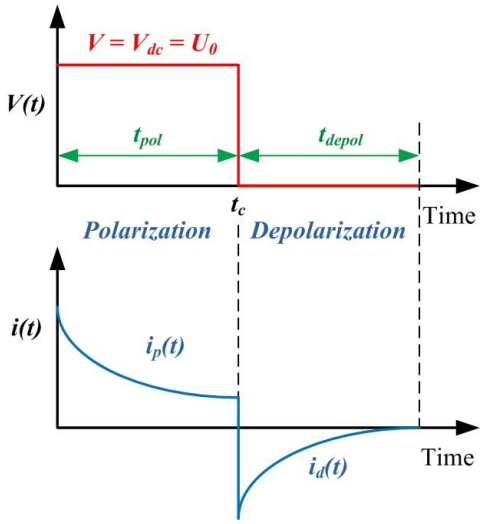

Figure 1.4: The characteristics of polarization and depolarization currents in a dielectric material exposed to a step voltage.

When a constant voltage U_0 is applied to the insulation under test, the resulting polarization current through the insulation (as illustrated in Figure 1.3) can be determined using equation (1.9).

$$i_p(t) = \left[C_0 U_0\right] \cdot \left[\varepsilon_\infty \delta(t) + f(t) + \frac{\sigma_0}{\varepsilon_0} \right] \quad \text{for } 0 < t < t_c \tag{1.9}$$

In equation (1.9), t_c represents the duration for which the field is applied to the test sample (i.e. charging time). After t_c, the excitation voltage is removed, and the test object is short-circuited. At this point, the displacement current ($\varepsilon_\infty \delta(t)$) does not contribute to the polarization current ($i_p(t)$) except at $t=0$. Thus, the resulting current primarily comprises two components: the conduction current, influenced by the conductivity (σ_0), and $f(t)$, the dielectric response function. Consequently, the dielectric response function $f(t)$ can be determined from the polarization current, provided the conduction current is known. Once the polarization process ends (at t_c), the voltage supply is disconnected, and the test object is short-circuited. The dipoles within the insulation then start to relax, releasing stored energy as they return to their original alignment [2, 16, 84-85]. This relaxation process generates a depolarization current i_d as the dipoles reorient. The depolarization current can be expressed as:

$$i_d(t) = -\left[C_0 U_0\right] \cdot \left[f(t) - f(t + t_c) \right] \quad \text{for } 0 < t < \infty \tag{1.10}$$

As previously noted, the dielectric response function $f(t)$ decreases monotonically. Thus, after a sufficiently long charging time t_c, the value of $f(t-t_c)$ becomes negligible compared to $f(t)$ and can be ignored [84]. Thus, the depolarization current in equation (1.10) simplifies to:

$$i_d(t) \approx -\left[C_0 U_0\right] \cdot \left[f(t) \right] \tag{1.11}$$

From equation (1.11), it is evident that once the depolarization current of a dielectric material is measured, the dielectric response function can be obtained. The typical nature of polarization and depolarization current has been shown in Figure 1.4.

1.8.1.2 Return Voltage Measurement

To further explore the dielectric phenomena, particularly the "after effects" of PDC measurement, the Recovery Voltage Measurement (RVM) technique is employed. In this process, a step voltage is applied to charge the sample for a specific time (t_{ch}), followed by grounding it to discharge for a period equal to half the charging time ($½t_{ch}$). Afterward, the sample is ungrounded, and the voltage across the insulation sample, known as the recovery voltage (RV), is recorded (i.e. V_r) [2, 87]. This voltage results from the active relaxation processes within the dielectric material, which didn't have sufficient time to fully relax during the brief discharging period. Consequently, the RV is a crucial indicator of the dielectric material's insulating properties. Figure 1.5 shows a typical recovery voltage waveform.

In the RVM methodology, the charging and discharging times are progressively increased while maintaining the same ratio between them. The peak recovery voltage ($V_{r(peak)}$) is recorded at each step. These peak values for different charging times (t_{ch}) are plotted to generate a $V_{r(peak)}$ versus t_{ch} curve, known as the Recovery Voltage Spectrum. This spectrum is then analysed for condition monitoring. Both PDC and RV waveforms have been found useful in assessing the condition of insulation.

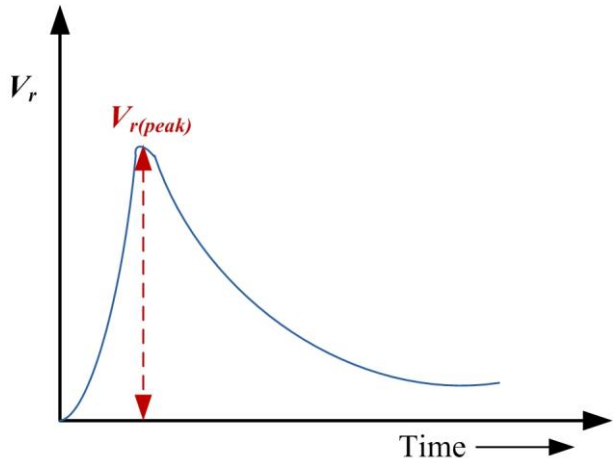

Figure 1.5: Nature of Recovery Voltage waveform.

1.8.2 Frequency Domain Dielectric Response Measurement

Time domain spectroscopy is commonly employed for monitoring the condition of the insulation dielectric. However, it has certain limitations. The primary drawbacks of TDS are the necessity for a high voltage source for measurements and its vulnerability to noise. As a result, researchers are exploring Frequency Domain Spectroscopy (FDS) as an alternative method for assessing the condition of oil-paper insulation. FDS uses a pure sinusoidal waveform for the excitation voltage. When this sinusoidal voltage is applied, the polarization process initiates, causing a dielectric response current to flow through the dielectric medium. This dielectric response current can be analytically derived by transforming time domain response current (i.e equation (1.8)) into the frequency domain using the Laplace transform, as illustrated in equation (1.12) [1, 2].

$$I(s) = [C_0] \cdot \left[\varepsilon_\infty sU(s) + sF(s)U(s) + \frac{\sigma_0}{\varepsilon_0} U(s) \right] \tag{1.12}$$

In equation (1.12), *s* represents the Laplace operator. By substituting *s* with the complex frequency $j\omega$, the equation (1.12) can be simplified as equation (1.13).

$$\bar{I}(\omega) = [C_0] \cdot \left[\varepsilon_\infty j\omega \bar{U}(\omega) + j\omega \bar{F}(\omega) \bar{U}(\omega) + \frac{\sigma_0}{\varepsilon_0} \bar{U}(\omega) \right] \tag{1.13}$$

In equation (1.13), $\bar{F}(\omega)$ is the Fourier transform of the dielectric response function *f(t)*. $\bar{F}(\omega)$ defines the susceptibility $\bar{\chi}(\omega)$ of the dielectric medium, as shown in equation (1.14) [16].

$$\bar{F}(\omega) = \bar{\chi}(\omega) = \chi'(\omega) - j\chi''(\omega) = \int_0^\infty f(t) \exp(-j\omega t) dt \tag{1.14}$$

In equation (1.14), $\bar{\chi}(\omega)$ represents the complex susceptibility of the medium. $\chi'(\omega)$ is the real part of $\bar{\chi}(\omega)$, while $\chi''(\omega)$ is the imaginary part. Consequently, the resultant dielectric response current $I(\omega)$ under sinusoidal excitation with angular frequency ω can be expressed as:

$$\begin{aligned}\bar{I}(\omega) &= \left[j\omega C_0\right]\cdot\left[\left\{\varepsilon_\infty + \chi'(\omega)\right\} - j\left\{\frac{\sigma_0}{\omega\varepsilon_0} + \chi''(\omega)\right\}\bar{U}(\omega)\right] \\ &= j\omega\left\{C'(\omega) - jC''(\omega)\right\}\bar{U}(\omega) \\ &= j\omega\bar{C}(\omega)\bar{U}(\omega)\end{aligned} \tag{1.15}$$

In equation (1.15), $\bar{C}(\omega)$ represents the frequency-dependent complex capacitance of the insulating medium. The real part, *C′(ω)*, indicates the energy storage in the medium during polarization. The imaginary part, *C″(ω)*, reflects the frictional loss due to interactions among dipoles under sinusoidal excitation. Therefore, the dielectric dissipation factor (*tanδ*), which represents the ratio of energy lost to energy stored within the dielectric medium, can be expressed as follows [1, 2, 16]:

$$\begin{aligned}\tan\delta(\omega) &= \frac{\left(\frac{\sigma_0}{\omega\varepsilon_0} + \chi''(\omega)\right)}{\left(\varepsilon_\infty + \chi'(\omega)\right)} \\ &= \frac{C''(\omega)}{C'(\omega)}\end{aligned} \tag{1.16}$$

It can be observed from equation (1.16) that the dielectric dissipation factor depends on the angular frequency (ω) of the applied sinusoidal excitation. Therefore, a pure sinusoidal excitation is applied to the insulation under test over a wide frequency range, typically from 1 mHz to 1 kHz, to analyze its dielectric behavior within this spectrum. This approach allows for the estimation of interactions among different dipolar groups [2]. By evaluating these interactions, the condition of the dry-type polymeric insulation can be predicted. Hence, the condition of the dry-type insulation is assessed by analyzing the corresponding *tanδ* profile obtained from FDS measurements.

1.8.3 Charge Trapping Measurement

In the process of condition assessment of dry-type insulation, it is evident that trapping and de-trapping processes play a crucial role in the conduction and space charge accumulation phenomena in solid dielectric materials. Consequently, over the past few decades, there has been increasing interest in investigating charge trapping behavior in polymeric insulating materials. Initially, space charge measurements in charged dielectric specimens were

conducted using destructive techniques, such as the dust figure method and the probe method [78, 88, 89]. Later, R.E. Collins introduced a non-destructive method for measuring space charge by perturbing the charges in a dielectric specimen with a thermal wave [90]. This method was subsequently refined, leading to the development of several non-invasive space charge measurement techniques. Among these techniques, the PEA and PWP methods are particularly notable [74-76]. These approaches have been utilized to investigate trapping behavior in polymeric materials. In such studies, a thin dielectric test sample is subjected to electrical stress and subsequently maintained in a short-circuit condition for a specified duration. By measuring the net charge at various time intervals during the voltage stressing and discharging phases, the collected data is used to model the trapping and de-trapping behavior of the dielectric material. In addition to space charge mapping techniques, methods such as surface potential decay, charging-discharging current, and others have also been utilized to study the trapping behavior of dielectrics.

1.8.3.1 Space Charge Distribution

In this section, a brief overview of various methods has been provided for extracting space charge distribution information in stressed dielectric materials.

- **Thermal Pulse and Step Method:** The thermal pulse method involves disturbing the specimen containing space charges using a thermal wave that penetrates the sample [90]. This disturbance creates an image charge in the electrodes, and as the thermal wave displaces the charge, it alters the values of the image charge, producing an electrical signal. By applying deconvolution techniques, the space charge distribution information can be deciphered from this electrical signal. A related technique is the thermal step method, which replaces the thermal pulse with a thermal step [78].

- **Laser Intensity Modulation Method (LIMM)**: In the LIMM technique, the metallized surfaces of a specimen are heated with a sinusoidally modulated laser beam, creating a temperature wave that diffuses through the sample [91]. This wave is attenuated and delayed during propagation, and its interaction with the space charges in the sample generates a pyroelectric current. From this current, space charge information can be extracted.

- **Optical Methods**: For optical methods, polarized light is passed through the transparent test object. The space charge distribution within the

material interacts with the optical wave, modifying its phase and other polarization properties [78]. By measuring these changes, information about the space charge distribution is obtained.

- **Pressure Wave Propagation (PWP) Method**: In the PWP method, a pressure wave is applied to perturb the space charge distribution. This pressure wave is generated using a piezoelectric crystal or laser shots. The wave disrupts the space charge distribution, producing an electrical signal in the electrodes, similar to the thermal pulse/step method [74]. Suitable signal deconvolution methods are then employed to extract information about the spatial distribution of the space charge.

- **Pulse Electro Acoustic (PEA) Method**: The PEA method involves applying a strong pulsating electrical field to a specimen containing space charges. The interaction between the externally applied electric field and the space charges produces a mechanical force, generating an acoustic wave detected by a piezoelectric transducer placed after the earth electrode [75, 76]. This transducer then produces a voltage signal from which space charge information can be extracted.

1.8.3.2 Surface Potential Decay

The isothermal surface potential decay (ISPD) method is a widely used technique for investigating trapping behavior in solid dielectrics. In this method, the dielectric specimen is charged through corona charging, during which ions accumulate on the surface of the specimen [78]. This ion accumulation leads to electron transfer on the surface to neutralize the ions, resulting in a gradual decrease in surface potential over time. This charge transfers process causes electron (or hole, depending on the charging polarity) trapping in the surface region. Theoretical models have been developed to link the energy distribution of traps with the surface potential decay. However, it is important to note that the potential decay is also influenced by dipolar polarization, neutralization through atmospheric ions, and conduction on the surface of the sample. These factors must be carefully considered before drawing conclusions about trapping behavior. Extensive research has been conducted on surface potential decay over the past few decades, but the results are not unanimous, indicating that further research is needed to improve this method.

1.8.3.3 Different others Methods

Iso-thermal relaxation currents or discharging currents have been utilized in early studies to understand trapping behavior of insulators and semiconductors [78, 92]. Similarly, charging and conduction currents have been analyzed to investigate charge trapping. However, progress in determining the trap energy distribution in a dielectric from these current measurements has been limited.

1.8.3.4 Limitations of Space Charge Measurement

Among all the methods discussed, the PEA and PWP techniques have significantly advanced our understanding of space charge behavior in dielectrics. Typically, to examine charge trapping and de-trapping processes, the sample is subjected to electrical stress and then held in a short-circuit condition for a specific duration. During this short-circuit phase, the total amount of charge stored in the sample is measured using these two techniques, allowing for the calculation of charge trapping parameters such as trapped charge, trap depth or energy, and trap distribution. However, both methods have comparable limitations. The measured signal does not directly reflect the space charge distribution in the sample. Therefore, transfer function analysis and deconvolution tools are applied to decipher the space charge distribution from the measured signal. Additionally, the measured signal is usually very low, necessitating proper de-noising for precise space charge estimation. While space charge measurement techniques have significantly advanced the study of charge trapping and de-trapping, the indirect nature of these measurements (via acoustic signals) presents challenges in the interpretation and analysis of the acquired data [78].
Another challenge associated with these measurement techniques is that they are mainly suited for thin dielectric samples with planar geometries. While the PEA method has been employed for space charge measurements in cables, its application to complex irregular insulation structures is very difficult [93]. For example, measuring space charge on an aged polymeric insulator used in transmission lines is particularly challenging. Thus, a direct approach for assessing charge trapping and de-trapping would be more advantageous for insulation diagnosis than indirect methods. One widely used direct technique for estimating charge trapping parameters is the Isothermal Surface Potential Decay method. In this method, the dielectric specimen is charged via corona discharge, and the surface potential decay of the sample is monitored over time. Parameters such as trap depth and trap density are derived from these surface potential decay measurements. However, this method is not directly applicable to electrical insulation systems that do not have planar geometries [78]. Setting up an experimental

arrangement for corona charging of insulation with a radial geometry, such as cables, is very challenging. For these reasons, a straightforward, low-complexity direct method suitable for investigating charge trapping in electrical insulations of various shapes or geometries would be extremely advantageous for engineers and industry people.

1.8.3.5 Importance of Charge Trapping Investigation

The exact mechanism of ageing in solid polymeric dielectrics is a topic of considerable discussion. However, it is widely accepted that trapped charges play a vital role in the accelerated ageing of polymeric materials. This section briefly discusses the knowledge gained over the last three decades on the fundamental principles of electrical ageing and the impact of trapped charges. The degradation of polymer dielectrics under thermal stress is traditionally explained through a thermodynamic approach, pioneered by Daikin [94]. According to this theory, the polymer is composed of chemical and morphological units called moieties that undergo local reactions. Ageing is considered to be dominated by a single reaction, involving an initial unaged state (i.e. state-1) and a final degraded state (i.e. state-2), each with associated Gibbs free energy (G_{FE1} and G_{FE2}, respectively). This reaction is partly reversible. Overall, Daikin's theory views ageing as a thermally controlled process. In [95], authors have described various chemical reactions related to ageing, most of which involve chain scission. The reaction rate is related to the energy difference (ΔG_{EF}) using the following equation (1.17) [78].

$$\tau_{aging} = \frac{kT}{h}\exp\left(-\frac{\Delta G_{EF}}{kT}\right) \tag{1.17}$$

$$\Delta G_{EF} = G_{EF2} - G_{EF1} \tag{1.18}$$

where τ_{ageing} is the reaction rate constant, G_{EF1} is the free energy of the unaged state, G_{EF2} is the free energy of the aged state, k is the Boltzmann's constant and h is the Planck's constant. The creation of the product state requires input energy (thermal or electrical), making ΔG_{EF} positive. As the ageing reaction is partly reversible, if a significant number of moieties convert from the unaged to the aged state, material degradation is triggered, limiting the insulation's lifetime. The fraction of polymer sites converted from the unaged to the aged state can be represented by the parameter B_{eq}, calculated as:

$$B_{eq} = \frac{c_{m2}}{c_{m1} + c_{m2}} \tag{1.19}$$

where c_{m1} and c_{m2} are the concentrations of unaged and aged moieties, respectively. This parameter B_{eq} is related to the energy difference ΔG_{EF} through the equation:

$$B_{eq} = \left(1 + \exp\left(\frac{\Delta G_{EF}}{kT}\right)\right)^{-1} \tag{1.20}$$

As B_{eq} increases with temperature, at a certain threshold temperature T_{th}, B_{eq} reaches a critical value (i.e. B^*_{eq}) indicating rapid degradation. This threshold temperature is related to B_{eq} through equation (1.21).

$$B_{eq}(T_{th}) = \left(1 + \exp\left(\frac{\Delta G_{EF}}{kT_{th}}\right)\right)^{-1} = B^*_{eq} \tag{1.21}$$

The effect of charge injection and extraction on tree initiation in XLPE cables was first discussed by Tanaka et al., who developed a model correlating tree inception time with applied electric stress [96]. In 1995, Dissado et al. introduced a new model incorporating the effect of trapped charges on insulation lifetime through thermodynamic modelling, which was further refined in subsequent years [97]. This model identified new parameters representing the electromechanical and electrostatic stresses associated with trapped charges.

When trapped charges are present in the insulation, they generate their own electric field, leading to mechanical stress, particularly in the region near the space charge (electrostriction effect). If a space charge Q occupies a spherical region of radius r_s with volume density ρ, the electromechanical energy W_{em} stored over a spherical region of radius r_s from the centre can be calculated using equation (1.22) [78].

$$W_{em} = \frac{3\beta_t^{\,2} q^4}{4480\pi^3 Y \varepsilon^4 r_s^5} \tag{1.22}$$

where β_t is the electrostriction coefficient and Y is Young's Modulus. This energy increases the ground state free energy per moiety by an amount A_pW_{em}, where A_p is a proportionality constant. If this mechanical stress leads to the scission of long polymer chains, the energy difference between the ground state and the reactant state decreases by a factor A_pW_{em}, given by [78]:

$$\Delta_m G_{EF} = \Delta G_{EF} - A_p W_{em} \tag{1.23}$$

As $\Delta_m G_{EF}$ decreases, the ageing reaction rate accelerates, and the threshold temperature T_{th} for ageing also decreases. Trapped charges thus simulate ageing reactions that would otherwise occur only at elevated temperatures, accelerating the thermal ageing process. Additionally, recombination of trapped charges of opposite polarity may release sufficient energy to damage the insulation, particularly in and around microscopic voids, where electromechanical stress can elongate void dimensions over time, ultimately leading to tree inception.

1.8.4 Insulation Resistance Measurement and Polarization Index (PI)

For Insulation Resistance (IR), the state of insulation is assessed by measuring the insulation resistance [98]. However, it is crucial to keep the temperature constant during this measurement, as variations in temperature can cause fluctuations in the insulation resistance. According to [16], a temperature increase of 10°C can reduce the IR value by half.

In the Polarization Index (PI) method, insulation resistance is measured at two different times—typically at 1 minute and 10 minutes—under a constant DC excitation voltage. The ratio of these measured resistance values is referred to as the PI value of the insulation [16, 98, 99]. By analyzing the PI value, one can assess the overall condition of the insulation. However, distinguishing between good and poor insulation based solely on PI values can be challenging if the insulation's charging current fluctuates [16]. Consequently, interpreting insulation condition using the PI method may occasionally yield inaccurate results.

1.9 Dielectric Response Function (DRF) of Dry-Type Insulation

Existing literature indicates that various environmental stresses degrade the insulating properties of the dry-type insulation, leading to changes in the dielectric material and altering the relaxation characteristics of different dipolar groups in the insulation [1, 16]. Consequently, during the polarization process, the dielectric response function *f(t)* in equation (1.24) is influenced by the different dipolar groups located in various regions of the polymeric insulation. The dielectric response function thus describes the fundamental memory properties of the insulating material [2, 16]. Research shows that the dielectric response function provides valuable information regarding the condition of the insulation [85]. By analysing this function, insights into the dielectric properties of the dry-type insulating medium can be obtained, which can then be used to assess the condition of the dry-type insulation. As a result, the modeling and analysis of the dielectric response function have become areas of significant interest for researchers. The literature also shows that the dielectric response function *f(t)* can be represented by a general response function [84]. The parametric form of this general response function is given by equation (1.24).

$$f(t) = \frac{A_r}{\left(\frac{t}{t_r}\right)^m + \left(\frac{t}{t_r}\right)^n} \tag{1.24}$$

where $A_r>0$, $m>n>0$, and $m>1$. In equation (1.24), t_r represents the effective relaxation time constant of the dielectric material. However, deriving the Fourier transform of the general response function is challenging, making it less commonly used for modeling the dielectric response function. As a result, different approaches are employed to model the dielectric response function. One such approach is using an empirical relaxation function known as the Kohlrausch-Williams-Watts (KWW) function [100]. It has been observed that the α and β relaxation processes in many dielectric materials conform to the KWW function [100]. These α and β processes can be fitted using the empirical formula given by equation (1.25).

$$f(t) = \exp\left[-\left(\frac{t}{\tau_{ar}} \right)^{b} \right] \tag{1.25}$$

where b is an adjustable parameter ($0<b<1$) and τ_{ar} is an apparent relaxation time. The difficulty with using the KWW function lies in the fact that its Fourier transform only exists when $b=0.5$ and $b=1$. This limitation is the main reason for the restricted use of the KWW function in modeling the dielectric response function of insulating materials. C.T. Moynihan et. al. addressed this issue by numerically fitting the empirical function with a weighted sum of single exponential decay functions, as shown in equation (1.26) [101].

$$f(t) = \sum_{g=1}^{n} A_g \exp\left(\frac{t}{\tau_g} \right) \tag{1.26}$$

where A_g is the amplitude of the exponential decay function representing the dielectric characteristics of dipole group g, and τ_g is the corresponding time constant. Due to the continuous decaying nature of equation (1.26), the dielectric response function $f(t)$ is absolutely integrable. Therefore, the dielectric characteristics of various dipoles in the dry-type insulation, can be used for modeling $f(t)$. This modeling approach not only provides computational flexibility but also describes the influence of dipoles on the dielectric response function. As seen in equation (1.11), the depolarization current of the insulation-dielectric has a linear relationship with $f(t)$. Hence, the depolarization current is used to model the dielectric response function $f(t)$ of dielectric media.

When a steady electric field is applied, dielectric material can both store and dissipate energy. Thus, the dielectric material can be described by its energy storage and dissipating elements [2]. It has been observed that exponential decay functions are used to characterize the dipoles in insulation material [2]. Consequently, various dipolar groups in the insulation can be represented by a series combination of energy dissipating (R_g) and storage (C_g) elements [2]. Literature indicates that the dielectric response function $f(t)$ in equation (1.26) can be modeled using several equivalent circuits that describe the dielectric characteristics of the dipolar groups [101]. Among these models, the X-Y model, the conventional Debye model (CDM), and the modified Debye model (MDM) are widely used [2, 16, 101].

1.10 Scope of the thesis

The objective of the work is to develop the condition assessment methodology of the dry-type insulation used in high voltage systems.

Chapter 2 of the thesis presents a new approach towards the development of a portable, integrated system that can perform PDC measurements of dry-type insulation both in the laboratory and on-site. It is to be mentioned here that the magnitude of the polarization and depolarization current of the dry-type insulation (i.e. solid dielectrics such as polymeric insulation) is quite low (in the range of sub-nA). In addition, the nature of the PDC of the dry-type insulation is faster decaying in nature than the conventional oil-paper insulation. Therefore, it is difficult to measure the PDC using conventional experimental setup. Hence, this chapter introduces a suitable data acquisition system to measure the PDC of the dry-type insulation. This developed data acquisition system also has the capability to measure the polarization current as low as in the range of pA with inherent noise immunity.

Chapter 3 discusses a practical methodology to estimate the charge trapping characteristics of the dry-type insulation based on polarization and depolarization current measurement. In addition, the relationship between thermal ageing and charge trapping properties of dry-type insulation (i.e. epoxy-based nano-composites) are also analysed. As dielectric materials age, its undergo extensive degradation, which significantly impacts space charge accumulation and charge trapping behavior, which are very useful parameters for evaluating insulation health in HVDC environments. This chapter introduces an enhanced model based on Isothermal Relaxation Current (IRC) to examine charge trapping behavior in pure epoxy and epoxy alumina (Al_2O_3) nanocomposites under various ageing conditions. A methodology using PDC measurements is proposed to identify the current component arising from dipolar relaxation within the measured total isothermal relaxation current, enabling a more precise assessment of trap distribution characteristics compared to traditional IRC measurements.

Chapter 4 introduces an advanced technique for accurately detecting the thermal ageing of the dry-type insulation using frequency domain spectroscopy (i.e. complex electric modulus). In this view, it is to be mentioned here that, the traditional methods of dielectric spectroscopy measurement are limited by electrode polarization and charge transport effects, particularly at high temperatures and low frequencies. Due to the

effect of these, the actual information of the insulation dielectric (i.e. different relaxation phenomenon of the dipoles) are not properly analysed in the lower frequency region. However, it is essential to realize the entire relaxation behaviour of the dipoles for accurate understanding of the insulation condition. To address these challenges, this chapter proposes the use of electric modulus (defined as the inverse of complex permittivity) with the help of Cole-Cole (C-C) model to quantitatively analyse the ageing behaviour of dry-type insulation (i.e. epoxy-alumina nanocomposites). Investigations revealed that the extracted parameters can be accurately used to sense the ageing condition of the insulation.

The described methodology in ***Chapter 4*** can provide distinct relaxation characteristics (i.e. particular relaxation frequency) of the dry-type insulation dielectrics. However, in case of polymeric insulation, the dielectric material has different dipolar groups depending upon the different polymeric chain length inside the material. Therefore, the relaxation characteristics of those different dipolar groups are also separate from each other which are not separately identified in the aforementioned method. Hence, for accurate condition estimation of the dry-type insulation it is utmost requirement to understand the distribution of those different dielectric relaxation phenomenon. In this context, ***Chapter 5*** introduces an advanced technique which can provide the relaxation frequency distribution of the different dipole groups from the analysis of the PDC. In addition, this method can identify the electrode polarization separately. Based on this method, the ageing state of dry type insulation (such as epoxy-alumina nano-composite and XLPE). The experimental investigation shows that the proposed method can effectively be applied for condition assessment of dry-type insulation used in real life high voltage equipment.

1.11 Originality of the Thesis

To the best of the author's knowledge, the following are the original contributions of this work:

i. Development of a data acquisition system for the measurement of the Polarization and Depolarization Current (PDC) of the dry-type insulation. This measurement of the PDC can suitably be utilized for the condition assessment of the dry-type insulation.

ii. A method has been proposed to estimate the charge trapping characteristics of the dry-type insulation based on the polarization and depolarization current measurement. Using the charge trapping parameters, the condition assessment as well as quality assessment of the dry-type insulation has been performed.

iii. A method has been proposed to estimate the ageing state of the dry-type insulation by identifying distinct relaxation characteristics based on frequency domain spectroscopy (i.e. electric modulus). It is to be mentioned here that, the proposed method has the ability to reveal the suitable relaxation characteristics by masking the effect of electrode polarization.

iv. A method has been proposed to estimate the ageing state of the dry-type insulation based on the relaxation frequency distribution enabling more accurate condition predictions.

Chapter 2

Development of PDC Measurement Experimental Setup for Dry-Type Insulation

2.1 Introduction

In the present time, many Time Domain Spectroscopy (TDS) measurement (like Polarization and Depolarization Current (PDC) measurement, Return Voltage Measurement (RVM)) and Frequency Domain Spectroscopy (FDS) measurement techniques have been frequently applied to diagnose the insulation system of any high voltage equipment [2, 16]. While TDS measurement techniques, such as PDC and RVM, are frequently used for oil-impregnated insulation, there is a need to explore these techniques for dry-type solid insulation due to different polarization mechanisms. Furthermore, PDC is preferred over RVM because it provides more detailed information about the insulation's condition, particularly for detecting moisture and ageing effects. In the case of oil-filed transformer insulation (i.e. oil-paper insulation), the polarization process is slow and may take several hours to complete the PDC measurement [2]. Several PDC measurement equipments are available for oil-filled transformer which applies a DC voltage external to the equipment under test, records the current in the range of microampere [1, 2]. However, the problem arises when the dielectric is solid (i.e. dry-type). In case of solid dielectrics (i.e. polymeric insulation) the polarization process are different from the polarization process of oil-paper insulation. In polymeric insulation, dipoles vary based on the polymer chain length, and these dipoles can be categorized into short polymeric chain (SPC) dipoles and long polymeric chain (LPC) dipoles. Similar type of dipoles (polymeric chain having similar length) create dipole group. There are different types dipolar groups are present inside the material. It is to be mentioned here that the polarization process of the different dipolar group are different from each other. Hence, when the DC voltage is applied across the insulation the smaller chain dipolar groups react very fast and according to their movement the polarization current starts to flow. The magnitude of the current is quite high (in the range of mA to sub-nA) and the duration is very short (in the range of few ms). These dipolar groups are aligned along the field direction very quickly. Result of that the contribution of the smaller chain dipolar groups ends with very short duration. However, the longer chain dipolar

groups start to move with application of DC electric field but their movement process are slow. Hence, the contribution of those bulky dipolar groups in the polarization process are also slow. This process may take few seconds to more than thousand seconds to complete the polarization process. Additionally, environmental noise can significantly affect the accuracy of data acquisition, making it challenging to distinguish the true PDC signal from noise. There is commercial unavailability of such instrument for the direct measurement of the PDC of the solid dielectrics. So, in this context, it is to be mentioned here that, the measurement of PDC for dry-type solid dielectrics is completely different and its data acquisition (DAQ) process is quite challenging as well. This chapter proposes a PDC measurement experimental setup and DAQ system for the condition assessment of dry-type solid insulation. The primary objective of the proposed scheme is to address the limitations of conventional measuring methods by employing innovative techniques to accurately capture the polarization process of solid dielectric materials, even in challenging noise conditions.
The developed setup has the capability of measuring the polarization and depolarization current of solid dielectrics with reasonable accuracy. The accuracy of the proposed setup is not dependent on the geometry of the sample. Also, this measurement technique is very simple and can be used for in-situ application. The developed set-up of the PDC measurement system is reliable, economical, and easy to operate and is inherently noise immune. The result obtained from this setup is verified with the well accepted conventional instruments.

2.2 Polarization Process of Dry-Type Insulation

The polarization current in dry-type insulation (such as polymeric insulation) is influenced by the nature of the dipoles, which in turn depends on the length of the polymer chains in the material. Depending on the polymeric chain length the dipoles are categorized into two types' i.e., short polymeric chain (SPC) dipole and long polymeric chain (LPC) dipole. It is important to note that the behaviors of these two types of dipoles, SPC and LPC, differ significantly under the influence of an electric field. When an electric field is applied, SPC dipoles rapidly align themselves in the direction of the field within a few milliseconds. In contrast, LPC dipoles, being bulkier, take a longer time—ranging from several seconds to thousands of seconds—to align in the direction of the electric field. Figure 2.1 illustrates the polarization process in dry-type insulation and the corresponding responses of different dipoles within the dielectric material. When there is no field the dipoles are

not organized (i.e. Case 0: at t < t_0 in Figure 2.1), they are present in their usual positions. After the application of a DC electric field, the polarization process starts, and SPC dipoles begin to orient. This orientation process is very fast (i.e. Case I: at $t = t_0$ to t_1, as shown in Figure 2.1). Therefore, the resulting current develops within the range of few mA to sub-nA and the current is decaying with very fast rate. After time t_1 the polarization of the SPC dipoles are near to complete and their contributions in the polarization process almost finish. Subsequently, LPC dipoles begin to slowly align along the electric field direction, as depicted in Case II of Figure 2.1. Therefore, due to the slower movement of the LPC dipoles, the polarization current continues to flow with lower magnitude (in the range of sub-nA to pA) with slower decaying rate. These LPC dipoles are almost completely oriented at time t_c (i.e. charging time). Hence, after time t_c, the polarization current has only component of the conduction current (i.e. Case III in Figure 2.1). Consequently, recording these rapidly decaying (or rising) currents, which have very low magnitudes, becomes challenging without the use of highly sophisticated data acquisition instruments.

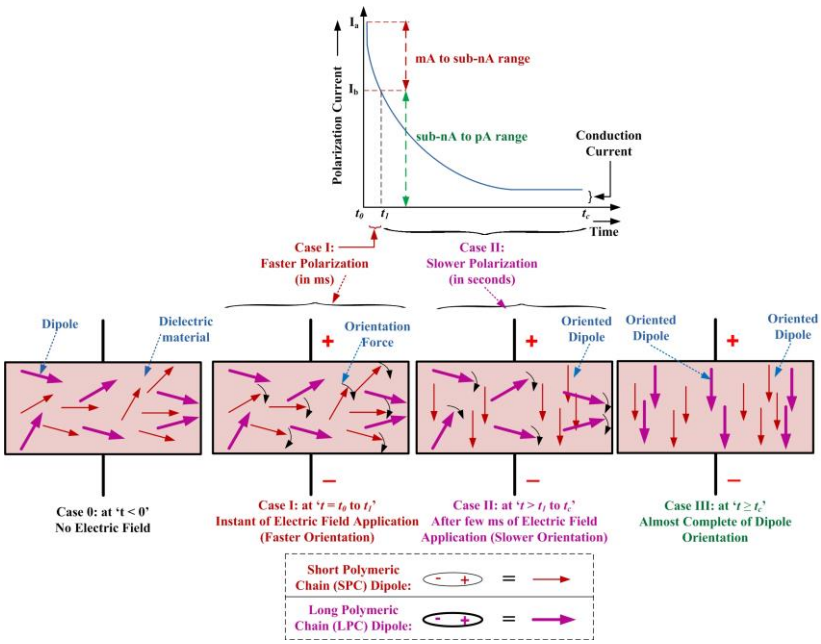

Figure 2.1 Schematic of polarization mechanism of solid dielectric with nature of the polarization current.

In case of conventional DAQ arrangement (ordinary mili-ampere or micro-ampere meter) for the PDC measurement of the dry-type insulation, it can measure the magnitude of the current in the range of mA to μA. In that range, the polarization current of the dry-type insulation is exponentially decaying in nature and it sustains for very short duration of time (few mili-seconds only i.e. Case I in Figure 2.1). Therefore, using this small duration polarization current, it is very difficult to assess the condition of the dry-type insulation. However, the major part of the current lies for longer duration (i.e. Case II in Figure 2.1) and is carrying the signature information of the test insulation is in the range of sub-nA to pA. In this context, it is yet to be mentioned that this low magnitude current may be suppressed by several environmental factors (such as temperature, noise etc.). Therefore, a proper DAQ system is required for the PDC measurement of the dry-type insulation.

2.3 Theory of Polarization and Depolarization Current (PDC)

A dielectric material becomes polarized when an electric field is applied across it, causing the positive and negative charges (dipoles) to shift relative to each other and align along the direction of the electric field. Under the influence of an applied electric field, the positive and negative charges, or dipoles, shift relative to one another and align with the electric field. This phenomenon is referred to as dielectric polarization. The relationship between the applied electric field ($E(t)$) and the resulting polarization ($\wp(t)$) in a dielectric material can be expressed mathematically as follows [2, 102]:

$$\wp(t) = \chi \varepsilon_0 E(t) \tag{2.1}$$

Here, ε_0 and χ are permittivity of the free space and susceptibility of the dielectric material, respectively. This susceptibility represents the all kinds of polarization taking place inside the dielectric materials. It can be inferred from (2.1) that the polarization $\wp(t)$ will vary by varying the electric field $E(t)$. Hence, it can also be said that any reduction in electric field magnitude will lead to the process of depolarization. If a charging voltage of $U(t)$ is applied two electrode having distance d, then the uniform electric field is developed across the electrodes can be written as,

$$E(t) = \frac{U(t)}{d} \tag{2.2}$$

In this context, according to the Gauss' law, the static charge density will appear on the surface of the electrode due to this electric field can be represented as,

$$Q_0(t) = \varepsilon_0 E(t) \tag{2.3}$$

When a dielectric material, characterized by its susceptibility (χ), is placed between two electrodes and subjected to an electric field, it becomes polarized, leading to an increase in surface charge density ($Q_1(t) = \wp(t)$). Finally, the total charge density ($Q(t)$) appearing at the electrode is the additive effect of the free space polarization and the polarization of the dielectric material. So, $Q(t)$ can be expressed as [102],

$$Q(t) = Q_0(t) + Q_1(t) \tag{2.4}$$

$$or, \qquad Q(t) = \varepsilon_0 E(t) + \wp(t) \tag{2.5}$$

$$or, \qquad Q(t) = \varepsilon_0 E(t) + \varepsilon_0 \chi E(t) \tag{2.6}$$

$$or, \qquad Q(t) = \varepsilon_0 (1+\chi) E(t) = \varepsilon_0 \varepsilon_r E(t) \tag{2.7}$$

Here, ε_r is the relative permittivity and it is also denoted as $(1+\chi)$. From (2.6), it can be understood that the response of the charge induced in free space occurs instantly and whereas the response form the dielectric material is delayed due to inertia. The total charge induced on the electrode surface can be represented by the dielectric displacement ($D(t)$), as given in equation (2.8).

$$D(t) = Q(t) = \varepsilon_0 E(t) + \wp(t) \tag{2.8}$$

Dielectric response can be defined mathematically using dielectric response function $f(t)$. This function $f(t)$ carrying the polarization property of the dielectric material. The time domain dielectric function can also be represented in the Laplace domain using the transfer function form. If the applied excitation is represented by delta function (i.e. $E\Delta t$) and the corresponding developed polarization ($\wp(t)$) can expressed with respect to $f(t)$ as [102],

$$f(t) = \left(\wp(t)\right) / \left(\varepsilon_0 E \Delta t\right) \tag{2.9}$$

$$or, \qquad \wp(t) = \left(\varepsilon_0 E \Delta t\right) f(t) \tag{2.10}$$

The properties of the dielectric response function, $f(t)$, which characterizes the material's polarization response, can be defined as follows [103]

i) Causality property: $f(t) \equiv 0$, for $t < 0$

ii) No permanent polarization property: $\underset{t\to\infty}{Lim}\left[f(t)\right] = 0$

iii) Integrality property: $\int_0^\infty \left[f(t)\right]dt = Finite$

iv) Superposition property: The total response resulting from individual excitations is obtained by summing all their contributions, thereby yielding the overall response caused by a sequence of elementary excitations.

Based on the properties of the dielectric response function *f(t)*, when the electric field *E(t)* is represented as a series of delta functions with strengths *E(t)dt*, the total response $\wp(t)$ can be determined by convolving the applied electric field with *f(t)* using the principle of superposition.

$$\wp(t) = \varepsilon_0 \int_0^t \left[f(\tau)E(t-\tau)\right]d\tau \tag{2.11}$$

For a step excitation $E(t)=E_0 \cdot u(t)$, where *u(t)* is the unit step function defined as 1 (*u(t)=1* for $t \geq 0$), the response can be formulated as:

$$\wp(t) = \left(\varepsilon_0 E_0\right)\int_0^t f(\tau)d\tau \tag{2.12}$$

From equation (2.8), the dielectric displacement can therefore be expressed as:

$$D(t) = \left[\varepsilon_0 E_0 u(t)\right] + \left[\left(\varepsilon_0 E_0\right)\int_0^t f(\tau)d\tau\right] \tag{2.13}$$

$$or, \qquad D(t) = \left[\varepsilon_0 E_0\right]\cdot\left[u(t) + \int_0^t f(\tau)d\tau\right] \tag{2.14}$$

When a steady electric field of magnitude E_0 is applied across a dielectric material with non-zero DC conductivity (σ_0), it results in a total current density *J(t)*, which includes both conduction and displacement currents. Therefore, the current density can be expressed as [102]:

$$J(t) = \left[\sigma_0 E_0\right] + \left[\frac{dD(t)}{dt}\right] \tag{2.15}$$

$$or, \qquad J(t) = [\varepsilon_0 E_0] \cdot \left[\varepsilon_\infty \delta(t) + f(t) + \frac{\sigma_0}{\varepsilon_0} \right] \tag{2.16}$$

The geometric capacitance C_0 of a test object can be described using the cross-sectional area A and the distance d between the electrodes as:

$$C_0 = (\varepsilon_0 A)/d \tag{2.17}$$

$$or, \qquad \varepsilon_0 = (C_0 d)/A, \; => (\varepsilon_0 E_0) = \{(C_0 d)/A\} \cdot \{U_0/d\} = (C_0 U_0)/A \tag{2.18}$$

Where U_0 represents the magnitude of the applied step voltage. By combining equations (2.16) and (2.18), the resulting current within the dielectric material can be formulated as:

$$i(t) = [J(t) \times A] = [A \times \varepsilon_0 E_0] \cdot \left[\varepsilon_\infty \delta(t) + f(t) + \frac{\sigma_0}{\varepsilon_0} \right] \tag{2.19}$$

$$or, \; i(t) = [C_0 U_0] \cdot \left[\varepsilon_\infty \delta(t) + f(t) + \frac{\sigma_0}{\varepsilon_0} \right] \tag{2.20}$$

The term $\delta(t)$ pertains to the current resulting from the instantaneous response of the free space charge in the dielectric material. The function $f(t)$ represents the component attributable to the polarization properties of the dielectric material, while σ_0 denotes the DC conductivity of the dielectric material. After the material has been charged for a sufficiently long period, the impact of the free space charge will diminish to zero. In this state, the polarization or charging current can be described using equation (2.20) as follows [1, 2]:

$$i_p(t) = [C_0 U_0] \cdot \left[f(t) + \frac{\sigma_0}{\varepsilon_0} \right] \tag{2.21}$$

After a charging voltage is applied for a sufficient duration, it can be assumed that the dielectric polarization has reached a steady state. At this point, when the voltage source is quickly turned off and the material is grounded, the oriented dipoles begin to return to their relaxed positions, resulting in the flow of depolarization current. After a total charging period of t_c when the unit step voltage U_0 has been removed, and the dielectric material is short-circuited to ground, the principle of superposition can be applied to write the depolarization current as [102]:

$$i_d(t) = [i_1(t + t_c)] + [i_2(t)] \tag{2.22}$$

Here, t represents the time measured from the moment when U_0 is removed. i_1 denotes the current resulting from the positive step voltage U_0, and i_2 signifies the current due to the negative step voltage which begins at t_c. By combining equations (2.21) and (2.22), the depolarization current can be expressed as:

$$i_d(t) = [C_0 U_0] \cdot \left[f(t + t_c) + \frac{\sigma_0}{\varepsilon_0} \right] - [C_0 U_0] \cdot \left[f(t) + \frac{\sigma_0}{\varepsilon_0} \right] \tag{2.23}$$

$$or, \quad i_d(t) = [C_0 U_0] \cdot [f(t + t_c) - f(t)] \tag{2.24}$$

It is important to note that the dielectric response function $f(t)$ decreases monotonically. Therefore, for sufficiently large values of the charging time t_c, $f(t)$ can be assumed to have diminished to an insignificantly small value, $f(t+t_c) \approx 0$ as t_c approaches infinity (i.e. $t_c \rightarrow \infty$). Therefore, the depolarization current from equation (2.24) can be written as:

$$i_d(t) \approx -[C_0 U_0] \cdot [f(t)] \tag{2.25}$$

Therefore, the dielectric response function can be accurately modeled using the experimentally obtained depolarization current data as follows:

$$f(t) \approx -\left[\frac{i_d(t)}{C_0 U_0} \right] \tag{2.26}$$

Figure 2.2 illustrates the typical behavior of polarization and depolarization currents when a step DC voltage of magnitude U_0 is applied across the insulation for the duration $t_0 \leq t \leq t_c$ [2]. After this period, the voltage is switched off and the insulation is grounded.

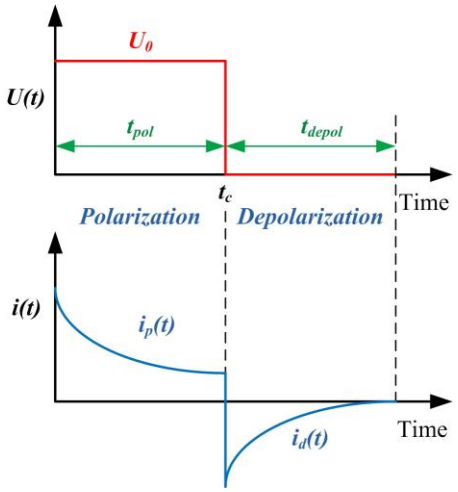

Figure 2.2 Nature of polarization and depolarization current under dc field excitation of *U(t)*.

2.4 Conventional PDC Measurement Suitable for Oil-Paper Insulation

In the context of oil-paper insulation, conventional PDC measurement techniques provide valuable diagnostic insights by measuring the polarization and depolarization currents. When a complex insulation system, such as oil-paper insulation in a transformer, is subjected to a steady applied voltage for polarization and depolarization current (PDC) measurement, various dipole groups within the insulation system align with the direction of the applied electric field. This alignment initiates the flow of polarization current, denoted as $i_p(t)$, through the insulating material [2]. Once the dipoles are oriented along the applied field, the polarization process is complete, and the resulting conduction current depends on the DC resistance of the insulation sample. During polarization, energy is stored within the insulation, which dissipates when the insulation terminals are short-circuited to ground, resulting in the flow of depolarization current. Upon removal of the excitation voltage, the insulation sample is short-circuited to ground to measure the depolarization current $i_d(t)$ as the dipoles return to their original positions, releasing the stored energy in the form of current flowing in the opposite direction. Figure 2.3 illustrates the experimental setup for the

conventional PDC measurement, which is appropriate for oil-paper insulation [2, 16]. During condition monitoring, a high DC voltage is applied to the insulation structure, and the resulting charging current through the dielectric, known as polarization current ($i_p(t)$), is recorded. In the next step, the DC voltage is removed, and the insulation sample is short-circuited, generating a discharge current flowing in the opposite direction, termed as depolarization current.

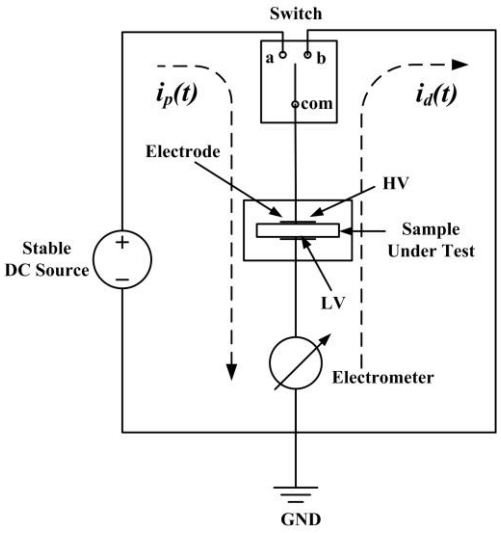

Figure 2.3 Schematic of the experimental setup for conventional PDC measurement.

The technique for measuring polarization and depolarization currents can be processed using two switches *i.e.* 'a' and 'b', as shown in Figure 2.3. The insulation sample is subjected to a high DC voltage U_0. To measure the polarization current, switch 'a' is closed while 'b' remains open for the duration t_c, during which the excitation voltage is applied. During this period, a polarization current in the nano-ampere range flows through the dielectric, denoted as $i_p(t)$, and is measured by an electrometer connected to the circuit. After t_c, the DC excitation is disconnected, 'b' is closed, and 'a' is opened. The stored energy in the insulation dissipates through 'b', and the depolarization current flowing in the opposite direction to the polarization current is recorded by the electrometer, denoted as $i_d(t)$ as shown in Figure 2.3. An electrometer configured as an ammeter is used to measure the current, automatically ranging based on the current input. A contactor connected in

parallel to the insulation sample supplies a high DC voltage (up to 1 kV DC) when turned on. The meter records the current versus time data for the charging or polarization current. The meter records the current vs. time data for the charging or polarization current. When the contactor is turned off after a specified time, the high voltage (HV) and low voltage (LV) terminals are grounded, allowing the meter to measure the discharging or depolarization current ($i_d(t)$). The measurement time for both polarization and depolarization current data varies from a few minutes to several hours, depending on the insulation condition and system requirements.

2.5 Limitations of the Conventional Setup

While conventional setups are effective for oil-paper insulation, they face several challenges when applied to solid dielectrics due to their unique properties. The PDC measurement of solid dielectrics is complicated due to the lower conductivity of the material under the influence of an electric field. The measured range of the current is in the pA range, whereas for conventional oil-paper insulation, this current is significantly higher, in the range of µA. As mentioned in the introduction, there are two primary challenges encountered during PDC measurement: identifying the actual PDC signal from the noisy background and manageing the system time constant. The polarization and depolarization process is very fast in solid dielectrics. Due to very low capacitance values (typically around 50 pF), the polarization and depolarization time constant is extremely short, on the order of nanoseconds. This necessitates the use of expensive data acquisition instruments capable of capturing such rapid events. To address this issue, a high-value resistor is connected in series with the sample to increase the overall time constant to a few seconds. This modification allows even a low-cost ADC with a sampling rate in the millisecond range to capture the current waveform with finer details. The detailed explanation for this approach is provided in Section 2.6.

2.6 Description of the Developed Experimental Setup

To address the limitations discussed in Section 2.5, a new experimental setup has been developed specifically for dry-type solid dielectrics. The schematic of the developed experimental process for PDC measurement is shown in Figure 2.4. The schematic of the experimental setup to acquire the polarization and depolarization current of solid dielectrics is presented in Figure 2.5. The photograph of the data acquisition module, resistance box,

and complete experimental setup is shown in Figure 2.6(a-c), respectively. A high voltage adjustable DC source, ranging from 200V to 10,000V at 1mA, has been used for this setup. A resistor R_{se} is connected in series with the sample under test. The theory behind incorporating this series resistor to increase the overall time constant (in the order of seconds) is explained in the previous section. The resistor also serves to limit the current, protecting the sample in the case of breakdown during testing. R_{se} is in the range of 1 GΩ to 10 GΩ, depending on the test insulation sample's properties, such as its insulation resistance, size, and material. The value R_{se} of the in GΩ range matches the high impedance of insulating materials to minimize loading effects and measurement errors. The test sample is placed between R_{se} and a measuring shunt resistance R_{sh}.The value of R_{sh} is in the range of 1kΩ to 10GΩ depending on the range of polarization and depolarization current of the dielectric material. A femtoampere electrometer (i.e. unity-gain non-inverting mode OP AMP such as ADA 4530 or equivalent) is used in the input stage as a buffer, in conjunction with a low-pass filter having cut off frequency 0.5 Hz to eliminate the influence of ambient noise [104]. It is yet to be mentioned here that the output voltage has been measured across the shunt resistance (R_{sh}) an ordinary digital storage oscilloscope (DSO). Thereafter, the measured output voltage is divided by the shunt resistance value to convert it into current. For embedded systems, the data can be recorded in local memory through an ADC to increase the system's portability.

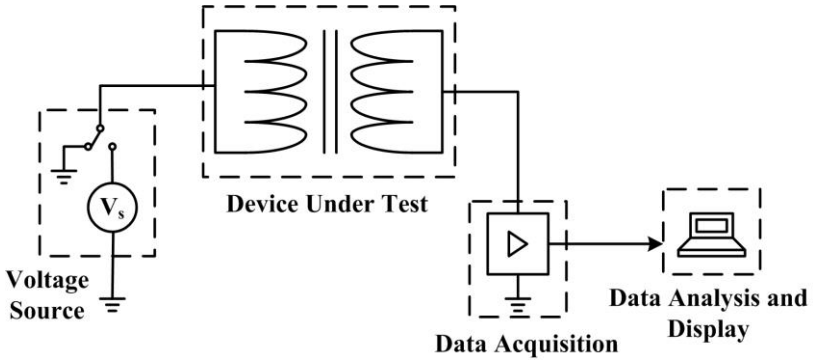

Figure 2.4 Schematic of the developed experimental process for PDC measurement.

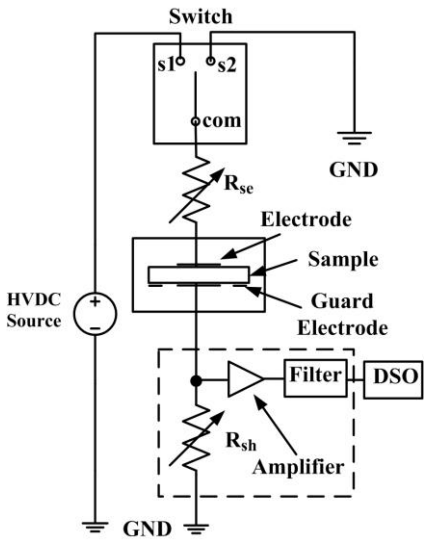

Figure 2.5 Schematic of the experimental setup for PDC measurement of solid dielectrics.

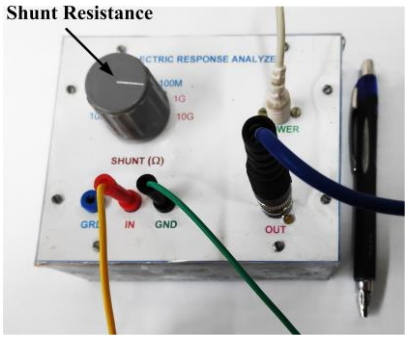

(a)

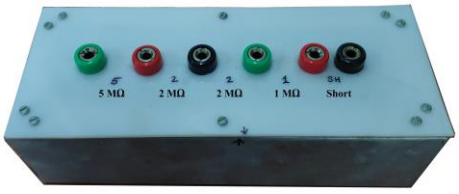

(b)

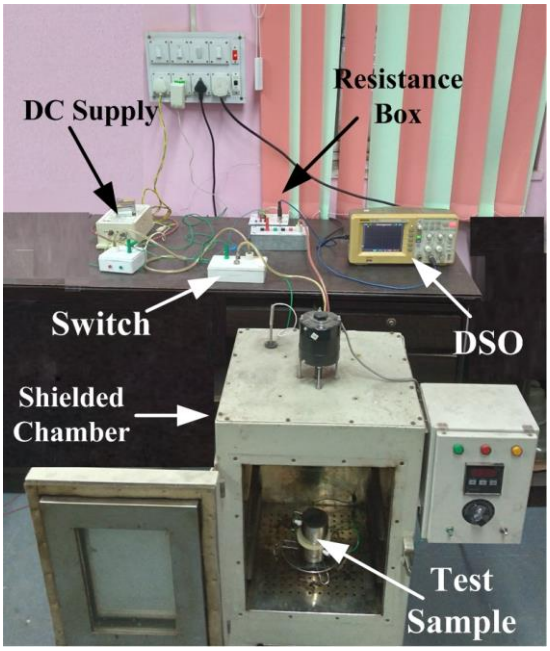

(c)

Figure 2.6 Photograph of the (a) data acquisition module, (b) series resistance box, and (c) complete experimental setup.

2.7 Experimental Procedure

Step-1: During the charging period the switch is in position 's1' in the schematic as shown in Figure 2.5. High voltage is applied to the sample, polarization current flows, and the nature of current is recorded in DSO. After sufficient time, the polarization current reaches a steady value. After recording the steady-state polarization current, the procedure then moves to the depolarization phase.

Step-2: The depolarization process starts when the switch is moved to position 's2'. The sample is short-circuited, and consequently, depolarization current begins to flow. This current is also recorded by the DSO. The photograph of the experimental setup, including all components, is shown in Figure 2.6(c).

2.8 Experimental Results

This comparison with conventional methods demonstrates the accuracy and reliability of the developed setup for measuring polarization and depolarization currents. In this work, LDPE (Low-Density Polyethylene) and XLPE (Cross-Linked Polyethylene) have been used as test samples to verify the performance of the developed setup. Five identical samples (each having dimensions of 10 cm × 10 cm × 1 mm) of LDPE and XLPE were collected from the local utility for experimental measurements. In this experimentation, LDPE test samples were used to study the effect of ageing through PDC measurement. Additionally, XLPE test samples were utilized to study the temperature effect on the PDC measurement process. LDPE test samples were subjected to thermal ageing at 100℃ for 800 hours. At every 100-hour interval, the samples were removed from the ageing chamber, cooled down to room temperature (25-32℃) for 24 hours, and then PDC measurements were performed. Similarly, XLPE test samples were placed in a controlled heat chamber (with a precision of 0.5℃) at different temperatures (30, 40, 50, 60℃) for at least four hours before PDC measurements were conducted.

Initially, the polarization current was measured for the unaged LDPE insulation. The same polarization current was also measured using a conventional complex experimental setup with an electrometer. For comparison and validation, the measured polarization and depolarization current for unaged LDPE samples using the developed DAQ module and an electrometer are shown in Figure 2.7. It is observed from Figure 2.7 that the developed DAQ module closely measures the polarization and depolarization currents for unaged LDPE samples at room temperature. It is also found that the deviation between the two methods is within 2%, validating the performance of the proposed experimental setup. Therefore, the developed DAQ module has been used for the PDC measurement of different dry-type test insulation samples.

To investigate the ageing characteristics of LDPE insulation, PDC measurements of aged LDPE samples were conducted under a 2 kV/mm DC field stress using the developed experimental setup at room temperature. The polarization currents of differently aged (unaged, 200, 400, 600, and 800 hours aged having capacitance values of 58, 56, 53, 49, and 45 pF, respectively) LDPE insulation are shown in Figure 2.8. The corresponding depolarization currents for the same set of samples are shown in Figure 2.9. It is yet to be mentioned here that during these measurements the shunt resistance value was chosen as 1 GΩ. It is evident from Figure 2.8 that the magnitude of the polarization current gradually increases with ageing

duration. This indicates that the conduction current, which is part of the polarization current measurement, gradually increases with ageing duration, providing useful information for investigating ageing characteristics. Similarly, it is observed from Figure 2.9 that the depolarization current gradually decreases with increasing ageing duration. Figure 2.9 also shows that the developed DAQ module can sense current magnitudes as low as a few hundred pA, demonstrating that the device is capable of measuring very low current magnitudes with reasonable sensitivity.

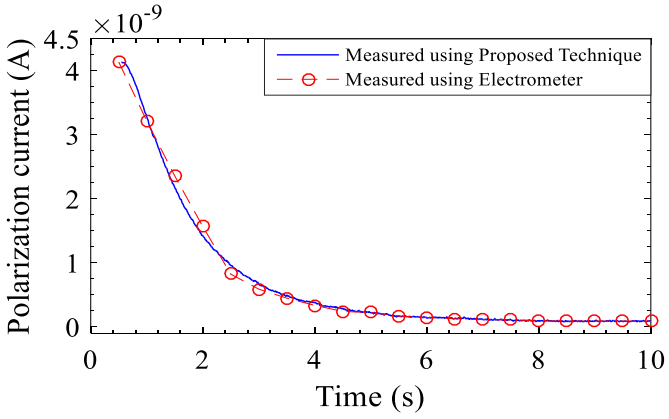

(a)

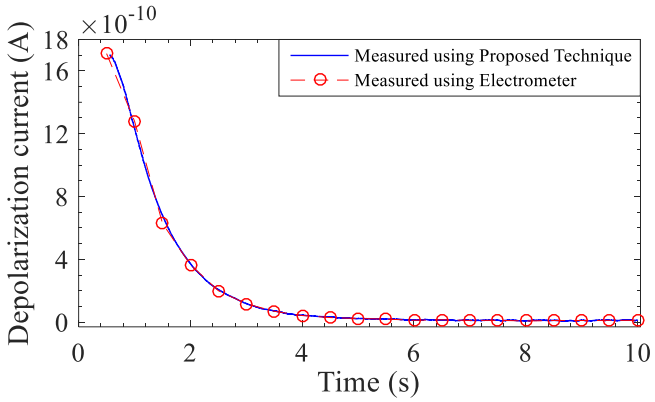

(b)

Figure 2.7 Comparison of PDC measurement using proposed technique and using electrometer: (a) polarization current, and (b) depolarization current.

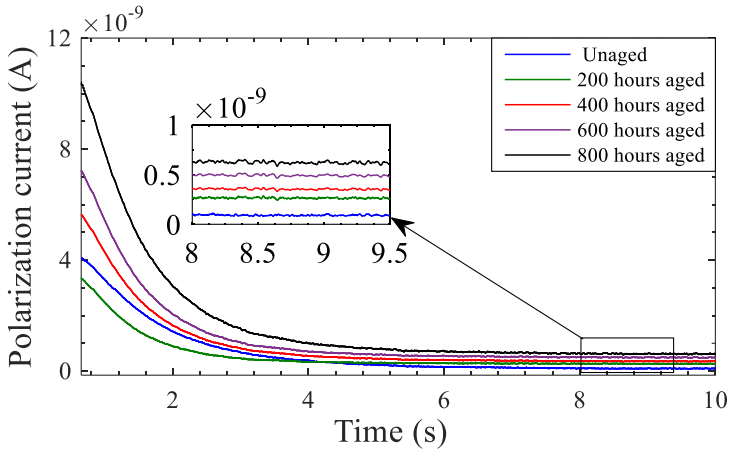

Figure 2.8 Polarization current of LDPE samples with different ageing condition.

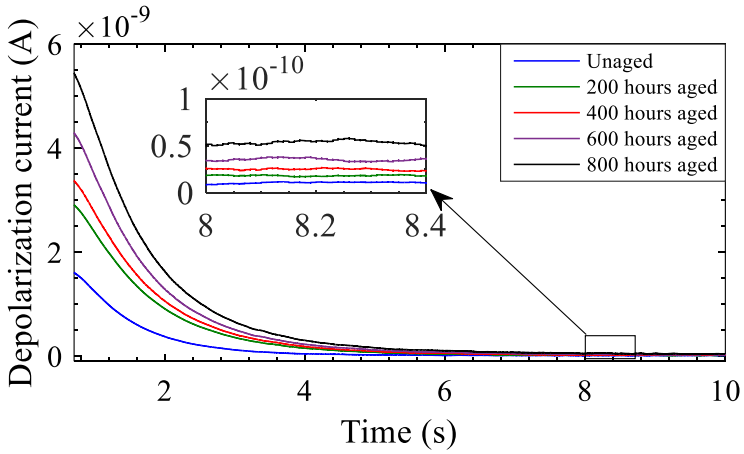

Figure 2.9 Depolarization current of LDPE samples with different ageing condition.

For studying the temperature effect on polarization and depolarization currents, PDC measurements were performed on XLPE samples using the developed experimental setup at different temperatures (30, 40, 50, 60℃). Figure 2.10 shows the polarization currents of XLPE samples maintained at different temperatures using a controlled chamber. The corresponding

depolarization currents are shown in Figure 2.11. It has been observed from Figure 2.10 that polarization current waveforms at different temperatures show the usual characteristics of insulating material, i.e., the polarization current is higher at higher temperatures than at lower temperatures. A similar observation can be made from Figure 2.11, where the magnitude of the depolarization current is even lower. These results indicate the potential of the developed instrument for on-site testing of dry-type insulation of high voltage equipment. From an experimental standpoint, it is important to note that the developed setup is capable of measuring variations in current as low as 100 pA with reasonable sensitivity.

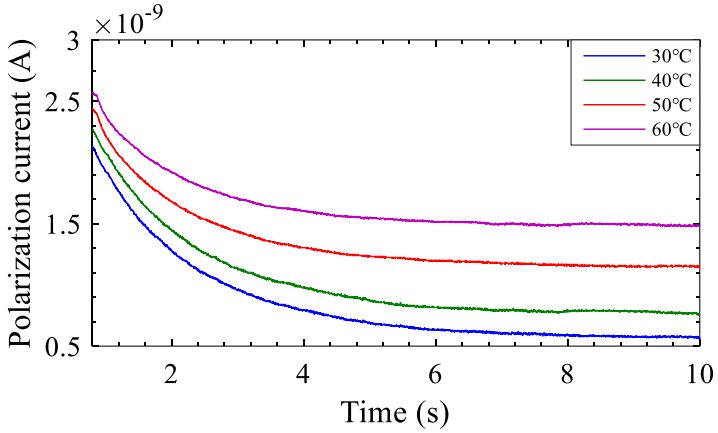

Figure 2.10 Polarization current of XLPE insulation samples at different temperatures.

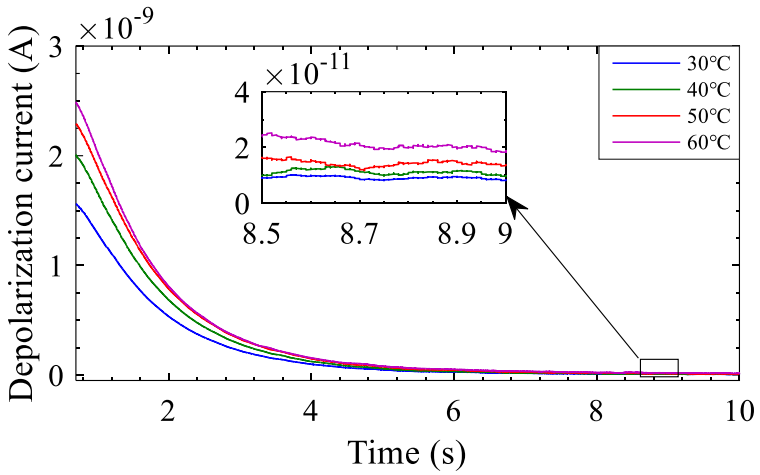

Figure 2.11 Depolarization current of XLPE insulation samples at different temperatures.

2.9 Conclusions

This chapter proposes an advanced Polarization and Depolarization Current (PDC) measurement technique suitable for the condition assessment of dry-type insulation. The time-domain spectroscopy-based diagnostic method developed in this study is specifically utilized to assess the severity of thermal ageing in LDPE material. Additionally, the effect of temperature on XLPE insulation is also investigated using the proposed PDC measurement experimental setup.

From the results presented in this chapter, several key conclusions can be drawn:

i) The polarization current measured with the developed setup shows a close agreement with the polarization current obtained using conventional methods under the same ambient conditions. This indicates that the new setup is reliable for accurately replicating standard measurement results.

ii) The developed setup is capable of detecting very small changes in polarization and depolarization currents, in the range of a few picoamperes (pA). This level of sensitivity is crucial for identifying subtle changes in insulation conditions that could indicate early stages of deterioration.

iii) The ability to measure such low currents with reasonable accuracy demonstrates the potential of this setup for use in practical condition monitoring and diagnostics of dry-type insulation systems. The results suggest that this technique can be applied for on-site testing of high

voltage equipment, providing a more efficient and economical alternative to existing methods.

Overall, these findings suggest that the proposed PDC measurement technique is a viable and effective tool for the condition assessment of dry-type insulation. The developed setup not only offers a reliable and sensitive measurement approach but also addresses several limitations of conventional PDC measurement methods, such as dealing with lower conductivity and noise issues in solid dielectrics. Therefore, it holds promise for broader applications in power system diagnostics and monitoring.

Chapter 3

Condition Assessment of Dry-Type Insulation Based on Charge Trapping Phenomenon

3.1 Introduction

In the ***Chapter 2***, an experimental setup has been developed to measure the Polarization and Depolarization Current (PDC) of dry-type insulation (i.e., polymeric insulation). PDC measurement is a non-invasive technique that can reveal important information such as conduction current, polarization current, and charge injection. Over the past two decades, nanocomposite-based polymeric materials have shown great potential for power engineering applications due to their improved electrical and non-electrical properties. This is because the addition of nanoparticles has significantly improved both the electrical and non-electrical properties of polymeric dielectrics [105-106]. A major challenge in using polymeric dry-type insulation in High Voltage Direct Current (HVDC) applications is the accumulation of space charge. Space charge buildup leads to localized overstress, insulation degradation, and potentially premature failure. Nanocomposites, however, exhibit less space charge accumulation compared to the base material [107-108]. Therefore, understanding space charge behavior (i.e., charge trapping characteristics) is crucial for assessing the condition of dry-type nanocomposite insulation. This chapter aims to investigate the charge trapping characteristics through PDC measurement.

The accumulation of space charge in a dielectric is mainly attributed to the presence of 'inhomogeneous regions' or traps which capture charges [109]. The duration for which the trapped charge will be confined in the trap is dependent on trap depth or trap-energy. Therefore, the energy distribution of traps has an overwhelming influence on the charge transport, charge accumulation and dielectric breakdown processes of a polymeric dielectric [110]. It may be inferred from the above discussion that the improvement in dielectric properties of nanocomposites is related to the alteration in trap distribution brought about by the addition of nanofillers. Compared to other dielectric properties of nano-composites, there is considerably less information on exactly how nano-fillers affect the trap distribution. It is noteworthy, that the nano-composite would experience service ageing during

practical application. With ageing, the trap distribution will also change. The change in trap distribution of a nano-composite will be in close relation with the percentage addition of nano-filler and extent of ageing. Therefore, the characterization of traps in a nano-composite in the presence of ageing may offer useful insight into understanding the charge dynamics of a nano-composite. This study attempts to enhance the understanding of the effect of nanofiller addition on trap distribution in polymeric dielectrics under ageing conditions. The base- material under study is epoxy resin, a widely used dry-type dielectric material, and the nano filler used is Alumina (Al_2O_3). It was selected because epoxy-alumina nano-composites have depicted significantly improved dielectric properties [32, 35, 38] i.e. higher breakdown strength, resistance to partial discharge, electro-thermal ageing, electrical treeing etc., and holds great promise for high voltage insulation applications.

In existing literature, several investigations have been performed to understand the space charge behavior in epoxy nano-composites with different filler materials [32, 39, 111-114]. Space charge behaviour of epoxy-MgO nano-composites were investigated in [112]. The effect of temperature gradient on epoxy-SiO_2 nano-composites have been studied in [113]. Pandey *et al.* studied the accumulation of space charge in epoxy-Al_2O_3 nano-composites in [114]. D. Saha *et.al*, investigated the behavior and properties of space charge in epoxy-hBn (hexagonal boron nitrade) nano-composites [115]. The effect of gamma radiation on space charge accumulation in epoxy-micro and nano-composites were studied in [116]. Similarly, Space characteristics of epoxy-graphene oxide nanocomposite were discussed in [117]. However, very few have investigated the charge trapping characteristics of the epoxy-alumina nano-composites.

The method employed for obtaining trap distribution is Isothermal Relaxation Current (IRC) [118-119] measurements with certain modifications in the analysis methodology. This modification is the inclusion of Polarization-Depolarization Current (PDC) measurements in IRC model. In the conventional IRC model, the relaxation current is attributed solely to the de-trapping of previously trapped charge carriers. This assumption holds true only for non-polar dielectrics. However, in polar dielectrics such as epoxy and epoxy-based nanocomposites, the relaxation current is influenced not only by charge de-trapping but also by the relaxation of dipoles. From PDC measurements, the contribution of dipoles in the relaxation current can be estimated and suitable corrections may be performed on the trap distribution analysis. The PDC measurements will also give information regarding ascertain the effect of nano-fillers on DC conductivity and dipolar

polarization process. Additionally, Frequency Domain Spectroscopy (FDS) measurements have also been performed on the nano-composites.

3.2 Theory

3.2.1 Basic Theory of Isothermal Relaxation Current

As discussed in Section 1.8, when a dielectric is placed under the application of an electric field (U_0), the dipoles begin to orient along the applied electric field, initiating the polarization process. The polarization current ($i_p(t)$) can be expressed as shown in equation (3.1) [1, 2].

$$i_p(t) = C_0 U_0 \left(\frac{\sigma}{\varepsilon_0} + \varepsilon_\infty \delta(t) + f(t) \right) \tag{3.1}$$

Here, σ, ε_0, ε_∞, $\delta(t)$, $f(t)$ and C_0 are the dc conductivity, permittivity of the free space, relative permittivity (at high frequency), impulse function, polarization function, and geometric capacitance of the dielectric, respectively. When the polarization current reaches to steady value at $t=t_c$, the applied d.c. field is removed and depolarization current ($i_d(t)$) flows through the shorted path,

$$i_d(t) = -C_0 U_0 f(t) \tag{3.2}$$

If the ambient temperature of the measurement condition remains the same, then the depolarization current is also known as the isothermal relaxation current (IRC).

3.2.2 Theory of Charge Trapping and De-trapping

In IRC measurements, the dielectric is stressed under a high voltage DC field for a sufficient time, and subsequently, it is discharged. During discharging, charges released from the traps produce a discharging current, which is measured. The process of releasing a trapped carrier is known as 'detrapping'. The trapped carrier can obtain the energy necessary to de-trap through various means, i.e., thermal collisions with the crystal structure, photon bombardment, impact ionization, etc. If the re-trapping of the released carriers is neglected, the rate of release of charge carriers within a trap depth range *dE* can be expressed as [120]

$$\delta n_t^{'} = f_0(E)N(E)e_n \exp\left(-\int_0^t e_n dt\right)dE \tag{3.3}$$

Where $n_t^{'}$ denotes the rate of release (de-trapping) of charge carriers, $f_0(E)$ represents the electrons' initial occupancy, and $N(E)$ indicates the energy distribution of traps across the energy gap. Additionally, e_n signifies the probability of an electron de-trapping per unit time from a trap level to energy E. The probability of de-trapping an electron from a trap level to energy E can be represented as follows:

$$e_n = \upsilon \exp\left(-\frac{E_t}{kT}\right) \tag{3.4}$$

Where υ, E_t, k and T are indicating the attempt to escape frequency, the trap depth, Boltzmann's constant and temperature, respectively.
If the contributions from all traps situated between the conduction band and the valence band are aggregated, then the equation (3.3) can be rewritten as

$$n_t^{'} = \int_{E_V}^{E_C} f_0(E)N(E)e_n(E,T)\exp\left(-\int_0^t e_n dt\right)dE \tag{3.5}$$

As all the de-trapped charge carriers are extracted from the dielectric, they generate a current in the circuit via the external electrodes. This current, $I_{de\text{-}trap}(t)$ is directly related to the trap distribution according to the following equation: [118-119]:

$$I_{de-trap}(t)t = \frac{qlkt}{2} N_t(E)\, f_0(E) \tag{3.6}$$

where q and l are denoting the electronic charge and electron injection depth, respectively. The current per unit electrode area can be readily calculated by dividing the total measured current by the electrode's surface area.

From the time (t_n) when a specific quantity of charge is extracted, the trap depth (E_{tn}) for that corresponding time can be calculated from the following equation:

$$E_{tn} = kT\ln(\upsilon t_n) \tag{3.7}$$

The trap density (N_t) at the trap depth E_t can be evaluated from

$$N_t = \frac{2I_{de-trap}(t)t}{qlkTf_0(E)} \tag{3.8}$$

Using equation (3.7) and equation (3.8), the trap density (N_t) at trap depth E_t can be calculated easily. In this present work, the values of υ and f_0 have been adopted as 6.2×10^{12} and 1/2, respectively [118].

3.2.3 Estimation of De-trapping Current

If the dielectric specimens under test are polar compound then, the relaxation current can be expressed as

$$I_r(t) = I_{de-trap}(t) + I_{dipol}(t) \tag{3.9}$$

where $I_r(t)$ is the total relaxation current, $I_{de\text{-}trap}(t)$ is the current due to de-trapping and $I_{dipol}(t)$ is the current due to dipolar relaxation. The current due to dipolar relaxation may be given as follows [1-2],

$$I_{dipol}(t) = C_0 U_0 f(t) \tag{3.10}$$

where, C_0 is the geometric capacitance, U_0 is the applied voltage and $f(t)$ is the dielectric response function. Under the assumption that $f(t)$ is independent of external excitation, the dipolar relaxation current at an excitation U_f can be given as,

$$I_{df}(t) = I_{dipol}(t) \times \frac{U_f}{U_0} \tag{3.11}$$

The process for separating the dipolar relaxation current from the de-trapping current is outlined in the following steps.

(i) At first PDC measurements are performed at electric fields of 1 *kV/mm*. At such low electric fields, there is no charge injection. Therefore, the measured depolarization current is due to dipolar relaxation only.

(ii) Now, the dielectric is stressed at a much higher voltage for sufficient and then it is discharged. The current due to dipolar relaxation is estimated using equation (3.11). Now using equation (3.10), the de-trapping current is separated.

3.2.4 Estimation of Trapping Parameters

The trap density at different trap depth is calculated from the de-trapping current using equation (3.7) and (3.8).

3.3 Experimental Arrangement

3.3.1 Preparation of Test Samples

The preparation of epoxy nanocomposite samples involved multiple steps. Initially, the base material epoxy resin (Bisphenol-A (CY1300), manufactured by Huntsman, density: 1.16 g/cm^3) and hardener (Triethyl Tetramine (TETA-HY956), manufactured by Huntsman, density: 1.02 g/cm^3) were heated at 40° C for 2 hours and degassed to remove the moisture and trapped air bubbles [35-36, 38, 121]. Similarly, Alumina nano-powder (Al_2O_3, APS: 65 nm, Make: Sigma-Aldrich, density: 4g/cm^3) was dried at 150° C for 24 hours before preparation of samples [38, 121]. The process of mixing was consisted of three stages which are mentioned below.

***Stage 1*:** The powdered nanoparticle (alumina) was mixed with epoxy resin. In this stage, the nano-particles was mixed with epoxy resin using a high-shear mechanical mixer at 750 r.p.m. speed for 1 hour followed by degassing and ultrasonic agitation at 24 kHz for 1 hour.

***Stage 2*:** The mixture was mixed with hardener through mechanical mixing and ultra-sonication. Ultrasonic agitation was performed for better dispersion of nano-particles. The degassing process was performed after each step to minimize the likelihood of trapped bubbles or moisture.

***Stage 3*:** The mixture was poured into molds and cured at 60°C for 4 hours inside a temperature-controlled oven. The detailed description of sample preparation is shown in a flowchart in Figure 3.1.

In this way, several samples with weight percentages of 1%, 2%, and 5% alumina nanoparticles were prepared. The diameter and thickness of the prepared samples were kept at 75 mm and 0.5 mm, respectively. The range of nano-particle concentration is carefully chosen by analysing the properties based on the available literature [35-39]. To study the dispersion of nano-particles in the polymer matrix, Scanning Electron Microscopy (SEM) was used. The obtained SEM images for pure epoxy and epoxy alumina nanocomposites with different filler loading are shown in Figure 3.2. From Figure 3.2, it can be observed that the nano-particles have been distributed uniformly.

***Stage 4*:** For thermal ageing, the samples were placed in a controlled thermal oven to undergo accelerated aging at a maintained temperature of 100°C. The heating oven used in this experiment featured a temperature accuracy of ±0.5°C. After each 200-hour ageing period, the oven was turned off; the samples were taken outside and cooled to room temperature. After this, PDC and IRC measurements were performed on the samples at ambient temperature (25°C).

The detailed description of sample preparation is shown in a flowchart in Figure 3.1. Following the procedure mentioned above, three samples with 1%, 2% and 5% alumina (Al_2O_3) nanocomposites by weight, mixed with epoxy resin, were prepared. Along with the nanocomposites, a pure epoxy resin sample with 0% nanofiller concentration was also prepared for the experiment. Every prepared sample has the thickness of 0.5 mm and diameter of 75 mm.

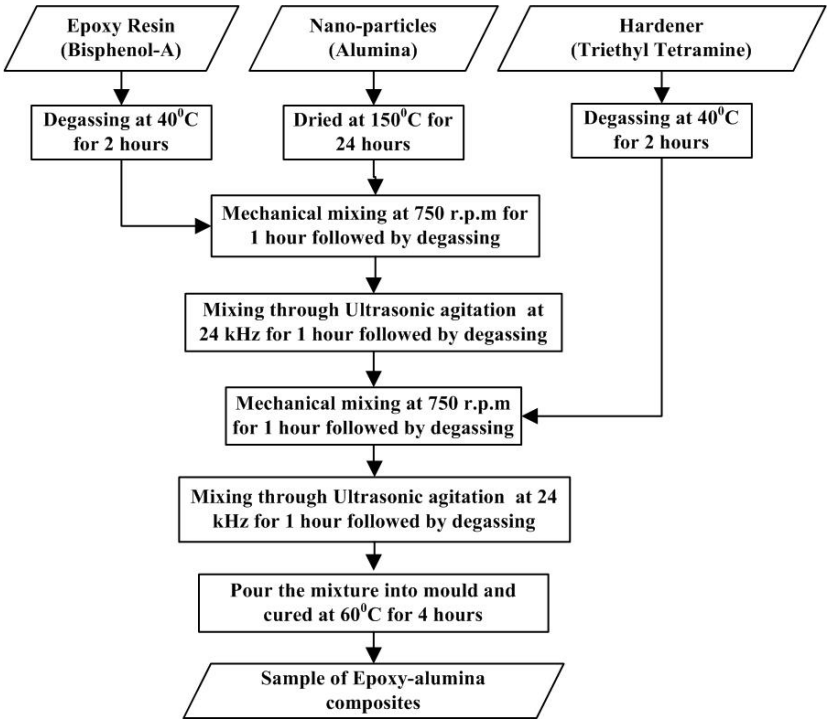

Figure 3.1 Flowchart showing sample preparation procedure.

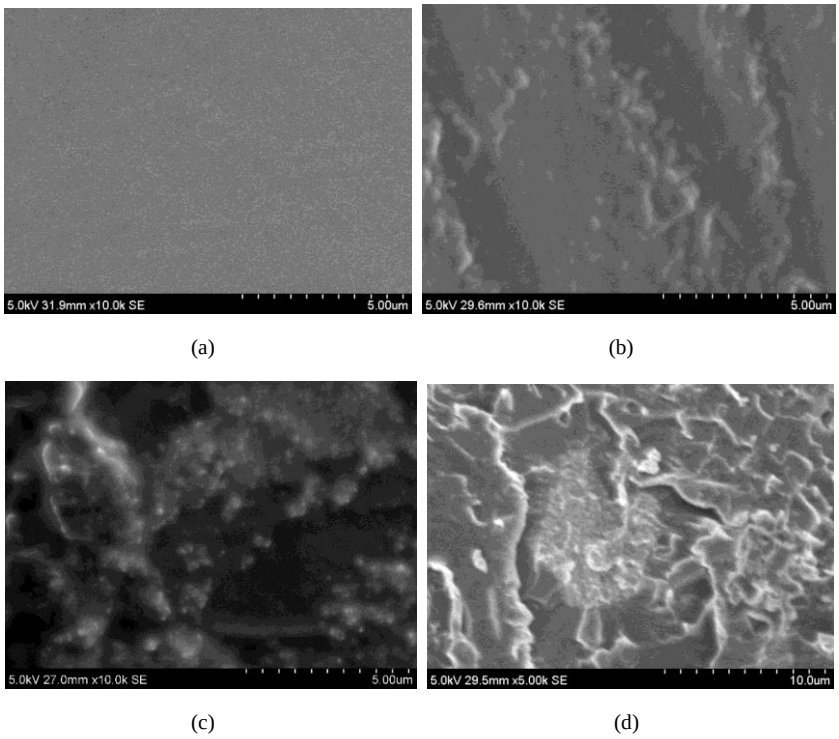

Figure 3.2 SEM images of (a) Pure epoxy, (b) Epoxy + 1wt% Al_2O_3, (c) Epoxy + 2wt% Al_2O_3, and (d) Epoxy + 5wt% Al_2O_3

3.3.2 Experimental Setup

The detailed description of the experimental setup has been discussed in Section 2.6 of ***Chapter 2***.The schematic and photograph of the experimental setup for performing the PDC and IRC measurements has been shown in Figure 2.5 and Figure 2.6 of ***Chapter 2***.

3.4 Experimental Results and Discussions

3.4.1 Effect of Nano-filler Concentration

At first, PDC measurements were performed on the prepared nanocomposites at 500 V DC. The measured polarization and depolarization currents are

shown in Figure 3.3 and Figure 3.4. It was observed from Figure 3.4, that depolarization current decreases with an increase in Al_2O_3 nano-filler concentration. This implies that Al_2O_3 nano-particles created hurdles in the polarization of the bulk material [121]. The presence of nanoparticles may cause entanglement of long polymer chains, which will lead to hindrance in the movement of the chains. This will restrict the polarization of epoxy-alumina nano-composites.
From the PDC measurements, the DC conductivity (σ_0) is calculated through the following equation (3.12) [84].

$$\sigma_0 \approx \frac{\varepsilon_0}{C_0 U_0}\left[i_p(t_p) - i_d(t_{dp})\right] \tag{3.12}$$

here, t_p and t_{dp} are the polarization and depolarization duration respectively. In present work, both the durations have been equal. ε_0, C_0 and U_0 are the permittivity of vacuum, geometric capacitance of the test sample and the applied voltage respectively.

The measured DC conductivity values for pure epoxy and epoxy-alumina nano-composites are tabulated in Table 3.1. It can be observed from Table 3.1 that with thermal ageing there is a slight decrease in the conductivity values. The variation in DC conductivity with nanofiller loading does not follow a clear trend. For 1 wt.% and 2wt% of filler loading, observed DC conductivity was slightly higher than that of pure epoxy. With more increase in nano-filler loading, DC conductivity decreased. The highest value was observed with 2wt % Al_2O_3 nano-composite. In all specimens, DC conductivity slightly decreased with progress in thermal ageing. This may be attributed to the post-curing reactions in epoxy [122], which generates deep traps. This has been discussed later in this section.

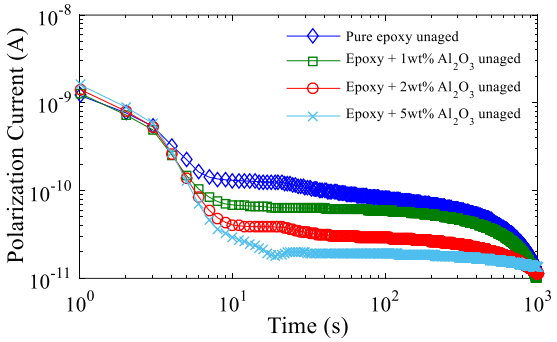

Figure 3.3 Polarization current of different samples at unaged condition.

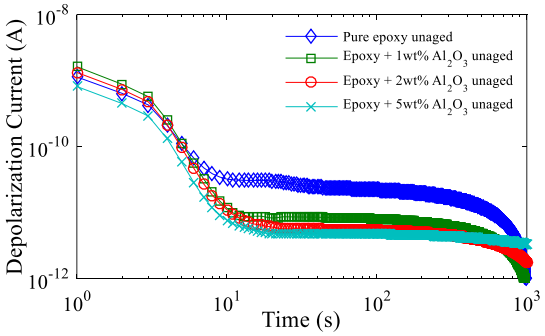

Figure 3.4 Depolarization current of different samples at unaged condition.

To get further information regarding the effect of ageing on the polarization processes in the nanocomposite, *tanδ* or dissipation factor measurements were also performed over the frequency range of 10^{-2} Hz to 10^{4} Hz. The results are depicted in Figure 3.5. It can be observed from Figure 3.5 that for all filler concentration, the dielectric losses increase with ageing. Another interesting piece of information from Figure 3.5 is that the peak region of dielectric losses slowly shifts towards higher frequencies with ageing. This occurs because the new polymer chains formed after chain scission are more flexible and can orient more easily in response to the electric field than the original, unbroken longer chains. Thermal ageing of epoxy resin also produces several polar groups, such as –OH groups, resulting from the breaking of the epoxide ring (–C–O–C) and the subsequent bonding of released O and H atoms [123].

Table 3.1: DC conductivity of all the samples.

Sample	**Ageing Status**	**DC Conductivity (S/m)**
Pure Epoxy	New	1.52E-16
	200 hours aged	1.45E-16
	400 hours aged	1.41E-16
Epoxy with 1wt% Al_2O_3	New	1.69E-16
	200 hours aged	1.66E-16
	400 hours aged	1.58E-16
Epoxy with 2wt% Al_2O_3	New	1.71E-16
	200 hours aged	1.68E-16
	400 hours aged	1.62E-16
Epoxy with 5wt% Al_2O_3	New	1.63E-16
	200 hours aged	1.59E-16
	400 hours aged	1.55E-16

Similarly, carbonyl groups (C=O) are generated through the oxidation of the main epoxy chain. Being polar, these compounds contribute to an increase in dielectric losses, especially in the frequency range of 0.1 to 10 Hz.

The effect of nano-filler concentration on the dissipation factor characteristics at different ageing stages is shown in Figure 3.6. It can be easily observed that with addition of nano-filler, the dielectric losses decrease. This can be explained as follows: The dielectric losses comprise mainly of two kinds, conduction losses and frictional losses. It has been already depicted in Table 3.1 that the conductivity slightly increases with nanoparticle concentration. The presence of nanoparticles in the polymer matrix often stretches the inter-lamellar distance around the nanoparticle [124]. This makes the motion of polymer chain under alternating field more difficult. As a result, frictional losses decrease. In the frequency region of 10^{-2}-10^{4} Hz, frictional losses are more prevalent compared to conductive losses. As a result, dielectric losses in nano-composites are less compared to pure epoxy, which makes the nano-composite comparatively less-aged. At the same time, epoxy-alumina nano-composites have shown greater resistance to partial discharges [125]. It was experimentally observed in [126], that the region around the alumina nanoparticle in epoxy is strongly bound and faces little erosion due to surface discharges when compared to the bulk material. This creates obstacles for growth of electrical trees. Altogether, these factors provide epoxy-alumina nanocomposite superior ageing-resistant properties.

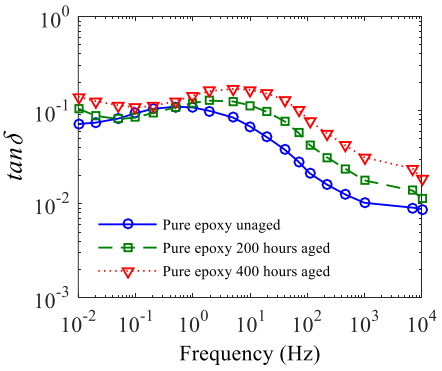

(a)

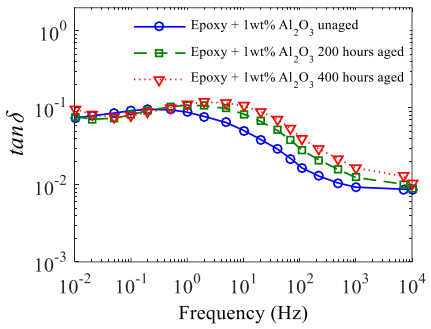

(b)

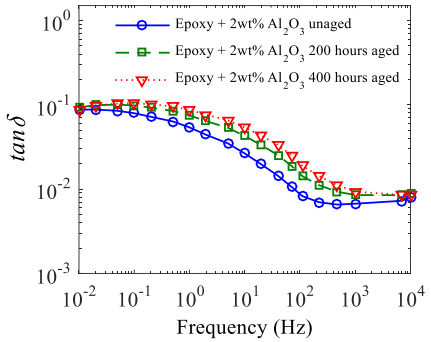

(c)

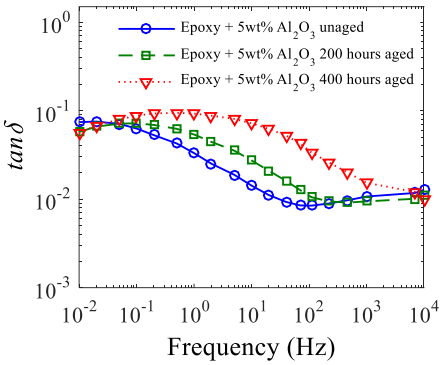

(d)

Figure 3.5 Dissipation factor measurements of pure epoxy and nano-composites, with different filler concentrations (a) Pure Epoxy (b) Epoxy + 1wt% Al_2O_3 (c) Epoxy + 2wt% Al_2O_3 (d) Epoxy + 5wt% Al_2O_3.

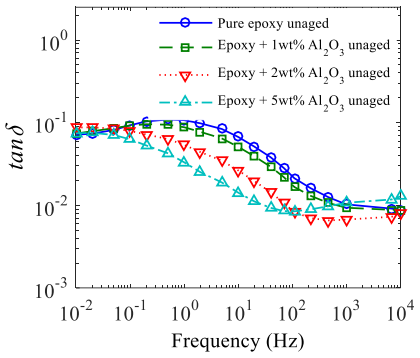

(a)

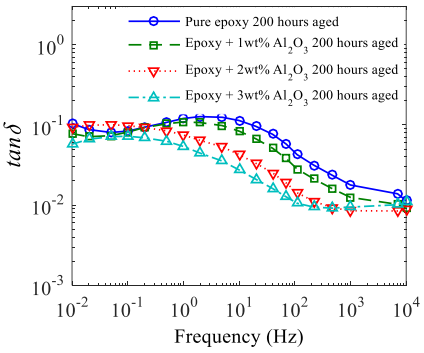

(b)

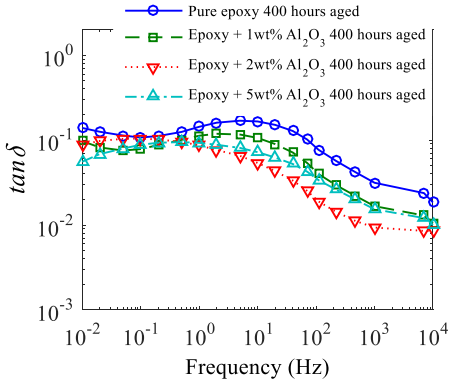

(c)

Figure 3.6 Effect of thermal ageing on FDS characteristics of epoxy nano-composites. (a) Unaged, (b) 200 hours thermally aged, (c) 400 hours thermally aged.

3.4.2 Effect of Thermal Ageing Duration

For analysis of charge trapping properties, the test samples were stressed at 10kV/mm electric field for around 1000 seconds and after that, the discharging currents were recorded. The discharging currents were recorded up to 1pA magnitude. Below this level, the current is highly affected by the noise and therefore discarded. From the measured currents, the de-trapping currents were separated using the methodology described in section 3.2.3. The de-trapping currents of pure epoxy and different epoxy nano-composites (epoxy resin with 1, 2 and 5wt% Al_2O_3) are shown in Figure 3.7 (a). The de-trapping currents of the same samples after 200 hours and 400 hours thermal ageing are shown in Figure 3.7(b) and (c). From the de-trapping currents, the net de-trapped charge of respective samples can be calculated using the following equation,

$$Q_{de-trapped} = \int_{t=0}^{t=t_f} I_{de-trap} dt \tag{3.13}$$

where, $I_{de\text{-}trap}$ is de-trapping current and t_f is the total measurement time of de-trapping current. The calculated net de-trapped charges for different samples are given in Table 3.2.

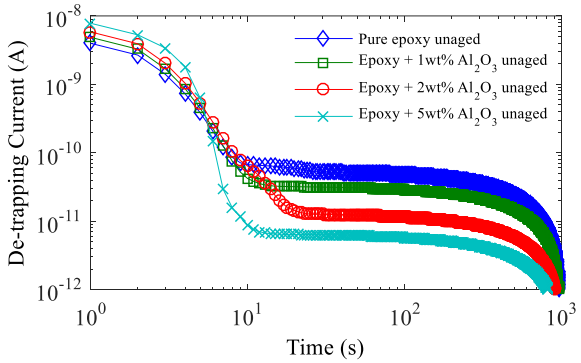

(a)

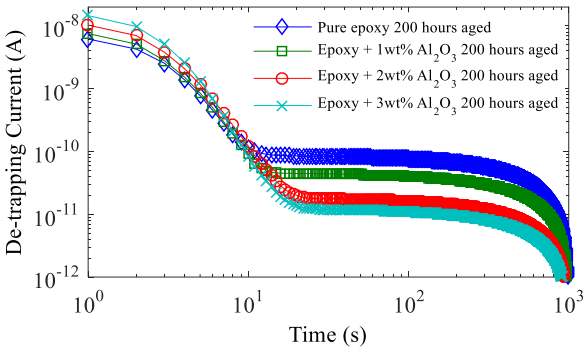

(b)

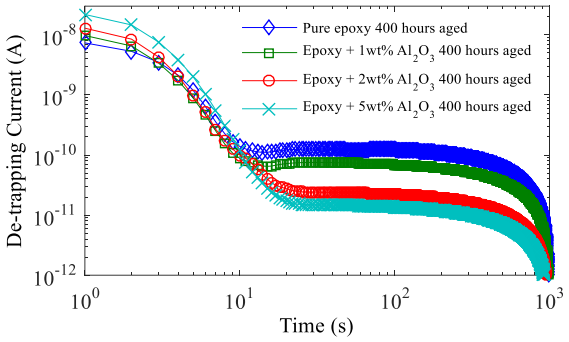

(c)

Figure 3.7 De-trapping Current of different epoxy nano-composite samples at (a) unaged condition, (b) 200 hours thermal ageing, (c) 400 hours thermal ageing.

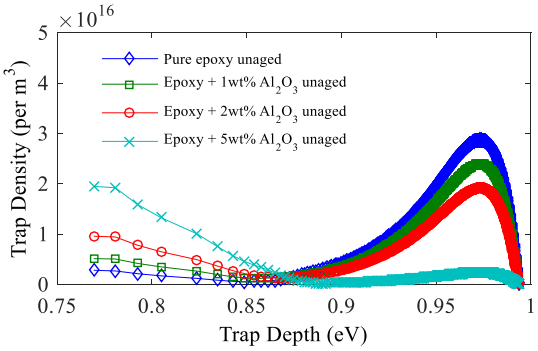

(a)

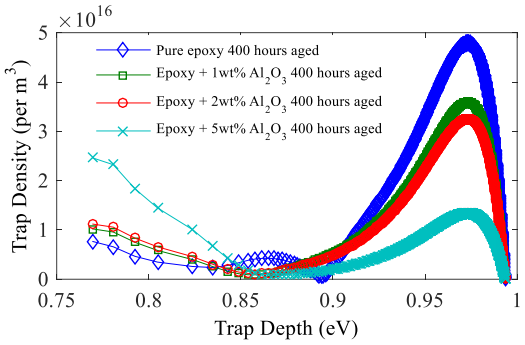

(b)

Figure 3.8 Distribution of trapped charge of samples at (a) unaged condition, (b) after 400 hours thermal ageing.

Table 3.2: Released charge for all the samples at 10kV/mm electric field stress.

Sample	**Ageing Status**	**Released Charge (nC)**
Pure Epoxy	New	35.791
	200 hours aged	58.156
	400 hours aged	84.526
Epoxy with 1wt% Al_2O_3	New	27.867
	200 hours aged	42.050
	400 hours aged	61.608
Epoxy with 2wt% Al_2O_3	New	21.658
	200 hours aged	37.327
	400 hours aged	44.631
Epoxy with 5wt% Al_2O_3	New	24.838
	200 hours aged	44.444
	400 hours aged	64.882

From Table 3.2, it can be observed that in general, the net de-trapped charge increases with thermal ageing. This is true irrespective of the nano-filler concentration. At the same time, the amount of total trapped charge in nano-composites is less compared to pure samples. To get a qualitative idea about the influence of nanofiller concentration on charge trapping, the trap distribution characteristics of pure epoxy and epoxy-alumina nanocomposites having different filler concentrations are shown in Figure 3.8. From Figure 3.8, two peaks in the trap distribution of every tested specimen are visible. One peak is at around 0.76 eV, corresponding to shallow traps. It should be mentioned here, due to measurement difficulties of transient currents just

after voltage application, it was not possible to obtain trap distribution below 0.76 eV. The other peak is around 0.97eV, corresponding to deep traps. Generally speaking, shallow traps are generated due to physical defects, whereas deep traps exist primarily due to chemical defects. Introduction of nanoparticles in the epoxy microstructure inadvertently causes significant physical defects. This is supported by the observations in Figure 3.8, where, the density of shallow traps increases steeply with increase in Al_2O_3 nanoparticle concentration. Comparatively, the density of filled deep traps decreases with nano-filler loading. It appears that Al_2O_3 nano-particles prevent deep traps to capture charges and generate more shallow traps in the dielectric microstructure. The explanation of this observation can be found in the relation between charge trapping and interfacial region surrounding the nano-particle. In recent years there has been significant experimental evidence [127] on the presence of localized electronic states with high concentration the interphase region around the nanoparticle. These localized states are ideal sites for charge trapping. Therefore, the probability of charge trapping increases with presence of nanoparticles.

On the other hand, it was experimentally observed in [128], that shallow traps have larger cross-section compared to deeper traps. The rate of charge trapping is proportional to the capture cross-section of traps. Consequently, shallow traps capture charge very easily. In the present case, it may happen that due to the presence of high density of shallow traps, charges are quickly captured in the adjacent layer of electrodes. This results in homo-charge accumulation, which reduces electric field density at the metal-dielectric interface, this in turn, reduces the Schottkey charge injection process [37, 129]. Accumulation of homo-charge in epoxy-alumina nano-composites have been observed with Pulse electro Acoustic measurements in [130]. As a result, deep traps do not get enough opportunity to capture charge carriers and remain unfilled. Therefore, the density of filled deep traps shows a decrease with Al_2O_3 nano-filler loading. As the charges are unable further penetrate in the dielectric specimen, the net amount of trapped charge is found to be less in epoxy-alumina nano-composites when compared to pure epoxy specimens.

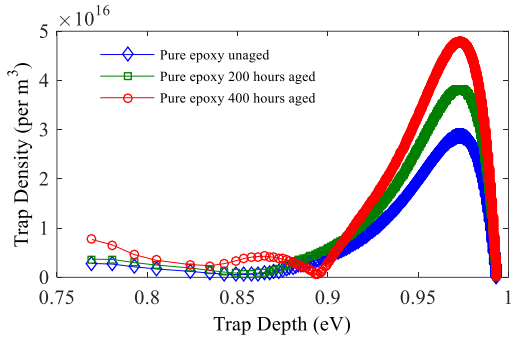
×10^16
5
4
3
2
1
0
Trap Density (per m^3)
Pure epoxy unaged
Pure epoxy 200 hours aged
Pure epoxy 400 hours aged
0.75
0.8
0.85
0.9
0.95
1
Trap Depth (eV)

(a)

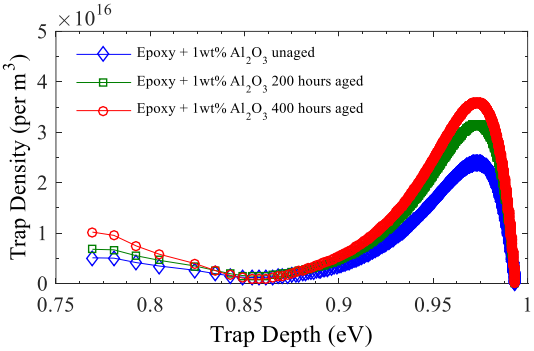
×10^16
5
4
3
2
1
0
Trap Density (per m^3)
Epoxy + 1wt% Al2O3 unaged
Epoxy + 1wt% Al2O3 200 hours aged
Epoxy + 1wt% Al2O3 400 hours aged
0.75
0.8
0.85
0.9
0.95
1
Trap Depth (eV)

(b)

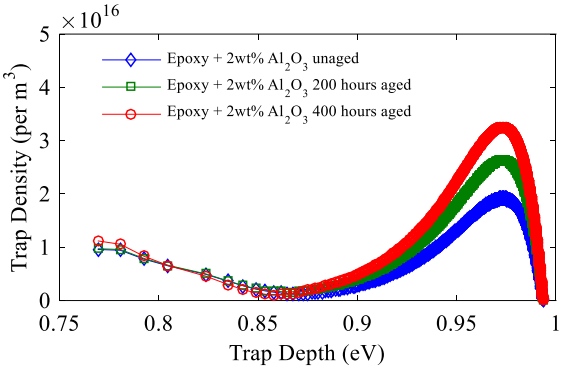
×10^16
5
4
3
2
1
0
Trap Density (per m^3)
Epoxy + 2wt% Al2O3 unaged
Epoxy + 2wt% Al2O3 200 hours aged
Epoxy + 2wt% Al2O3 400 hours aged
0.75
0.8
0.85
0.9
0.95
1
Trap Depth (eV)

(c)

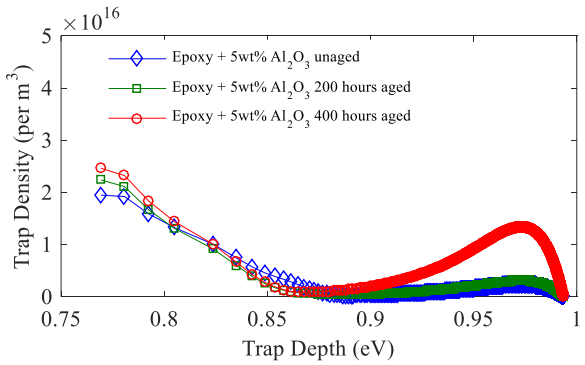

(d)

Figure 3.9 Distribution of trapped charge of differently aged samples (a) Pure Epoxy (b) Epoxy + 1wt% Al_2O_3 (c) Epoxy + 2wt% Al_2O_3 (d) Epoxy + 5wt% Al_2O_3.

Table 3.3: Comparison of trap depth obtained from the enhanced IRC model with values reported in other published studies.

Reported Articles	**Trap depth (eV)**
Gao et. al. [131]	0.70 - 0.85
Yu et.al [132]	0.90 - 1.05
Neelmani et. al. [129]	0.725 - 0.825
Present work	0.75 - 1

The effect of ageing on trap distribution of pure epoxy and epoxy-alumina nano-composites are shown in Figure 3.9. It can be easily observed that the density of deep traps increases with ageing. It has been already discussed that thermal ageing leads to chain scission and breaking of bonds. This results in a chemical non-uniformity across the dielectric. This leads the generation of new traps in the dielectrics, apart from the traps generated in the interfacial region. It has been already discussed that chemical defects lead to the generation of deep traps. The DC conduction in polymers is often influenced by the 'hopping' of charge carriers from one trapping site to another. If deep traps are present in the charge transport path, it will effectively reduce the conductivity by confining the charge for long durations. In that case the effective DC conductivity can be given through the following equation,

$$\sigma_{eff} = \sigma_{sh}\tau_{dtp} / (\tau_{dtp} + \tau_{deep}) \tag{3.14}$$

where σ_{eff} , τ_{dtp} , σ_{sh} is the effective conductivity, the time between two trapping events into deep traps, and τ_{deep} the retention time of charges after

being captured by deep traps. As the retention time is more for deep traps, the overall conductivity reduces with a greater number of deep traps. This also explains the experimental observation Table 3.1, where, DC conductivity decreased with ageing.
A comparison of trap density obtained in this work and other investigations reported in the literature is shown in Table 3.3. It can be observed from Table 3.3 that the findings regarding trap depth in the present work have wider range compared to other values reported in literature. This is because two different trap depth peaks corresponding to shallow and deep traps were noticed in present work, but in other works only one trap depth peak was noticeable.

3.5 Conclusions

In this chapter, a methodology has been proposed to estimate the trapping parameters (i.e., trap depth and trap density) from the IRC measurements of the dry-type insulation. In this investigation, epoxy-alumina nanocomposite was used as a dry-type insulation. The thermal ageing of this insulation has also been studied through the de-trapping characteristics based on isothermal relaxation current measurements. In addition, the contribution of dipolar relaxation in IRC measurements has been identified and separated through PDC measurements conducted on the same specimens at much lower electric field strengths. It has been revealed that the effect of nanoparticle addition and thermal ageing on trap distribution is not similar. The effect of thermal ageing is more pronounced on deep traps, where the density of filled traps significantly increased with thermal ageing. On the other hand, Al_2O_3 nanoparticle addition enhanced shallow trap density.
The effect of thermal ageing on the DC conductivity of pure epoxy and epoxy-alumina nanocomposites is not significant. Overall, the nanocomposites performed much better than pure epoxy in terms of space charge accumulation.

Chapter 4

Condition Assessment of Dry-Type Insulation Using Electric Modulus

4.1 Introduction

As discussed in ***Chapter 3***, the charge de-trapping characteristics of polymeric (dry-type) insulation can be estimated from polarization and depolarization current measurements. However, when these measurements are taken over an extended period, electrode polarization may occur. Electrode polarization refers to the buildup of a charge layer on the surface of an electrode when it is in contact with the insulating material. This charge accumulation can alter the behavior of the insulation. This occurs as charges migrate within the insulation and accumulate on the electrode surface, leading to polarization. Consequently, the true relaxation behavior of the dielectric material is obscured by this effect. A similar issue can arise during frequency domain measurements, particularly at low frequencies (near 1 mHz). Therefore, to accurately understand the dielectric material's relaxation behavior, the effect of electrode polarization must be eliminated.

Several studies in existing literature have explored the ageing behavior of insulating materials based on their relaxation phenomena [2, 36-39, 122]. However, as noted, the relaxation behavior of polymer dielectrics is not fully understood due to the effects of electrode polarization and charge transport, particularly at high temperatures and low frequencies [80]. Electrode polarization is the phenomena for the charge accumulation is occurs near the electrode. Result of that, this electrode polarization obscures the bulk relaxation process of the insulation and makes it complicated to extract the exact dielectric behaviour [80]. To address this, the present work proposes a quantitative analysis using electric modulus to more accurately estimate the thermal ageing state of epoxy-alumina nanocomposite insulation. The complex electric modulus ($M^*(\omega)$), defined as the inverse of complex permittivity ($\varepsilon^*(\omega)$), is a powerful tool for analyzing the relaxation behavior of insulating materials. Its advantage lies in its ability to reveal relaxation processes within the insulation that are often obscured by electrode polarization and charge transport effects, especially at low frequencies and higher temperatures [80].

The application of electric modulus to study the dielectric behavior of polymer dielectrics, such as epoxy resin [80] and ethylene-propylene-diene copolymer (EPDM) [133], has been well-documented. Parameters extracted from the electric modulus have also been used to estimate the moisture content in composite oil-paper insulation [134]. Additionally, recent studies have reported temperature correction techniques for electric modulus and activation energy computation for diagnosing oil-paper insulation [135]. Despite these successful applications, electric modulus has rarely been applied to study the thermal ageing behavior of polymeric insulation. As the growing popularity of epoxy and its nanocomposites as dry-type insulation in equipment such as dry-type transformers, rotating machines, and switchgear [37], this chapter employs electric modulus to study the relaxation behavior and quantitatively estimate the thermal ageing of epoxy nanocomposites.

In this chapter, three types epoxy alumina nano-composite samples with different filler concentrations (0 wt%, 1 wt% and 2 wt%) were prepared and the samples were thermally aged up to 400 hours (in steps of 100 hours) in the laboratory. Initially, frequency domain spectroscopy measurement (FDS) of the unaged as well as the thermally aged samples was done to obtain the variation of real ($\varepsilon'(\omega)$) and imaginary part ($\varepsilon''(\omega)$) of complex permittivity over the frequency range from 1 mHz to 10 kHz. From the frequency variation of complex permittivity, real ($M'(\omega)$) and imaginary part ($M''(\omega)$) of complex electric modulus of the same samples were obtained. Investigations revealed that the peak frequency of the $M''(\omega)$ spectrum (also known as the relaxation peak frequency) obtained for different nano-composite samples are sensitive to the change in the thermal ageing duration. In order to gain better insight into the relaxation behavior of the epoxy nano-composites, the variation of $M'(\omega)$versus $M''(\omega)$for the different samples were further fitted using Cole-Cole model. It was observed that the fitting parameters of the C-C model vary with the thermal ageing duration of the nano-composite samples. Based on the experimental investigations, two characteristic parameters, namely the relaxation peak frequency and the C-C distribution parameter have been used in this chapter to describe the thermal ageing of the epoxy-nano composite samples quantitatively. It was observed that using the above mentioned parameters, the thermal ageing of the epoxy nano-composites can be estimated closely with an acceptable error percentage (i.e. $\leq 8\%$).

4.2 Theoretical Background

4.2.1 Brief Theory of Frequency Domain Spectroscopy

As discussed in Section 1.8.2, when a sinusoidal excitation voltage $V(\omega)$ is applied on the insulator under test, the current $I(\omega)$ flowing through it can be expressed as [2, 16, 37]

$$I(\omega) = j\omega\overline{C}(\omega)V(\omega) \tag{4.1}$$

In equation (4.1), $\overline{C}(\omega)$ is the complex capacitance of the insulator which can be further divided into real and imaginary parts as

$$\overline{C}(\omega) = C'(\omega) - jC''(\omega) \tag{4.2}$$

The real part ($C'(\omega)$) signifies the energy storage component, whereas the imaginary part ($C''(\omega)$) represents the losses occurring within the dielectric medium, including both resistive and dielectric losses. The relationship between the $C'(\omega)$ and $C''(\omega)$ with the real ($\varepsilon'(\omega)$) and imaginary part ($\varepsilon''(\omega)$) of complex permittivity is given by

$$\varepsilon'(\omega) = \frac{C'(\omega)}{C_0} \tag{4.3}$$

$$\varepsilon''(\omega) = \frac{C''(\omega)}{C_0} \tag{4.4}$$

Here, C_0 is the capacitance of the of the empty electrode system which depends on geometry factor i.e. the area of cross section and the distance between the electrodes. In this chapter, FDS measurement was done from 1 mHz to 10 kHz to observe the variation of $\varepsilon'(\omega)$ and $\varepsilon''(\omega)$ with frequency, which can provide insight into the insulator condition.

4.2.2 Concept of Electric Modulus

When an alternating electric field with angular frequency (ω) is applied across an insulation, charge accumulation occurs near the electrodes, especially at low frequencies. This phenomenon, known as electrode polarization, not only significantly increases permittivity but also obscures the bulk relaxation process of the dielectric material, complicating the analysis of its behavior. In such cases, the complex electric modulus is a

valuable tool for examining the relaxation behavior of polymer dielectrics [80]. The complex electric modulus ($M^*(\omega)$) is defined as the reciprocal of complex electric permittivity ($\varepsilon^*(\omega)$), where conductive effects are disregarded. Complex permittivity, which varies with frequency, is given by $\varepsilon^*(\omega)=\varepsilon'(\omega)-j\varepsilon''(\omega)$, where the real part ($\varepsilon'(\omega)$) represents the energy storage component, and the imaginary part ($\varepsilon''(\omega)$) represents losses, including both polarization and conduction losses within the insulator. The complex electric modulus $M^*(\omega)$ can also be expressed in terms of the real and imaginary parts of the complex capacitance as follows [134]:

$$M^*(\omega) = \frac{1}{\varepsilon^*(\omega)} = \frac{1}{\varepsilon'(\omega) - j\varepsilon''(\omega)}$$

$$= \frac{\varepsilon'(\omega)}{\varepsilon'^2(\omega) + \varepsilon''^2(\omega)} + j\frac{\varepsilon''(\omega)}{\varepsilon'^2(\omega) + \varepsilon''^2(\omega)}$$

$$= M'(\omega) + jM''(\omega) \tag{4.5}$$

Here, $M'(\omega)$ denotes the real part and $M''(\omega)$ represents the imaginary part of $M^*(\omega)$. According to equation (4.5), if $\varepsilon'(\omega)$ and $\varepsilon''(\omega)$ increase significantly due to electrode polarization at low frequencies, $M'(\omega)$ and $M''(\omega)$ become smaller, as $\varepsilon'(\omega)$ and $\varepsilon''(\omega)$ appear in the denominator. Consequently, the high permittivity caused by electrode polarization, which obscures the relaxation process in the permittivity spectrum, does not affect the electric modulus spectrum. Also, it follows from (4.5) that the relaxation shifts to a high frequency in the electric modulus spectrum, compared to permittivity spectrum. Therefore, analyzing the electric modulus spectrum offers a clearer understanding of the relaxation behavior in epoxy nanocomposites compared to examining the permittivity spectrum.

4.2.3 Cole-Cole Model

The complex permittivity $\varepsilon^*(\omega)$ can be expressed in terms of Cole-Cole (C-C) relaxation which is given by [122, 135]

$$\varepsilon^*(\omega) = \varepsilon_\infty + \frac{\varepsilon_s - \varepsilon_\infty}{1 + (j\omega\tau)^\beta} \tag{4.6}$$

Here, ε_s and ε_∞ are the relative permittivity values at the infinite and near-zero frequencies, respectively and τ is the relaxation time constant. The parameter β is the relaxation time distribution parameter varying from 0 to 1. The

parameter β governs the shape of the C-C plot in the argand plane. The $M^*(\omega)$ is the reciprocal of the $\varepsilon^*(\omega)$, which can be expressed as [80]:

$$M^*(\omega) = \frac{1}{\varepsilon^*(\omega)} = \frac{1}{\varepsilon_\infty + \frac{(\varepsilon_s - \varepsilon_\infty)}{(1+(j\omega\tau)^\beta)}}$$

$$= \frac{1}{\varepsilon_\infty} - \frac{(1/\varepsilon_\infty) - (1/\varepsilon_s)}{1+(j\omega\tau)^\beta.(\varepsilon_\infty/\varepsilon_s)}$$

$$= \frac{1}{\varepsilon_\infty} - \frac{(1/\varepsilon_\infty) - (1/\varepsilon_s)}{1+(j\omega\tau_M)^\beta}$$

$$or,\quad M^*(\omega) = M_\infty - \frac{M_\infty - M_s}{1+(j\omega\tau_M)^\beta} \tag{4.7}$$

Now, (4.7) is the C-C relaxation expressed in terms of complex electric modulus ($M^*(\omega)$). Here, $M_s=1/\varepsilon_s$ and $M_\infty=1/\varepsilon_\infty$ and the electric modulus relaxation time constant $\tau_M=\tau.(\varepsilon_\infty/\varepsilon_s)^{(1/\beta)}$. The variation of $M'(\omega)$ and $M''(\omega)$ in the argand plane also looks like a semi-circular plot and for β=0, the center will lie on the real axis. One interesting observation from (4.7) is that the distribution parameter β remains unchanged when the C-C relaxation is expressed in terms of $M^*(\omega)$. It is to be noted that experimental observation on real dielectrics have revealed that C-C plot does not form a semicircle rather it is an arc of the circle and the center point of the circle lies below the real axis [122]. The shifting of the center of the semicircle on C-C plot signifies the distributive relaxation process of the polymer dielectric materials. Smaller value of β denotes the wider distribution of relaxation time and vice-versa.

4.3 Experimental Details

4.3.1 Preparation of Test Samples

The detailed description of sample preparation has been discussed in Section 3.3.1 of ***Chapter 3***. Following the sample preparation procedure, two types of test samples with 1% and 2% alumina (Al_2O_3) nano-composites by weight mixed with epoxy resin were prepared. Along with the nano-composites, a pure epoxy resin sample with 0% nano-filler concentration was also prepared for the purpose of experiment. Every prepared sample has the thickness of

0.5 mm and diameter of 75 mm. For thermal ageing, the prepared samples were kept inside a controlled heat chamber (temperature accuracy of 0.5° C) where the accelerated thermal ageing was executed at fixed temperature of 100° C. For each of the prepared nano-composite samples, thermal ageing was done for 100 hours, 200 hours, 300 hours and 400 hours, respectively. After thermal ageing was done, each sample were taken outside and cooled down to room temperature (25° C) before the start of the experiment.

4.3.2 Experimental Procedure

Frequency domain spectroscopy (FDS) was performed on the prepared test samples using the IDAX-300 test equipment. The schematic diagram and actual photograph of the measurement setup are shown in Figure 4.1 and Figure 4.2, respectively. For FDS measurement, a sinusoidal voltage of magnitude 141.4 $V_{r.m.s}$ was applied across the sample under test through cylindrically shaped brass electrodes (radius 30 mm and thickness 11.5 mm). The frequency range for FDS measurements was 0.001 Hz to 10 kHz. FDS measurement has been performed from high frequency to low frequency at room temperature of 25° C, which was continuously monitored using a thermometer. After each measurement was done the terminals of the test samples were kept short circuited for sufficient duration to eradicate the memory effect.

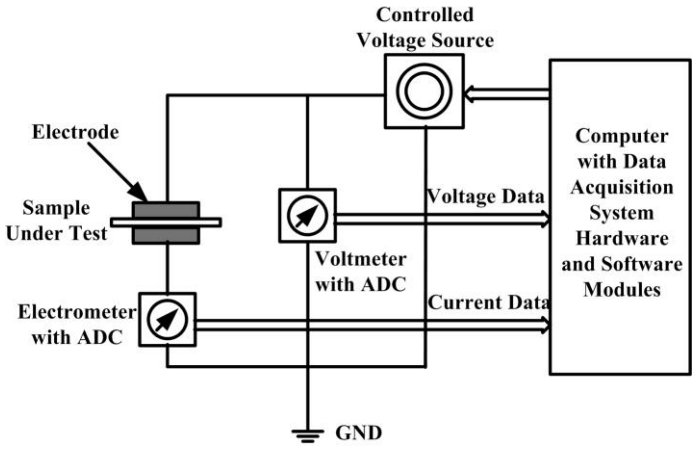

Figure 4.1 Schematic diagram of the experimental setup.

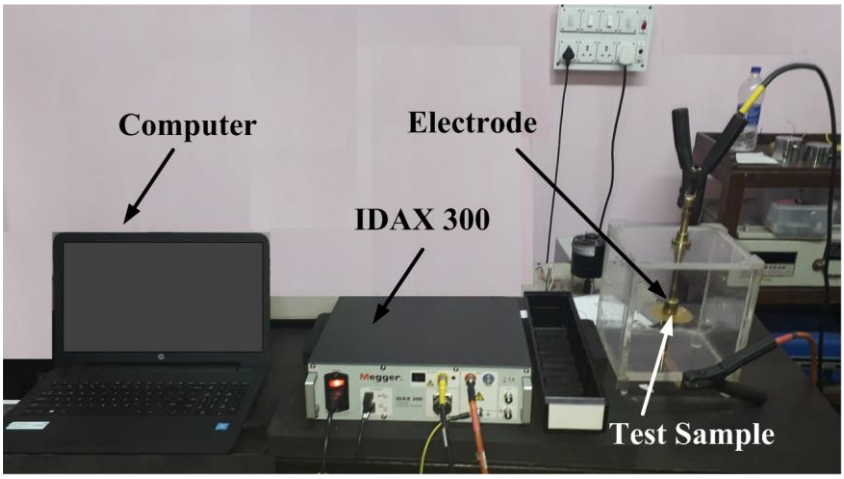

Figure 4.2 Photograph of the experimental setup.

4.4 Experimental Results and Discussions

4.4.1 Variation of Real and Imaginary Part of Electric Modulus with Ageing Duration

The FDS measurement of the epoxy nano-composite samples (unaged and thermally aged up to 400 hours) were conducted over a frequency range of 1 mHz to 10 kHz to observe the $\varepsilon'(\omega)$ and $\varepsilon''(\omega)$ with frequency variation. Then using equation (4.5), the $M'(\omega)$ and $M''(\omega)$ were computed and plotted against frequency to observe the influence of thermal ageing on epoxy nano-composite samples. The frequency variation of $M'(\omega)$ and $M''(\omega)$ with ageing duration for the three test samples (pure epoxy and epoxy with 1wt% and 2wt% Al_2O_3 nano-filler) is shown in Figure 4.3(a-c) and Figure 4.4 (a-c), respectively. From Figure 4.3 (a-c), it can be observed that thermal ageing has definite influence on the $M'(\omega)$ spectrum of the epoxy nano-composite samples. For all three test samples, the value of $M'(\omega)$ computed at each frequency is found to increase with the increase in measurement frequency but decreases with the ageing duration.

This is evident from the $M'(\omega)$ curves obtained for the test samples (see Figure 4.3 (a-c)), which shows a downward and and rightward shift with the

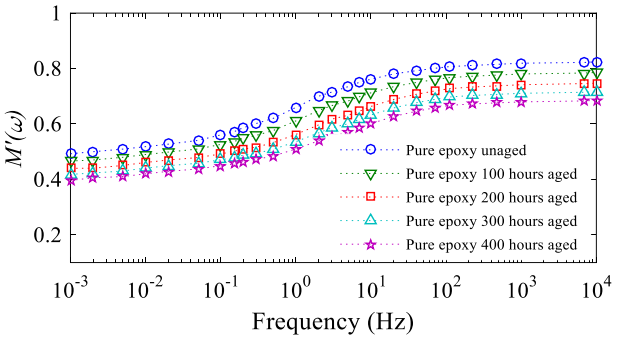

(a)

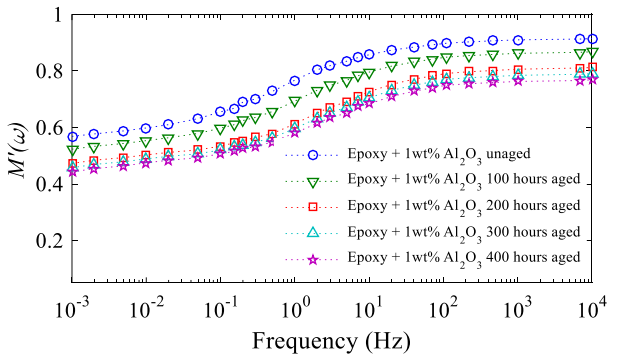

(b)

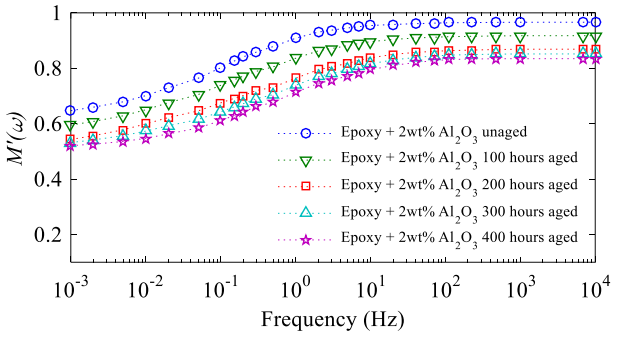

(c)

Figure 4.3 Variation of M'(ω) with frequency for different ageing duration (hours) (a) Epoxy resin (b) Epoxy resin + 1wt% Al_2O_3 (c) Epoxy resin + 2wt% Al_2O_3.

increase in thermal ageing duration. The variation of $M''(\omega)$ with frequency resembles a bell shaped curve that attains peak at a particular frequency known as the relaxation peak frequency (f_p). With the increase in the ageing duration, f_p shifts towards the higher frequencies for all three test samples. The value of f_p indicates the frequency at which the dielectric loss peak occurs. From the knowledge of f_p, the relaxation time constant has also been computed in this chapter for better understanding the relaxation behavior of the epoxy nano-composites with the change in thermal ageing duration. The relaxation time constant (τ_p) indicates the time taken by the dipoles to rearrange after the applied electric field is removed. The relaxation time constant (τ_p) can be derived from the peak

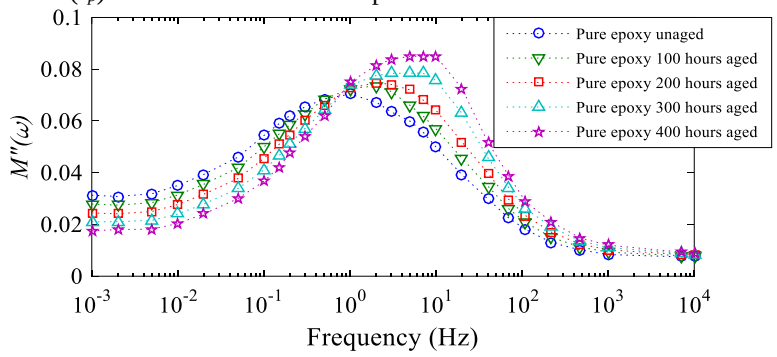

(a)

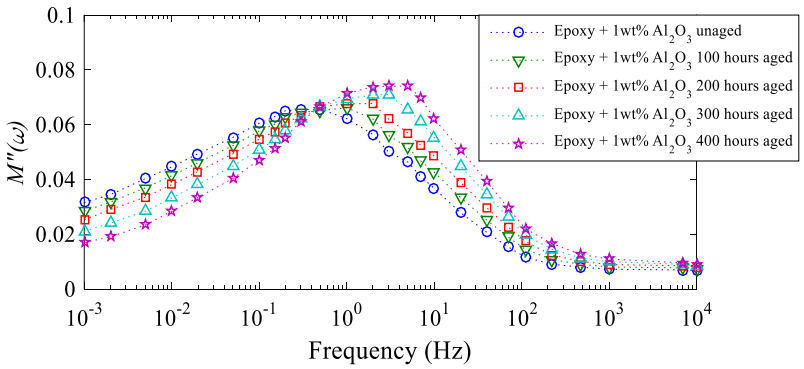

(b)

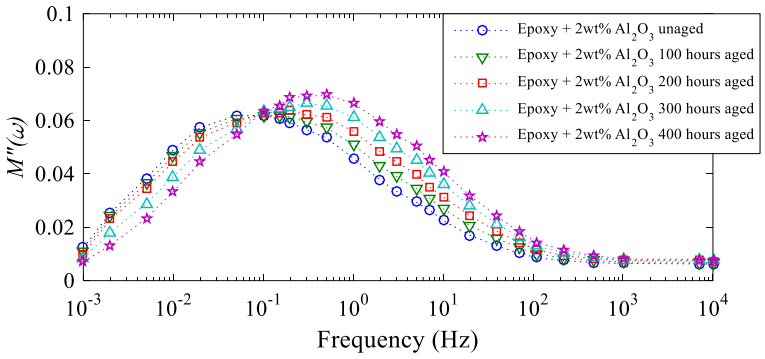

(c)

Figure 4.4 Variation of $M''(\omega)$ with frequency for different ageing duration (hours) (a) Epoxy resin (b) Epoxy resin + 1wt% Al_2O_3 (c) Epoxy resin + 2wt% Al_2O_3.

frequency (f_p) using the following relation [134]

$$\tau_p = \frac{1}{\omega} = \frac{1}{2\pi f_p} \tag{4.8}$$

The variation of f_p and τ_p obtained for three test samples with different ageing duration (in hours) is shown in Table 4.1.

Table 4.1: Variation of relaxation time constant and peak frequency with ageing duration

Sample	**Ageing duration (hours)**	f_p **(Hz)**	τ_p **(s)**
Epoxy	0	1.01	0.157
	100	2.01	0.079
	200	4.02	0.039
	300	7.01	0.022
	400	9.91	0.016
Epoxy + 1 wt% Al_2O_3	0	0.51	0.312
	100	1.02	0.156
	200	2.10	0.075
	300	3.54	0.044
	400	5.04	0.031
Epoxy + 2 wt% Al_2O_3	0	0.10	1.592
	100	0.15	1.061
	200	0.25	0.636
	300	0.31	0.513
	400	0.52	0.306

From Table 4.1, it can be observed that f_p increases with the increase in ageing duration for all test samples. It happens because thermal ageing leads to chain scission and breaking of long polymeric chains, thereby producing new polymeric chains of shorter length. These new chains are more flexed to orient according to the electric field than the old lengthy chains [37]. Also, it can be observed from Table 4.1 that for a particular ageing duration, the value of f_p decreases with the increase in Al_2O_3 nano-filler concentration. It may be due to the involvement of nano-particles in the polymeric matrix, which creates an interfacial region surrounding the nano- particle. Available literature shows that this interfacial region may have its own unique glass transition temperature [136, 137]. As a result, the motion of molecular chains in epoxy nano- composites under alternating fields will not be as smooth as in pure epoxy. Additionally, due to filler loading the degree of cross linking in the polymer matrix decreases and creates more side chains as well as branch chains. Therefore, the intensity of the orientation polarization weakens [37]. Also, the variation of τ_p with the ageing duration and the nano-filler concentration shows an inverse behavior as compared to f_p. Now, from the existing literature [135], we know that the relaxation peak frequency f_p is an important parameter, which can be used to describe the relaxation behavior of the polymer dielectric materials in a quantitative manner. Therefore, f_p is used in this chapter as a metric to study the relaxation properties of epoxy-nano composites quantitatively. The variation of f_p with the ageing duration (in hours) for three test samples is portrayed in Figure 4.5. From the nature of variation of f_p with the ageing duration (in hours) as depicted in Figure 4.5, an empirical relation has been derived using least square curve fitting technique, that relates f_p obtained from $M''(\omega)$ spectrum with the ageing duration (in the increase in the ageing duration. From Figure 4.4 (a-c), which shows the variation of $M''(\omega)$ with frequency, it can be seen that the $M''(\omega)$ curves for three test samples reveal an upward hours), which is given by

$$aging(hours) = \frac{1}{b_1} \ln\left(\frac{f_p}{a_1}\right) \tag{4.9}$$

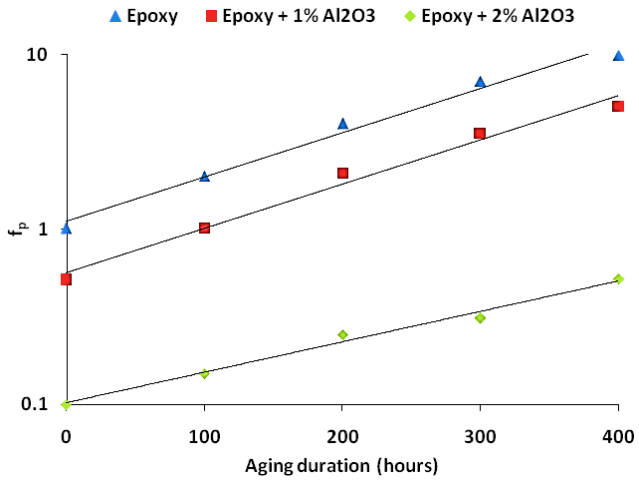

Figure 4.5 Variation of f_p with ageing duration (hours)

Using equation (4.9), thermal ageing of different epoxy nano-composites can be estimated if f_p is known, which can be obtained from $M''(\omega)$ spectrum of the test samples. The variation of the coefficients of the equation (4.9) for different test samples is presented in Table 4.2. It can be observed from Table 4.2 that the coefficients a_1 decrease while b_1 is almost insensitive with the increase in nano-filler concentration. Therefore, from the above analysis, it is evident that both $M''(\omega)$ and $M''(\omega)$ characteristics are sensitive to the change in ageing duration of the epoxy nano- composite samples.

Table 4.2: Variation of slope and intercept values of the equation (4.9) for different test samples

Sample	a_1	b_1	R^2
Epoxy	1.11	0.006	0. 982
Epoxy + 1 wt% Al_2O_3	0.55	0.005	0. 985
Epoxy + 2 wt% Al_2O_3	0.10	0.004	0. 988

Besides, the relaxation peak frequency can be used to estimate the ageing state of the epoxy nano-composites. In the next, section, further analysis was carried out using Cole-Cole model for better understanding of the change in dielectric relaxation behavior of the epoxy nano-composite samples with thermal ageing.

4.4.2 Analysis using Cole-Cole Model

The variation of $M''(\omega)$ is plotted against $M'(\omega)$ for three test samples in Figure 4.6 (a-c), which represents a semicircular arc. From Figure 4.6 (a-c) it can be observed that the $M''(\omega)$ versus $M'(\omega)$ curves for different test samples are sensitive to the change in ageing state. Also, it can be observed that the curves shift towards the left and become narrow in width with the increase in ageing duration of the test samples. For better understanding of the variation of the dielectric relaxation behavior of the epoxy nano-composites, the variation of $M''(\omega)$ versus $M'(\omega)$ curves were fitted using Cole-Cole (C-C) model. It can be observed that the variation in the relaxation behavior of the epoxy nano-composites with the change in ageing duration can be well approximated using the C-C model. The variation of the C-C model parameters with ageing duration (in hours) for different test samples is shown in Table 4.3. In this contribution, three parameters namely C-C distribution parameter (β), C-C time constant (τ) and width of the C-C plot ($\Delta M = M_s - M_\infty$) have been extracted to quantify the differences in ageing duration between different types of nano-composite

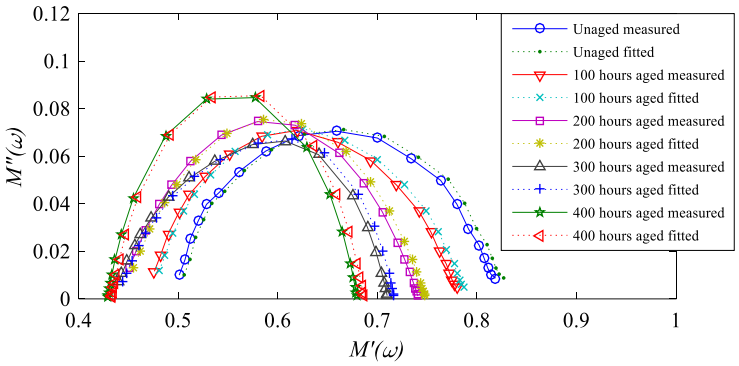

(a)

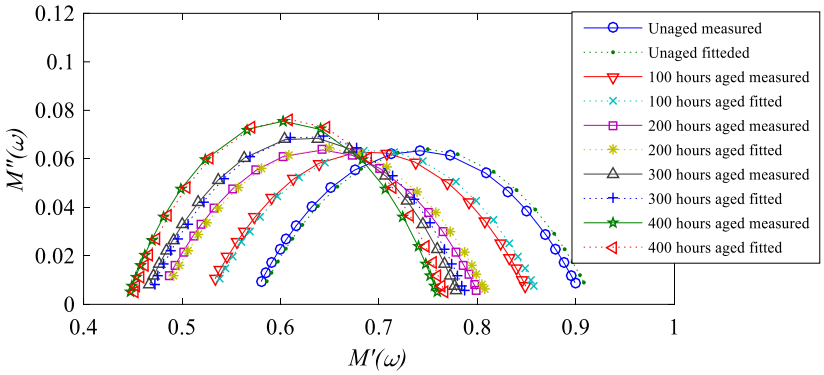

(b)

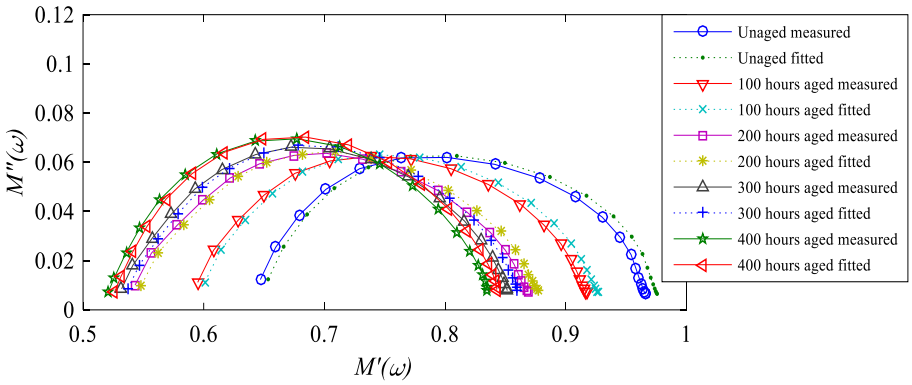

(c)

Figure 4.6 Variation of $M'(\omega)$ versus $M''(\omega)$ for different ageing duration (hours) (a) Pure Epoxy (b) Epoxy resin + 1wt% Al_2O_3 (c) Epoxy resin + 2wt% Al_2O_3.

samples. It can be seen from Table 4.3 that the parameters used to fit the C-C model are sensitive to the change in thermal ageing duration of the test samples. The parameters β and ΔM decreases with the increase in ageing duration whereas τ shows an increasing trend with the ageing duration. Considering the effect of adding nano-fillers, it can be observed that both β and ΔM shows a slightly increasing trend whereas, τ increases slightly with the addition of nano-fillers. Since, β is an indicator of the distribution of relaxation time, hence it can be said that with the increase in thermal ageing leads to wider distribution of relaxation times as β decreases. On the contrary,

Table 4.3: Variation of C-C parameters with ageing duration

Sample	**Ageing duration (hours)**	***β***	***τ***	**$\Delta M = Ms - M_\infty$**	***RMSE***
Epoxy	0	0.371	0.146	0.328	0.0012
	100	0.345	0.147	0.319	0.0010
	200	0.282	0.148	0.301	0.0011
	300	0.268	0.150	0.294	0.0014
	400	0.219	0.152	0.283	0.0017
Epoxy + 1wt% Al_2O_3	0	0.440	0.162	0.341	0.0018
	100	0.412	0.164	0.337	0.0019
	200	0.385	0.166	0.333	0.0017
	300	0.350	0.167	0.325	0.0015
	400	0.314	0.168	0.320	0.0020
Epoxy + 2wt% Al_2O_3	0	0.534	0.175	0.344	0.0031
	100	0.507	0.176	0.341	0.0040
	200	0.461	0.178	0.338	0.0037
	300	0.435	0.179	0.332	0.0035
	400	0.402	0.180	0.325	0.0041

addition of nano-fillers results in narrower distribution of relaxation time as β increases. Among the three C-C fitting parameters, it can be observed that only the parameter β is more sensitive to the change in ageing duration compared to other parameters. The variation of β with ageing duration (hours) is shown in a graph in Figure 4.7.

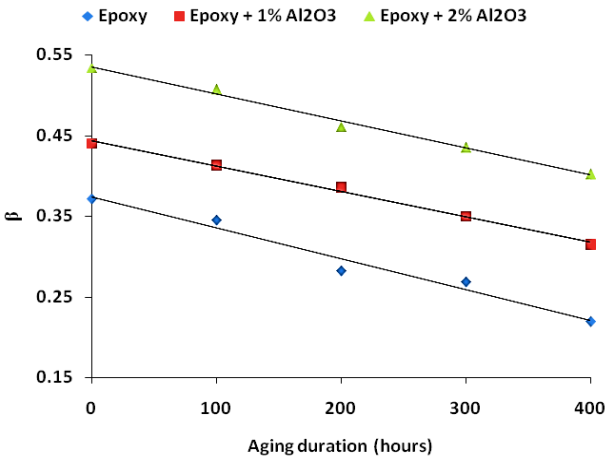

Figure 4.7 Variation of C-C distribution parameter β with ageing duration (hours).

From the nature of variation as shown in Figure 4.7, an empirical relation has been established between β and ageing duration (hours) using least square curve fitting technique which is expressed as

$$aging(hours) = \frac{\beta + c_1}{m_1} \tag{4.10}$$

Using (4.10), it is possible to estimate the thermal ageing state of the epoxy nano-composites if the value of β from the C-C model is known. In Table 4.4, the variation of the slope and intercept values of (4.10) for different test samples is shown. It can be seen from Table 4.4 that between the slope (m_1) and the intercept (c_1), the latter is more sensitive showing an increasing trend with the increase in the nano-filler concentration. Thus, from the above analysis, it is conclusive that the variation of the $M''(\omega)$ plotted against $M'(\omega)$ can be fitted using C-C models and the fitted parameters are sensitive to the change imageing duration of the epoxy nano-composite samples.

Table 4.4: Variation of slope and intercept values of equation (4.10) for three samples

Sample	m_1	c_1	R^2
Epoxy	0.0004	0.373	0.988
Epoxy + 1wt% Al_2O_3	0.0002	0.443	0.995
Epoxy + 2wt% Al_2O_3	0.0003	0.535	0.992

4.4.3 Validation of the Proposed Technique

In order to verify whether the thermal ageing of the epoxy nano-composite samples can be accurately estimated using the parameters derived from the electric modulus spectrum, three additional epoxy nano-composite samples thermally aged for 150 hours were prepared in the laboratory for the purpose of verification. Initially, FDS measurement was done on the three new test samples to obtain the imaginary part of the complex permittivity $\varepsilon''(\omega)$, from which $M''(\omega)$ were computed using (4.5). From the variation of $M''(\omega)$ with frequency, the relaxation peak frequency f_p was computed for the three new test samples, and using (4.9), ageing duration of the epoxy nano-composite samples were estimated using the parameters mentioned in Table 4.2. Moreover, the relative percentage errors in sensing the ageing duration (with respect to actual ageing duration) were also computed for the three new test samples and the results are presented in Table 4.5. In addition, the variation of $M'(\omega)$ and $M''(\omega)$ in the complex plane for the three new test samples were also fitted using C-C model to observe their relaxation behaviors and finally the C-C model distribution parameter β of the respective test samples were obtained. Then, using (10), the ageing duration of the three epoxy nano-

Table 4.5: Sensing of thermal ageing using relaxation peak frequency

Sample	f_p **(Hz)**	**Ageing duration (hours)**	**Estimated Ageing duration (hours) using equation (4.9)**	**Error (%)**
Epoxy	2.51	150	140	6.7
Epoxy + 1wt% Al_2O_3	1.12	150	142	5.3
Epoxy + 2wt% Al_2O_3	0.18	150	143.5	4.3

Table 4.6: Sensing of thermal ageing using C-C distribution parameter

Sample	β	**Ageing duration (hours)**	**Estimated Ageing duration(hours) using equation (4.10)**	**Error (%)**
Epoxy	0.315	150	138.5	7.6
Epoxy + 1wt% Al_2O_3	0.405	150	141.0	6.0
Epoxy + 2wt% Al_2O_3	0.485	150	140.5	6.3

composite test samples were also estimated using the parameters mentioned in Table 4.3 and the relative percentage errors with respect to the actual ageing duration were computed which are presented in Table 4.6. From Table 4.5 and Table 4.6, it can be observed that the thermal ageing of the epoxy nano-composites can be estimated using equations (4.9) and (4.10), respectively with acceptable error (i.e. $\leq$8%). Further, observations from Table 4.5 and Table 4.6 reveal that the thermal ageing of the test samples can be better estimated using equation (4.9) compared to equation (4.10), which is evident from the relative error percentage reported in the above tables for all three test samples. Therefore, it can be said from the above observations that compared to the C-C model distribution parameter β, relaxation peak frequency f_p is more reliable and useful for sensing of the thermal ageing of the epoxy nano-composites. Nevertheless, it can be observed from Table 4.5 and Table 4.6 that for all three test samples, the relative error percentages in sensing the thermal ageing lies within the acceptable range, which indicates the two aforesaid parameters proposed in this chapter, can be used to estimate the thermal ageing of the epoxy nano-composites. It is to be mentioned here that, if moisture or other factors influence the ageing condition, therefore, it may alter in the shift of the f_p and broaden the relaxation time distribution, affecting β. Hence, it may affect the coefficients of the derived equations and impose error in accuracy of estimation. To improve reliability, the derived equations based on those indicators should be used with updated coefficients alongside compensation models.

4.5 Conclusions

In this chapter, an advanced technique using complex electric modulus is proposed for sensing the thermal ageing of the epoxy-nano composite insulation samples. The epoxy nano-composite samples mixed with different filler concentrations of Al_2O_3 were prepared and were thermally aged for 100 hours 200 hours, 300 hours and 400 hours, respectively. Initially, FDS measurement was done on the prepared samples to analyze the variation of $\varepsilon'(\omega)$ and $\varepsilon''(\omega)$ across the frequency range of 1 mHz to 10 kHz. In order to unfold to relaxation behavior of the epoxy nano-composites which were masked using electrode polarization effect, an advanced approach employing complex electric modulus $M^*(\omega)$ was employed in this chapter. From the frequency variation of $\varepsilon'(\omega)$ and $\varepsilon''(\omega)$, $M'(\omega)$ and $M''(\omega)$ were computed for the epoxy nano-composite samples from which the relaxation peak frequency (f_p) and the relaxation time constant (τ_p) were derived. It was observed that both f_p and τ_p are sensitive to the change in nano-filler concentration as well as thermal ageing duration of the epoxy nano-composite samples. The value of f_p increases with the increase in ageing duration while decreases with the increase in nano-filler concentration. Based on their nature of variation, an empirical relationship between f_p with the ageing duration (hours) has been established in this chapter for sensing the ageing duration of the epoxy nano-composites quantitatively. Besides, for better understanding of the change in relaxation behavior of the epoxy nano-composites with the change in ageing duration, the variation of $M'(\omega)$ and $M''(\omega)$ plotted in the complex plane were modeled using C-C model. Investigations revealed that the different fitting parameters of the C-C model were found to be sensitive to the change in thermal ageing duration. Among the different fitting parameters, specifically C-C distribution parameter (β) was found to be more sensitive to the change in thermal ageing duration. Using curve fitting, an empirical relationship between β and thermal ageing duration (hours) has also been established for sensing the thermal ageing of the epoxy nano-composites. Finally, three new samples were tested to verify whether the parameters f_p and β can accurately estimate the ageing state for different epoxy nano-composites. It was observed that between f_p and β, the former can be used to estimate the thermal ageing more accurately with an acceptable error. Thus, it can be concluded that the proposed framework employing complex electric modulus can be applied for accurate sensing of the thermal ageing of the epoxy nano-composites.

Chapter 5

Condition Assessment of Dry-Type Insulation Using Dielectric Relaxation Current Analysis

5.1 Introduction

As discussed in ***Chapter 4***, the electric modulus has been employed to study the relaxation characteristics of polymeric (dry-type) insulation. The electric modulus technique effectively reduces the effects of electrode polarization, revealing the intrinsic relaxation behavior of dipole groups. In ***Chapter 4***, the relaxation characteristics were studied using the electric modulus and the Cole-Cole model. Existing literature reports that the relaxation behavior of dielectric materials is generally analyzed using various modeling techniques, including the Debye model, Cole-Davidson model, and Havriliak-Negami (H-N) model, among others [1-2, 122, 138-140]. These techniques model dielectric relaxation characteristics based on multiple distinct relaxation times [138-140]. In the case of polymeric dielectric materials, different dipolar groups, depending on their polymer chain lengths, exhibit different relaxation times. As a result, the relaxation times of these dipolar groups are often closely spaced, exhibiting only minor variations. This makes it challenging to separate closely related relaxation times within the dielectric material using the aforementioned models. As a result, the modeling of relaxation currents using these methods (such as the Debye, Cole-Cole, Cole-Davidson, and H-N models) may sometimes deviate from the actual measured relaxation current, potentially obscuring crucial information about the insulation characteristics. To address this, the proposed Relaxation Frequency Distribution (RFD) method has been developed. This method can account for closely related relaxation times when modeling the dielectric relaxation current. Thus, it can be concluded that using the RFD method provides a more accurate representation of the inherent characteristics of the insulation.

As discussed in ***Chapter 1***, transformer and rotating machines are the major equipment of power system network. Failure of these equipments lead to power disruption and momentary loss in production of heavy industries. These failures are primarily due to the insulation degradation of these equipments. Thus, continuous monitoring and improvements in insulation quality are increasingly emphasized by researchers. Presently, epoxy and its

nano-composites are accepting as dry-type insulation for high voltage equipment due to its promising electrical characteristic. However, these insulations experience thermal, electrical, chemical, and mechanical stress during their service life, accelerating the ageing process [39-43, 141-142]. This ageing process results in degradation of insulating properties that may lead to pre-matured and catastrophic breakdown in long run.

Similarly, nowadays, the most commonly used insulating material in new underground cable installations is cross-linked polyethylene (XLPE) [143-146]. However, during its service life, the XLPE-cable insulation has been endured to various stresses that may result in insulation fault. Major cause of cable faults is the degradation of the insulation. The degradation of XLPE insulation is accelerated by electrical, thermal, mechanical, and environmental stresses [144-145]. One of the major concerns of the underground cable is the moisture inrush in cable insulation [146-149]. Over time, soil moisture may penetrate the insulation or enter through a damaged outer sheath [147, 150]. Moisture ingress in high-voltage cables leads to the formation of water trees within the insulation, resulting in irreversible damage and potentially causing premature insulation failure [146-147]. Replacing faulty cables can also be an expensive and space-consuming process [146, 149]. Therefore, research activities have been actively involved to understand the degradation process of the XLPE insulation. Hence, from technical and economic point of view, it is important to periodically perform the diagnostic tests of the in-service underground cable insulation for checking its condition status before the complete failure [151]. Moreover, regular diagnostic testing along with proper maintenance can help to extend the life span of the in service power cable. Considering the above mentioned fact, a proper condition monitoring scheme is required to estimate the actual deterioration of the cable insulation.

Due to the ageing, the insulation properties are altered which in turns affects its relaxation characteristics. Hence, the relaxation characteristics of the dipoles within the dielectric insulation needs to be investigated to assess its condition. The relaxation characteristics of insulating materials can be better understood by analyzing the depolarization current. The dielectric relaxation function ($r(t)$) can be estimated from the relaxation current, which indicates the fundamental memory properties of the insulation material [16, 85]. Once the relaxation function $r(t)$ is determined, the characteristics of the insulation can be accurately estimated. Therefore, the proper estimation of the relaxation function is the area of interest for the researchers.

In this investigation, the ageing characteristics of the epoxy nano-composite (EPNC) and XLPE cable insulation have been estimated based on the RFD technique. For this purpose, epoxy-alumina nano-composite samples (with unfilled, 1wt% and 2wt% alumina concentration) and XLPE cable insulation samples (having different moisture content) were prepared in the laboratory. These prepared samples were undergone different degree of artificial electro-thermal ageing for experimental purpose. Thereafter, the depolarization currents of the prepared test samples were measured using the developed experimental setup. The depolarization currents of the test samples have been used for modelling their relaxation characteristics.

5.2 Theoretical Background

5.2.1 Brief Theory of Dielectric Relaxation Current

In time domain spectroscopy, a DC voltage of preset magnitude is applied to the insulation under test to initiate the polarization process. After a designated period for voltage application, the voltage source is disconnected and replaced by a short circuit, allowing the corresponding dielectric relaxation current to be measured. The dielectric relaxation current (DRC) is then analyzed to assess the dipole relaxation behavior within the insulation material. This technique, used to assess the condition of the insulation, is known as Polarization and Depolarization Current (PDC) measurement [1-2, 85]. The detailed theory is discussed in Section 1.8.

5.2.2 Concept of Relaxation Characteristics Modelling

According to the classical Debye model (DBM) [1, 2, 85], the dielectric response function *r(t)* of an insulating material can be expressed as follows, where the model assumes a single characteristic relaxation time constant (τ_{DM}).

$$r(t) = \frac{A}{\tau_{DM}} e^{(-\tau/\tau_{DM})} \tag{5.1}$$

Where, τ_{DM} is the relaxation time constant of the dipoles. *A* is the amplitude of the exponential function. When a step input excitation $E(t)=E_0U(t)$ is applied, the dielectric polarization can be described by the following equation [102, 139].

$$\wp(t) = \varepsilon_0 E_0 \int_0^t r(t)dt \tag{5.2}$$

$$or, \quad \frac{d}{dt}\wp(t) = \varepsilon_0 E_0 r(t) \tag{5.3}$$

Here, ε_0 is the permittivity of free space. Now, using equations (5.1), (5.3) can be modified as

$$\frac{d}{dt}\wp(t) = \varepsilon_0 E_0 \frac{A}{\tau_{DM}} e^{(-\tau/\tau_{DM})}$$

$$\text{or,} \quad \wp(t) = \int \frac{d}{dt}\wp(t)dt = \varepsilon_0 E_0 \frac{A}{\tau_{DM}} \int e^{(-\tau/\tau_{DM})}dt$$

$$= \frac{\varepsilon_0 E_0 A}{\tau_{DM}}(-\tau_{DM})e^{(-\tau/\tau_{DM})} + \lambda$$

$$= -\tau_{DM}\varepsilon_0 E_0 \frac{A}{\tau_{DM}} e^{(-\tau/\tau_{DM})} + \lambda \tag{5.4}$$

$$= -\tau_{DM}\varepsilon_0 E_0 r(t) + \lambda \tag{5.5}$$

Here, λ is the integration constant and response function *r(t)* is monotonically decreasing in nature. After sufficient long time, the response function reaches to 0.

$$\lim_{t\to\infty} r(t) = 0$$

Therefore, the magnitude of the λ can be calculated as,

$$\lim_{t\to\infty}\wp(t) = 0 + \lambda$$

$$or, \quad \lambda = \lim_{t\to\infty}\wp(t) \tag{5.6}$$

Now the $\wp(t)$ would be

$$\wp(t) = -\tau_{DM}\frac{d}{dt}\wp(t) + \underset{t\to\infty}{Lim}\,\wp(t) \tag{5.7}$$

At steady state i.e. $t\to\infty$,

$$\underset{t\to\infty}{Lim}\,\wp(t) = \wp_0 = \varepsilon_0 E_0 \int_0^\infty r(t)dt = \varepsilon_0 E_0 \chi_0 \tag{5.8}$$

Here, χ_0 is the steady-state susceptibility, defined as $\chi_0 = \int_0^\infty r(t)dt$.

Combining equations (5.7) and (5.8), the dielectric response with single relaxation time (τ_{DM}) can be expressed as,

$$\tau_{DM}\frac{d}{dt}\wp(t) + \wp(t) = \underset{t\to\infty}{Lim}\,\wp(t) = \varepsilon_0 E_0 \chi_0 \tag{5.9}$$

Equation (5.9) can further be expressed in terms of relaxation frequency ($\nu = (1/\tau_{DM})$) and expressed as [139],

$$\frac{1}{\nu}\frac{d}{dt}\wp(t) + \wp(t) = \underset{t\to\infty}{Lim}\,\wp(t) = \varepsilon_0 E_0 \chi_0 \tag{5.10}$$

5.2.3 Mathematical Design of the Relaxation Frequency Distribution (RFD) Function

According to DBM relaxation mechanism [138, 152], the dielectric molecules are considered as spherical in shape with having single relaxation. However, in practice, not every molecule is spherical. Moreover, in the case of solid polymeric dielectric the molecules form polymeric chains of different length with different attributes. With ageing, the length of polymeric chain becomes shorter. Thus, the relaxation characteristics of polymeric chains differ based on ageing, as the molecular structure becomes increasingly disordered, leading to variation in relaxation times. In solid nano-composites materials, the properties of the relaxation process are different depending upon the degree of interaction between the molecules and their axis of rotation. This phenomenon indicates the frequency dispersion of the relaxation process over a wide range. Therefore, in order to understand the

relaxation process, the corresponding recorded depolarization current data is converted into distribution domain over a wide frequency range. These distribution domain data have been utilized for evaluating the distribution density function (*r(v)*). This distribution density function (*r(v)*) can be expressed as the rate of change of relaxation of the total polarization ($\wp_{total}$ i.e. total polarization at any time instant *t*) with respect to relaxation frequency (*v*) [139].

$$r(v) = \frac{1}{P_{total}} \frac{d\wp_{total}}{dv} \tag{5.11}$$

$$vr(v) \equiv R(v) \tag{5.12}$$

Here, *R(v)* is the total summation of the individual relaxation function of each dipole group having distinct relaxation frequency. The *R(v)* has been calculated using the numerical procedures as given in [139, 153-155]. The function *R(v)* in equation (5.12) can be correlated with the depolarization current as described by equation (5.13). The *R(v)* is similar to the Fourier Transform. However, as the measured data is discrete in nature, so iterative method has been adopted for calculating *R(v)* as given in [153-155]. Where $\wp_{0total}$ represents as the total polarization in the dielectric under equilibrium condition (i.e. $t \rightarrow \infty$). The method reported in [139], the overall distribution of frequency has been denoted by *R(v)* (in equation (5.12)).

5.2.4 Identification of RFD Function from Relaxation Current Data

As reported in [1, 85], individual dipolar relaxation current nature becomes exponential. Since the depolarization current is the superposition of individual dipolar relaxation currents, $i_r(t)$ in equation (5.13) is expressed as the sum of exponential currents from each dipole.

$$i_r(t) = \wp_{0total} \int_0^\infty R(v) e^{-tv} dv \tag{5.13}$$

Equation (5.13) can be represented in discrete form by a linear set of discrete equation (in equation (5.14)) with different set of (v_k, R_k). The present investigation is oriented towards the modelling of relaxation current. In depolarization phase (relaxation current), conduction current becomes zero

and only the dipolar relaxation current flows. Saha *et al* modelled the depolarization current as a superposition of individual dipolar relaxation current [85]. Following that method, in this work, the depolarization current has been modelled as summation of relaxation current of each dipole (which is independent to the other dipoles) obtained through RFD (as given in equation (5.14)).

$$i_r(t_{di}) = \wp_{0total} \sum_{\substack{k=1 \\ i=1,2,\ldots N}}^{N} \Delta \nu_k R_k(\nu_k) e^{-t_{di}\nu_k} \qquad (5.14)$$

Direct solutions of equation (5.14) are generally difficult to obtain due to the ill-conditioned nature of the corresponding matrix, requiring the application of iterative numerical methods. The procedures for solution of similar kind of equation are being reported in [140]. In the present investigation, a numerical iterative method is being adopted to calculate the frequency distribution spectra of the relaxation process from the measured depolarization current.

5.3 Experimental Arrangement

In this section, the experimental procedure has been discussed along with the preparation of the test samples.

5.3.1 Preparation of Test Samples

In this chapter, two different types of dry-type insulation were considered for experimental analysis and mathematical model development. These two types of insulation samples are epoxy-alumina nano-composites and XLPE cable insulation. The epoxy nano-composite samples were prepared, and their ageing process conducted in the laboratory, while the XLPE cable insulation samples were collected from a local power utility, with moisture content ageing performed in the laboratory.

5.3.1.1 Preparation of Epoxy Nano-Composites

Epoxy-alumina nano-composite samples have been prepared by mixing different percentage of alumina nano-particle in base epoxy resin. The details of the sample preparation have been described in Section 3.3.1. Table 5.1 shows the samples prepared along with percentage of alumina. The prepared samples were subjected to accelerated electro-thermal ageing process at 100°C (in order to keep the ageing temperature close to maximum operating

temperature (120℃) of class E insulation [156]) and 6 kV, 50Hz field stress (considering the twice the nominal operating electric stress as reported in [39]) in a controlled heat chamber. The total duration of the ageing process was 600 hours. After every 100 hours, the samples were removed from the heat chamber and allowed to cool to 27°C for 2 hours. Depolarization current of the test samples were measured using the developed experimental setup.

Table 5.1: Test Sample Details of Epoxy-Alumina Nano-Composites

Name	**Description**
EpA0	Pure epoxy
EpA1	Epoxy + 1wt% Al_2O_3
EpA2	Epoxy + 2wt% Al_2O_3

5.3.1.2 Preparation of XLPE Cable Insulation

In the present investigation, 11 kV XLPE cable samples (single core: aluminum) with specified dimensions (as outlined in Table 5.2) were collected from the local power utility and used for experimental purposes. The photograph of the cable sample has been shown in Figure 5.1(a). Moisture inrush in cable insulation is a lengthy and slow process. Therefore, in the present investigation, an experimental process has been adopted where a specified amount of water (i.e., actual moisture content) has been injected into the cable insulation to emulate the water tree. Prior to experimentation, all XLPE cable samples were dried at 50°C for 24 hours to eliminate residual moisture. After that, the moistures (i.e. distilled water) have been injected in the artificially created holes (diameter: 0.5 mm, depth: 2.9 mm) in the XLPE cable insulation. Then, the moisture induced holes have been sealed with the glue and kept it in closed chamber at least 72 hours before the experimentation. The photograph of the cable sample with artificially created hole is shown in Figure 5.1(b). The schematic of the XLPE cable cross-section (with dimensions) is depicted in Figure 5.2. It is to be mentioned here that, actual water trees in cable insulation have the dimensions of few μm in range [147]. Therefore, it is very difficult to emulate such actual tree structure inside the cable insulation. Considering this fact, in this experimentation, an artificial hole was created in the insulation layer. It is yet to be mentioned here that, the volume of the hole is nearly equalized with the total water volume in the tree structure of the net insulation. Thereafter, a known amount of water was inserted into the created holes. Finally, the m.c. inside the cable insulation can be defined as equation (5.16).

$$m.c. = \frac{v_w}{v_i} \times 10^6 \quad ppm \tag{5.16}$$

Where, v_w denotes the injected moisture volume and v_i represents the insulation volume. It is reported, in a real life aged cable, typical length of water trees is in the range of 20-200 μm, its width varies within 0.2-0.5 μm, and number concentration is around 10-20 per mm^3 [147, 157]. It is also reported in [147] that, the moisture content of a practical aged cable is less than 100 ppm with respect to the insulation volume. Considering these facts, in this investigation, the m.c. of the XLPE cable samples were varied from pristine to 105ppm, in step of 15ppm. It is to be mentioned here that, the moisture stress has been done following the guidelines given in [147, 158-159]. The details of the XLPE samples are tabulated in Table 5.3.

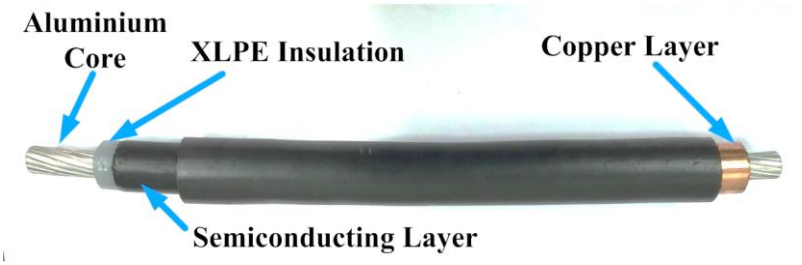

(a)

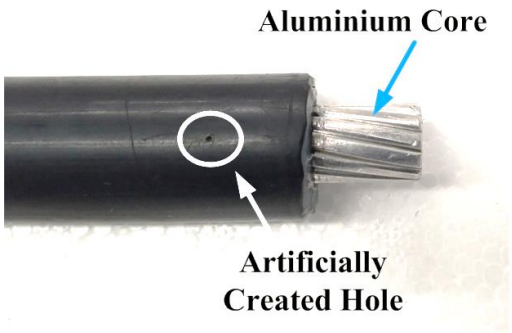

(b)

Figure 5.1 Photograph of (a) Test XLPE cable sample, (b) Artificially created hole in XLPE cable sample.

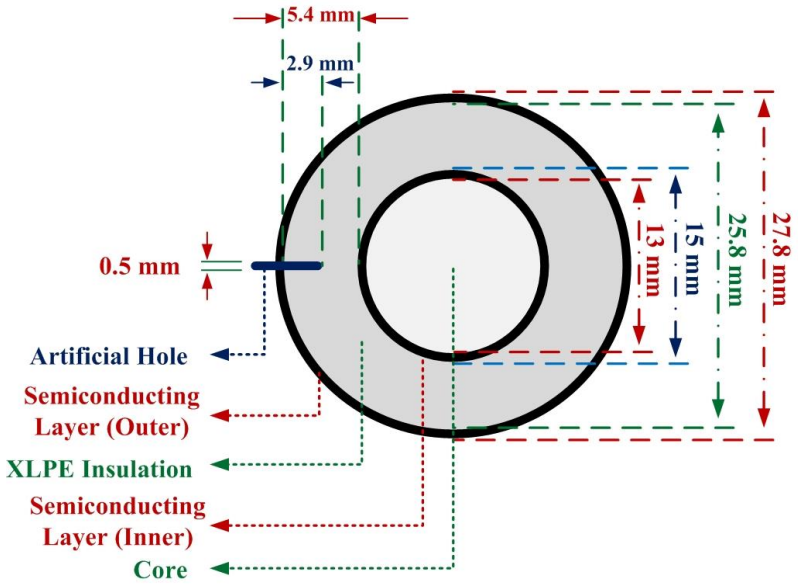

Figure 5.2 Schematic of cross-sectional view of XLPE cable sample.

Table 5.2: Information about the Test XLPE Cable Sample

Properties	Specifications
Rating	11 kV
Core Material	Aluminum
Length	32.5 cm
Diameter of Core	13 mm
Thickness of the Insulation	5.4 mm

Table 5.3: Test Sample Details of XLPE Cable Insulation

Sample Nomenclature	Moisture Content (m.c.) (ppm)
S_0	--
S_1	15
S_2	30
S_3	45
S_4	60
S_5	75
S_6	90
S_7	105

5.3.2 Experimental Procedure

An experimental setup (as shown in Figure 2.6(c) of *Chapter 2*) was prepared in the laboratory to record the polarization and depolarization currents (PDC) of the epoxy nano-composite test samples. Similarly, for the measurement of PDC in the XLPE cable insulation, an experimental setup was prepared as illustrated in Figure 5.3(a). A high voltage dc source is connected to the test electrodes through a two-way switch. The test sample is placed in between the electrodes. When the switch is turned to position 'P_1', the d.c. voltage is applied to the test sample and the polarization current is recorded. Thereafter, the depolarization current has been measured by shifting the switch position to 'P_2'. The experimental set-up photograph for the PDC measurement of XLPE cable insulation is shown in Figure 5.3(b).

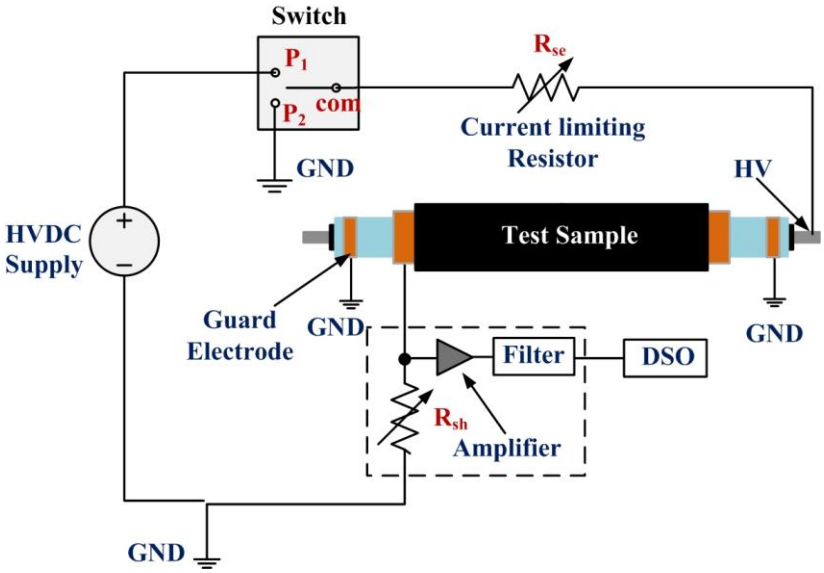

(a)

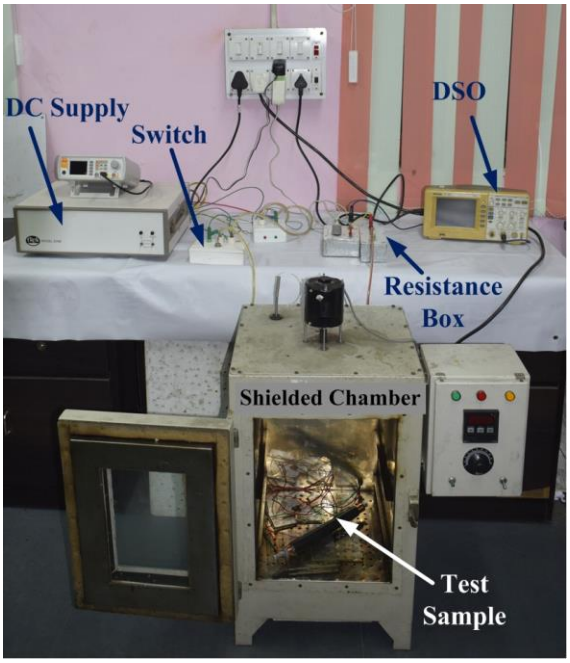

(b)

Figure 5.3 (a) Schematic of experimental setup for XLPE cable insulation samples, (b) Hardware module of experimental setup for XLPE cable insulation samples.

5.4 Experimental Results and Discussions

For experimental analysis, two different types of insulating materials are considered such as epoxy nano-composite and XLPE cable insulation. The electro-thermal ageing state of the epoxy nano-composite was initially analyzed, and an estimation method for ageing duration was subsequently derived. Thereafter, the moisture content of the XLPE cable insulation has been analyzed and suitable mathematical moisture content estimation technique has been developed.

5.4.1 Analysis Based on Epoxy Nano-Composites Insulation

In this sub-section, the results and analysis of the epoxy nano-composite insulation has been discussed.

5.4.1.1 Variation of Depolarization Current with Ageing Duration

The PDC measurement of the test samples (EPNC with unaged and electro-thermally aged) were performed under 1kV/mm d.c. electric field stress. The measured depolarization currents of the test samples have been shown in Figure 5.4(a) and Figure 5.4(b). As shown in Figure 5.4(a), the depolarization current increases progressively with the duration of ageing. The addition of nano-fillers to the base epoxy resin forms new bonds with the base resin molecules, modifying the material's macromolecular structure. Therefore, the length of the macromolecular polymeric chains is enhanced which results in reduction of degree of freedom of the dipoles during the application of electric field. This fact in turn reduces the vibration of the long chain dipoles and subsequently the polarization process. Figure 5.4(b) illustrates that increasing alumina nano-particle concentration leads to a decrease in depolarization current. It may be due to the presence of nano-particles which may enhances the polymeric chain and creates new entanglement [36-37]. Entanglement of the polymeric chain within the test samples opposes its vibration. The decrement of vibration in turn reduces the polarization process within the test sample.

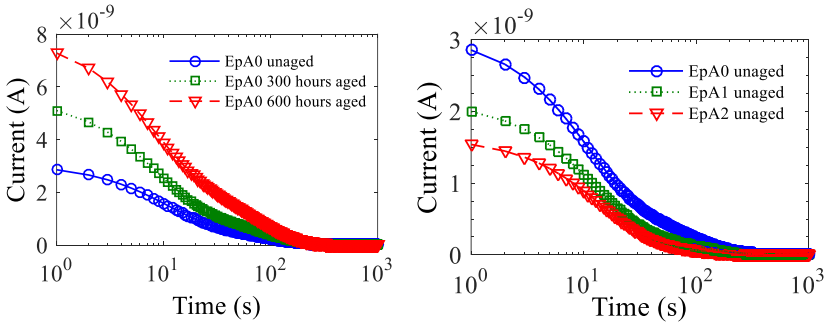

Figure 5.4 Relaxation current of (a) EpA0 with different ageing state, (b) unaged epoxy-alumina nano-composite with different filler concentration.

5.4.1.2 Analysis using Frequency Distribution Function

Based on the measured depolarization current of the test samples, their frequency domain distribution function has been evaluated following the procedures adopted in [154-155]. The evaluated frequency domain distribution function (for 10, 100, 700, 1000 iterations) of the pure epoxy unaged sample have been shown in Figure 5.5(a). Depolarization currents

were calculated for each evaluated frequency domain distribution function (as shown in Figure 5.5(a)) and compared with their corresponding measured values, as depicted in Figure 5.5(b). It may be observed Figure 5.5(b) that, the error involved for the evaluated depolarization current becomes minimum for 1000 iterations. Considering this fact, the relaxation frequency distribution frequency (RFD) for each test sample have been evaluated after 1000 iterations.

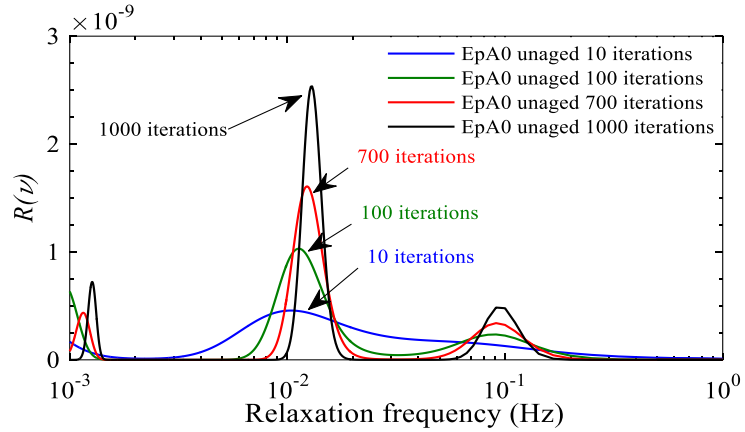

(a)

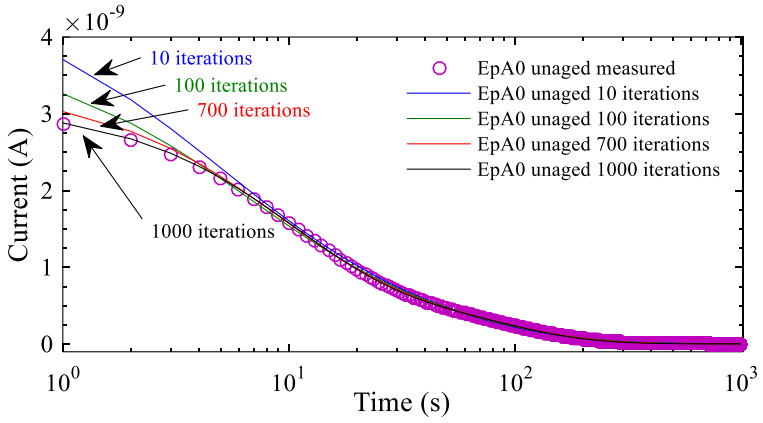

(b)

Figure 5.5 (a) Relaxation frequency distribution functions of EpA0 unaged, (b) relaxation current of EpA0 unaged (measured and fitted from RFD functions at different iterations instant).

In case of epoxy-alumina nano-composites, the macromolecular polymeric chains undergo polarization process when an electric field is applied to it. Depending on the length of the chains, the macromolecular polymer can be sensitive at different frequencies. As shown in Figure 5.5(a), most of the polymeric chains have relaxation time of nearly 100 s. This fact illustrates that the information about the condition of the polymeric insulation can be obtained through investigating the peaks near 0.01 Hz. Some polymeric chains become longer and exhibit sensitivity at lower frequencies, such as 1 mHz. Similarly, there are few polymeric chains whose length is smaller and sensitive at 0.1 Hz.

Due to the ageing of the epoxy insulation, the scissions reactions take place within the insulation resulting the development of short-chain macromolecular dipoles. Besides, due to the scission reaction, number of dipolar groups are increased which results in increment of RFD peak (as can be seen from Figure 5.6). These short-chain macromolecular dipoles are more sensitive to higher frequencies which results in increment of relaxation peak frequency (f_p). On the other hand, as the number of dipoles increase due to the ageing of epoxy insulation, the interactions among the dipoles also enhances during the application of excitation voltage. The increment of interactions among the dipoles in turn enhance the frictional loss within the insulation and hence the dielectric loss. Therefore, the higher value of RFD peak (M_p) indicates higher dielectric loss within the insulation. Due to ageing of epoxy resin at high temperature, hydroxyl group is oxidised in the presence of air. As a consequence, the macromolecular polymeric chain is broken within epoxy resin which further generates a radical as shown in Figure 5.7 [3, 142]. Moreover, the *C-H* bond of the carbon atom attached to the benzene ring is also ruptured and more free radicals are produced as the sample degrades (as shown in Figure 5.7).

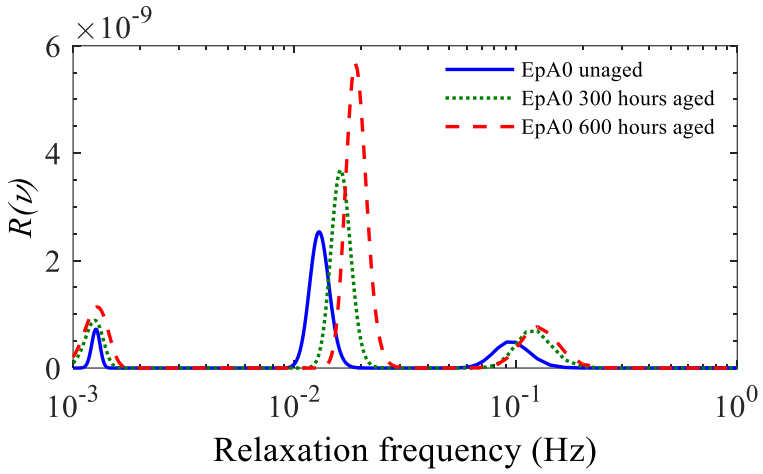
×10-9
6
4
2
0
R(ν)
EpA0 unaged
EpA0 300 hours aged
EpA0 600 hours aged
10-3
10-2
10-1
100
Relaxation frequency (Hz)

(a)

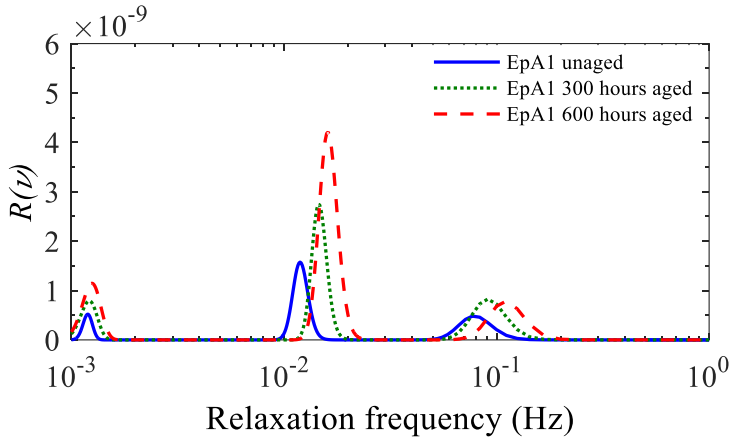
×10-9
6
5
4
3
2
1
0
R(ν)
EpA1 unaged
EpA1 300 hours aged
EpA1 600 hours aged
10-3
10-2
10-1
100
Relaxation frequency (Hz)

(b)

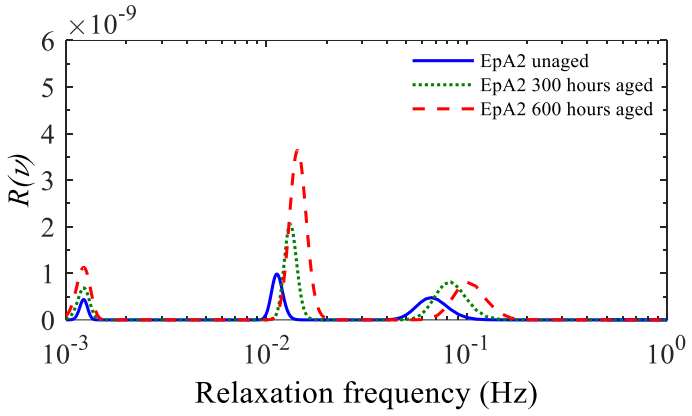

(c)

Figure 5.6 Relaxation frequency distribution functions at different ageing state of (a) EpA0, (b) EpA1, (c) EpA2.

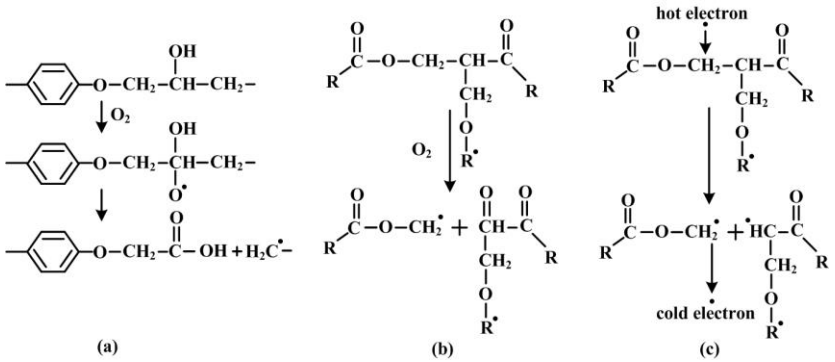

Figure 5.7 Chemical changes (a) oxidation-induced decomposition of hydroxyl, (b) breakage of C–H bond, (c) hot electron bombarding a molecular chain.

The spectrum of RFD function with variation of different filler concentration at specified ageing (unaged and 600 hours aged) state are shown in Figure 5.8(a) and Figure 5.8(b), respectively. From Figure 5.8(a) and Figure 5.8(b), it may be observed that, the major peak of the RFD function shifted towards lower frequency region with increment of alumina nano-particle concentration in the base epoxy resin. The lower magnitude major peak is observed for EpA2 during unaged condition. This may be due to the enrichment of nano particles, new bond or entanglement creates with nano-

particle and base epoxy resin. The polymeric chain length also enhances and forms new attribute or branches. The development of new attributes in polymeric chains may restrict the movement of the molecule during the application of electric field and reduces the peak (M_p) [37, 111]. This phenomenon results in minimization of dielectric loss with increment of the nano-particle concentration. Besides that, the shifting of major peak towards the lower frequency range with increment of nano-particle concentration signifies decrement of relaxation rate.

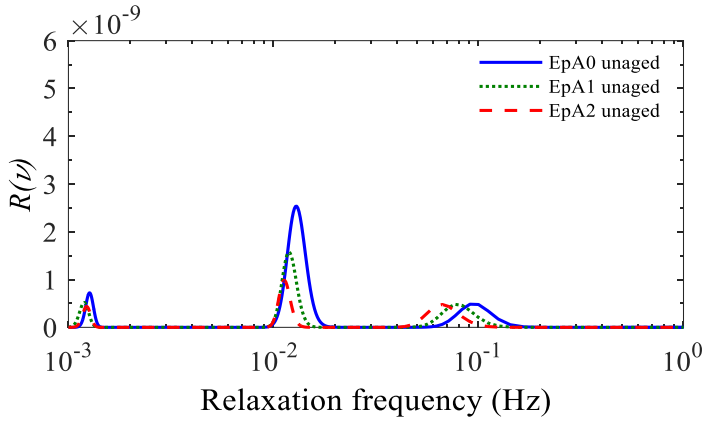

(a)

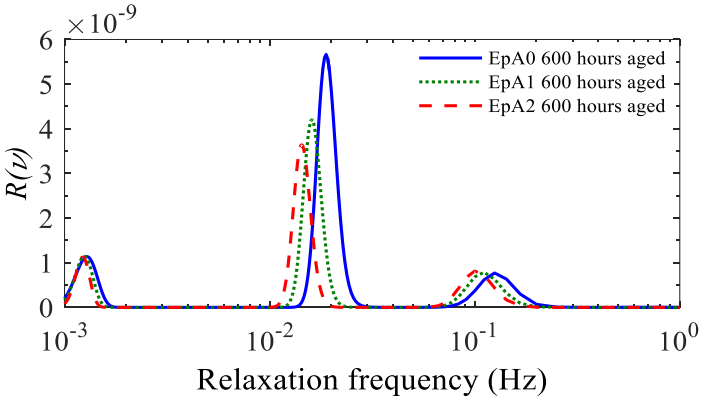

(b)

Figure 5.8 Relaxation frequency distribution functions of epoxy-alumina nano-composite with different filler concentration at (a) unaged, (b) 600 hours aged.

5.4.1.3 Estimation of Ageing Duration of Epoxy Alumina Nano-Composites Samples

The relaxation peak frequency (RPF) of the test samples obtained from the RFD function with different ageing state are shown in Table 5.4. It may be observed from Table 5.4 that, the RPF (f_p) value increases with the increment of ageing period and decreases with the enhancement of alumina nano-particles concentration.

Table 5.4: Relaxation Peak Frequency of Epoxy-Alumina Nano-Composites

Ageing duration (hours)	**f_p (Hz)**		
	EpA0	**EpA1**	**EpA2**
0	0.012987	0.011905	0.010615
100	0.013333	0.012500	0.011495
200	0.014493	0.013333	0.012358
300	0.016129	0.014493	0.013158
400	0.016949	0.014925	0.013333
500	0.018182	0.015625	0.013514
600	0.018868	0.016129	0.014286

As the RPF varies with ageing duration, it can be a very good ageing marker of the insulating material. Therefore, in the present work, RPF has been used to estimate the ageing state of EPNC insulation. The variation of RPF (f_p) with ageing durations has been shown in Figure 5.9. Based on the variation of f_p (as shown in Figure 5.9), an empirical relation for estimating the ageing duration was derived, as shown in equation (5.15). It is to mention here that the relationship in equation (5.15) has been derived using least square curve fitting (LSCF) technique.

$$aging\ \ duration\ \ (hours) = \frac{1}{\mu_2} \ln\left(\frac{f_p}{\mu_1}\right) \qquad (5.15)$$

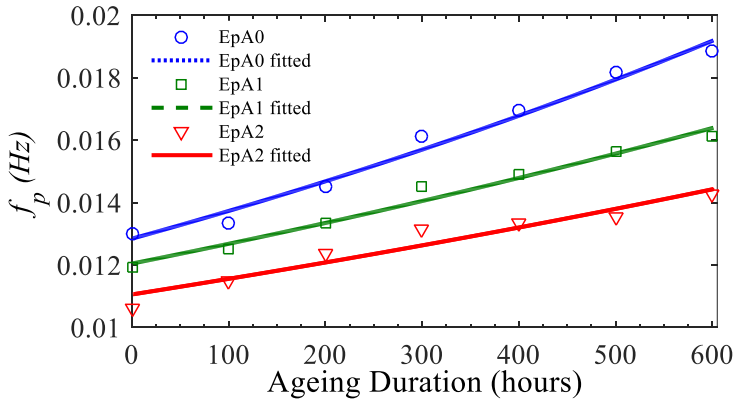

Figure 5.9 Variation of relaxation frequency (f_p) with ageing duration.

The estimated coefficients ('μ_1' and 'μ_2') of the equation (5.15) for different EPNC has been presented in Table 5.5. Table 5.5 shows that both coefficients, 'μ_1' and 'μ_2', decrease as the alumina nano-particle concentration increases. Therefore, the above analysis illustrates that the characteristics of the RFD function with respect to frequency are sensitive to variation of ageing state of the test samples (EPNC). Therefore, once the RPF (f_p) is evaluated from RFD function spectrum, then using equation (5.15), the electro-thermal ageing state of EPNC can be estimated.

Table 5.5: Fitted Coefficients of equation (5.15)

Parameter	**EpA0**	**EpA1**	**EpA2**
μ_1	0.012850	0.012050	0.011060
μ_2	0.000669	0.000513	0.000443
R^2	0.981800	0.977900	0.930600
RMSE	0.000342	0.000260	0.000367

From the RFD function spectra (in Figure 5.6 and Figure 5.8), it can be observed that the magnitude (M_p) of the RFD function at peak frequency (f_p) increases with increment of ageing duration. As discussed in Section IV-B, generation of more free radicals due to the scission reaction of macromolecular polymeric chain (effect of ageing), increases the number of dipoles as well as their relaxation frequencies. This fact enhances the value of f_p and M_p with ageing. Therefore, M_p can be an important ageing sensitive parameter to understand the ageing state of the insulating material. The

computed M_p values of the EPNC samples have been shown in Table 5.6. The variation of M_p values with ageing duration have been plotted in Figure 5.10. From the nature of the variation of the M_p values (estimated from Figure 5.6 and Figure 5.8), an empirical relation has been derived with M_p and ageing duration (in hours) using LSCF technique which is expressed as:

$$aging\ \ duration\ \ (hours) = \frac{M_p - p_2}{p_1} \tag{5.16}$$

Table 5.6: Relaxation Peak Magnitude of Epoxy-Alumina Nano-Composites

Ageing duration (hours)	***M*$_p$**		
	EpA0	**EpA1**	**EpA2**
0	2.53E-09	1.57E-09	4.33E-10
100	2.90E-09	2.13E-09	1.18E-09
200	3.22E-09	2.43E-09	1.65E-09
300	3.69E-09	2.74E-09	2.06E-09
400	4.34E-09	3.06E-09	2.62E-09
500	5.03E-09	3.55E-09	3.08E-09
600	5.67E-09	4.21E-09	3.65E-09

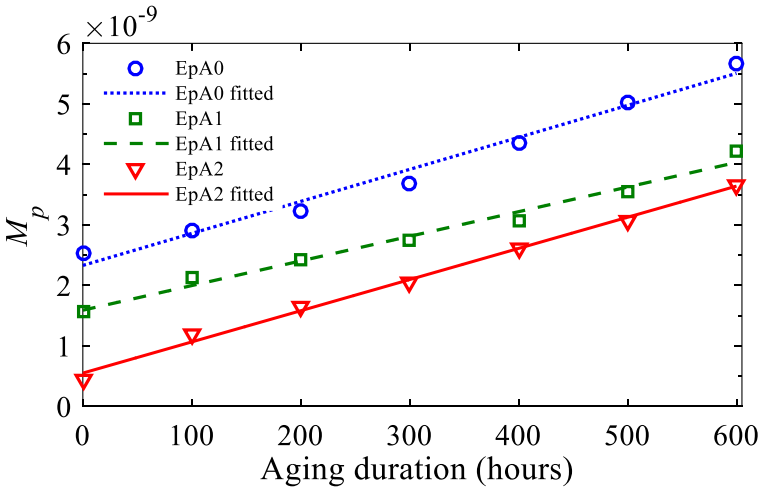

Figure 5.10 Variation of relaxation peak ('M_p') with ageing duration.

The parameters (p_1 *and* p_2) of equation (5.16) for EPNC samples have been shown in Table 5.7. It may be observed from Table 5.7 that, the variation of p_1 and p_2 decrease with increment of nano-particle. Therefore, from the above relation it can be suggested that the M can be an ageing sensitive parameter. Using relation (5.16), electro-thermal ageing state of different EPNC insulation can be estimated, if the M value from the RFD function spectra is evaluated.

Table 5.7: Fitted Coefficients of equation (5.16)

Parameter	EpA0	EpA1	EpA2
p_1	5.29E-12	4.07E-12	5.15E-12
p_2	2.33E-09	1.59E-09	5.51E-10
R square	0.9796	0.9818	0.9953
RMSE	1.81E-10	1.31E-10	8.40E-11

5.4.1.4 Validation of the Proposed Model for Epoxy Nano-Composites

In order to experimentally validate whether the ageing (electro-thermal) state of EPNC can properly be estimated using equations (5.15) and (5.16), three additional electro-thermally aged (450 hours aged) EPNC samples (EpA0, EpA1 and EpA2) were prepared. Initially, the PDC measurements were performed on these test samples. The RFD function for each of the samples was computed using the procedures as discussed in Section 5.2. From the RFD function, the RPF (f_p) was estimated for all the three samples of EPNC. Using equation (5.15), the ageing state of the EPNC samples were estimated by the help of the parameters shown in Table 5.3. The relative percentage errors of the estimated ageing duration (with respect to the actual ageing duration in hours) have been calculated for three test samples and presented in Table 5.8. Again, the magnitude of the peak of the RFD function (M_p) for these test samples have been computed adopting the procedures given in Section 5.2. Using equation (5.16), the ageing duration of the three EPNC samples have been calculated using the parameters given in Table 5.5. The relative percentage error of the estimated ageing duration with respect to the actual ageing duration has been calculated and shown in Table 5.9. It may be observed from Table 5.8 and Table 5.9 that the electro-thermal ageing state of the test samples can closely be estimated by using equations (5.15) and (5.16). The calculated errors of the estimated ageing duration using equation (5.15) are within 4.5%. On the other hand, the estimated errors of the ageing duration for same test samples by using equation (5.16) are within 5.5%. Therefore, it can be understood that the proposed method can reliably estimate the ageing state of the EPNC insulation.

Table 5.8: Estimated Ageing State Using *fp*

Sample	f_p (*Hz*)	Ageing duration (hours)	Estimated ageing duration by equation (5.15)	Error (%)
EpA0	0.01714	450	430.93	4.23
EpA1	0.01504	450	431.75	4.06
EpA2	0.01342	450	437.07	2.87

Table 5.9: Estimated Ageing State using Magnitude of the Relaxation Peak (*'M_p'*)

Sample	M_p	Ageing duration (hours)	Estimated ageing duration by equation (5.16)	Error (%)
EpA0	4.58E-9	450	425.33	5.48
EpA1	3.33E-9	450	427.51	4.99
EpA2	2.78E-9	450	432.81	3.82

5.4.2 Analysis Based on XLPE Insulation

In this sub-section, the results and analysis of the XLPE cable insulation has been discussed.

5.4.2.1 Variation of Depolarization Current with Moisture Content

At first, the PDC measurement was performed on the XLPE cable samples at 1 kV d.c. voltage. Based on PDC measurement, the relaxation current of the test XLPE cable samples were recorded. Figure 5.11 shows the recorded relaxation current, normalized by cable length, for XLPE cable samples with varying moisture content. As shown in Figure 5.11, the relaxation current increases proportionally with the moisture content (m.c.) in the XLPE cable insulation.

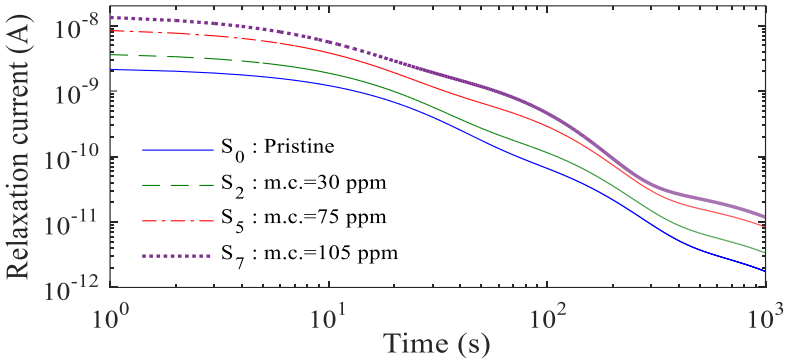

Figure 5.11 Relaxation current of XLPE cable insulation with different moisture content.

5.4.2.2 Investigation using Frequency Distribution Functions

From the relaxation currents of different samples, the relaxation frequency distribution (RFD) functions have been calculated using the procedure described in [85, 139]. The estimated RFD functions of different XLPE samples (i.e. S_0 to S_7) have been presented in Figure 5.12. As the XLPE is a polymeric insulation, it has several polymeric chains of different lengths which are formed different dipolar groups. When an electric field is applied across the insulation, these dipolar groups are oriented along the field direction. In this context, it is to be mentioned here that depending upon the nature of the dipolar groups their relaxation process also varies with different time instants. Therefore, the dipolar groups are sensitive to different frequencies. As a consequence, the distribution of RFD function has different relaxation peak. Hence, from Figure 5.12, it has been observed that, the RFD function of all XLPE cable samples three distinct peaks i.e. first peak at near 1 mHz, second peak near 10 mHz and the third peak near 100 mHz range. Those three peaks represent different relaxation zone, at where the dipolar groups of the insulating material are more sensitive. The first peak, observed at very low frequencies (near the 1 mHz range), is likely caused by electrode polarization effects [160]. The second peak (at 10 mHz range) which is sensitive to the inter-cluster polarization. The third peak, observed at higher frequencies (near 100 mHz), corresponds to the presence of trapped or loosely bound charges caused by impurities or localized defects in the XLPE insulation layer [138]. It can be understood from Figure 5.12 that, among those three peaks, the second and third peaks are related to the condition of the insulation. In addition, the second peak carrying the information of the cluster (i.e. group of dipoles having similar

relaxation phenomenon), which is one of the promising signature for assessment of the insulation condition and the third peak relating to the impurities or defects in XLPE insulation which in turn signifies the deterioration of the insulation. Comparing those, the second peak has larger magnitude. It is yet to be mentioned here that, with increment of m.c. in the XLPE insulation the second peak increases prominently than the other peaks. It defines that the number of clusters formation due to moisture in the XLPE insulation are sensitive to relaxation frequencies near the 10 mHz range. Figure 5.12 shows that the magnitude of the second peak increases as the moisture content (m.c.) in the XLPE insulation rises. This fact in turn indicates that the magnitude of the peak represents the dielectric loss (which is due to the friction loss of the dipolar groups during relaxation).

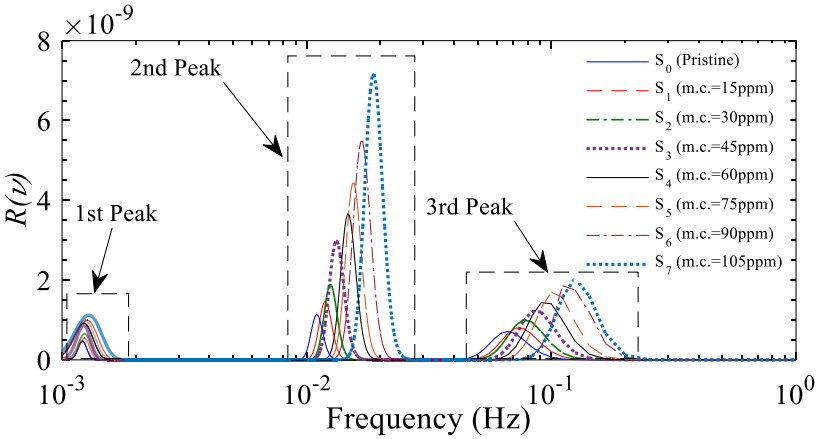

Figure 5.12 Relaxation frequency distribution functions of the XLPE cable insulation with different moisture content.

According to Dissado-Hill cluster model, in normal XLPE insulation there are several dipoles which have similar relaxation characteristics form individual cluster (i.e. intra cluster) and the several clusters are attached with each other through inter-cluster movement (as shown in Figure 5.13) [161-162]. In addition, the intra-cluster is formed with long-chain polymer with partial regularity. But, when the water molecules get into the insulation, they may create structural disorder as well as generation of localized coupled vibration regions in the presence of electric field [163]. Result of that, it helps to form new smaller size dipole clusters. Therefore, with inrush of the moisture, the number of cluster are increased. In

addition, the moisture is a polar group, during field stress it responds more effectively than the normal XLPE insulation. It has also been observed from Figure 5.12 that the highest peak (i.e. 2nd peak) is shifted towards the higher frequency with increment of m.c. in the XLPE insulation. It can be explained that, the increase of moisture ensures the formation of more polar cluster groups. As the polar groups are increased in the insulation, they are more flex to the electric field which ensures the increase of the relaxation rate. Therefore, the required relaxation time by the cluster groups are also less, which in turn reduces the relaxation time.

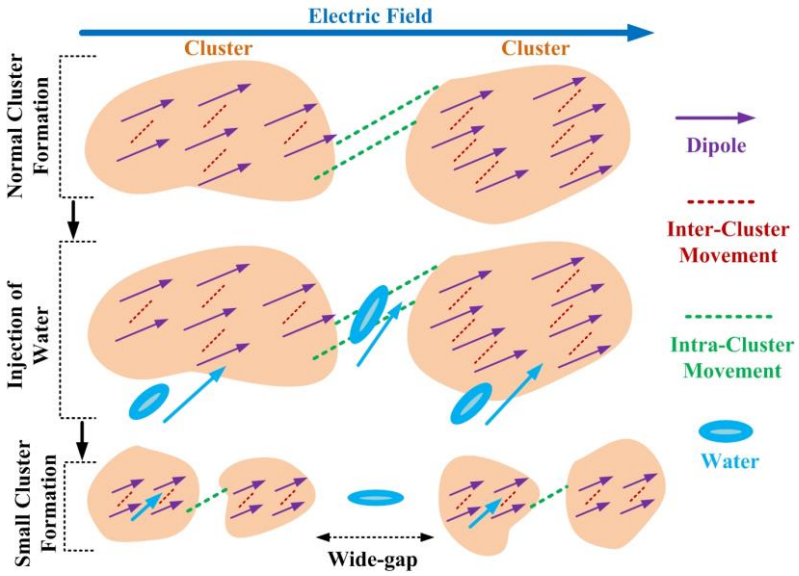

Figure 5.13 Cluster model of the XLPE insulation.

In addition, the crystallinity of XLPE insulation has two regions, i.e. crystalline region and amorphous region. The macromolecular polymeric chains are cross-linked and create lamella or lamellar crystal region. In between lamellar crystal regions, there are several amorphous regions where the polymeric chains are shorter in length and the degree of freedom of the chain movement is higher than the crystalline region [164]. Injection of water molecules in the XLPE insulation, the amorphous regions are widened and they (water molecules) try to bend or stretch the lamellar crystal region (as shown in Figure 5.14) as well as lead to form short polymeric chains. Hence, increment of amorphous regions may promote to enhance the degree of freedom of the dipolar movement. Therefore, with

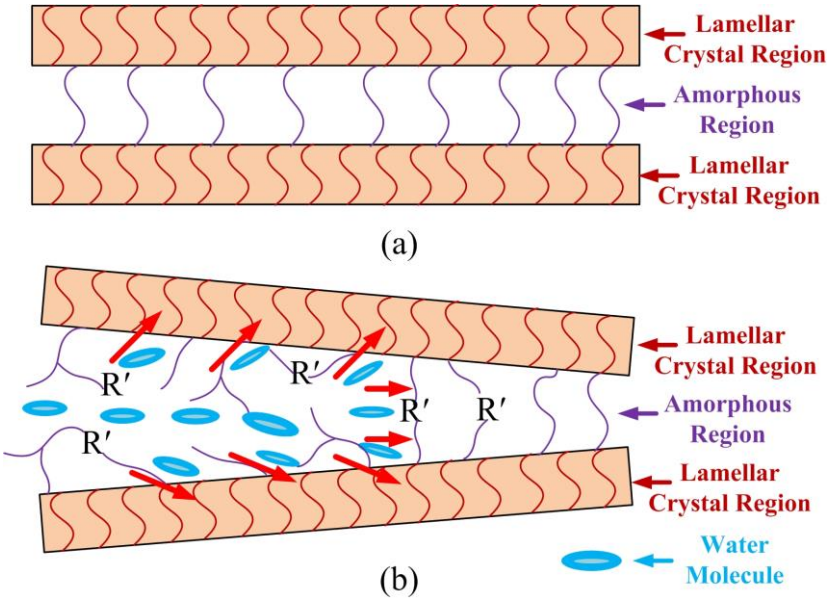

Figure 5.14 Schematic of XLPE insulation (a) under normal condition, (b) with water induced XLPE (with impact of water micro-beads).

increment of the m.c., the dipoles may orient themselves faster, in turn increase the relaxation rate. On the other side, the third peak which implies the defect or impurity in the insulation, that also signifies the insulation's condition. As the water content increases, the defects in the insulation also increase. This fact in turn increases the magnitude of the relaxation peak (3rd peak) with increment of m.c. As, the relaxation phenomenon changes in the insulation due to water injection, therefore this water injection (i.e. degradation of the XLPE insulation) is indirectly affects the relaxation phenomenon. Result of that, relaxation time get reduced and the relaxation frequencies (i.e. the relaxation of the 2nd and 3rd RFD peaks) are shifted towards higher frequency with increase of moisture content. From the above investigation it has also been identified that the magnitude of the relaxation peaks (i.e. 2nd and 3rd peak magnitude: M_{p2} and M_{p3}, respectively) and the corresponding relaxation frequencies (i.e. frequency at which peaks occur: f_{p2} and f_{p3}, respectively) are sensitive to the m.c. of the XLPE insulation. Therefore, M_p and f_p can effectively be utilized as m.c sensitive markers of the XLPE cable insulation.

5.4.2.3 Estimation of the Moisture Content of XLPE Cable Samples

The magnitude of the 2nd and 3rd relaxation peaks (i.e. M_{p2} and M_{p3}) have been estimated from the RFD function spectra of the test insulation samples as shown in Figure 5.12. The estimated M_{p2} and M_{p3} values of the different XLPE samples have been represented in Table 5.10.

Table 5.10: Relaxation Peak (*'M_p'*) of XLPE cable samples

Name	M_{p2}	M_{p3}	$\xi = (M_{p2} / M_{p3})$
S_0	1.1361E-09	7.1449E-10	1.5901
S_1	1.4696E-09	8.4816E-10	1.7327
S_2	1.8980E-09	1.0053E-09	1.8879
S_3	2.9813E-09	1.4157E-09	2.1058
S_4	3.6615E-09	1.5355E-09	2.3846
S_5	4.4360E-09	1.7001E-09	2.6093
S_6	5.4827E-09	1.8583E-09	2.9504
S_7	7.1598E-09	2.0524E-09	3.4885

It can be observed from Table 5.10 that the peaks magnitude (both M_{p2} and M_{p3}) increase with the increment of the m.c. in the XLPE insulation. As peak-magnitude represents the polarization loss and it varies with moisture content, therefore, it may be an effective m.c. sensitive marker. In this investigation, the values of M_{p2} and M_{p3} were used to estimate the moisture content (m.c.) of the XLPE insulation. The variations of M_{p2} and M_{p3} with moisture content have been plotted in Figures 15(a) and 15(b), respectively. Based on the variations of M_{p2} and M_{p3} (as plotted in Figure 15), an empiric relationship has been derived to obtain the m.c. of the XLPE insulation as stated in equation (5.17). It is to be mentioned here that this relation has been obtained by using least square curve fitting (LSCF) technique.

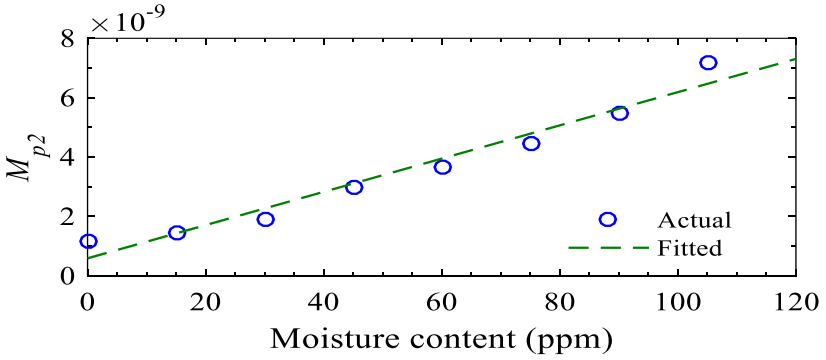

(a)

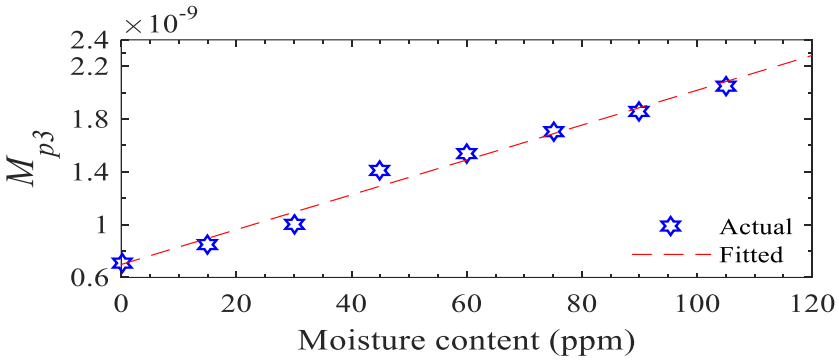

(b)

Figure 5.15 Variation of relaxation peak with moisture content (a) M_{p2}, and (b) M_{p3}.

$$m.c.\ (ppm\ ) = \frac{M_p - \alpha_2}{\alpha_1} \tag{5.17}$$

The calculated coefficients (i.e. α_1 and α_2) of the equation (5.17) for both M_{p2} and M_{p3} have been tabulated in Table 5.11. Therefore, using these coefficients the m.c. of the XLPE insulation can be estimated by equation (5.17).

Table 5.11: Fitted Coefficients of equation (5.17)

Parameter	Value	
	M_{p2}	M_{p3}
α_1	5.597E-11	1.319E-11
α_2	5.896E-10	6.988E-10
R^2	0.9824	0.9723

Apart from the M_{p2} and M_{p3} values, another parameter ξ have been calculated, which is the ratio of M_{p2} and M_{p3} (i.e. $\xi = M_{p2} / M_{p3}$). The calculated ξ values have been shown in Table 5.10. It has been observed from the Table 5.10, the ξ value increases with the ingress of the moisture in the XLPE insulation. Since, the ξ is sensitive to m.c., hence it can be used as an m.c. ingression indicator. Therefore, an empirical relationship (i.e. equation (5.18)) has been developed between m.c. and ξ value using LSCF technique. Figure 5.16 shows the variation of ξ values with moisture content (m.c.). The estimated co-efficients of the (5.18) have been tabulated in Table 5.12.

$$m.c.(ppm) = \lambda_1(\xi)^{\lambda_2} + \lambda_3 \tag{5.18}$$

Table 5.12: Fitted Coefficients of equation (5.18)

Parameters	Value
λ_1	-334.5
λ_2	-0.7599
λ_3	235.3
R^2	0.9987

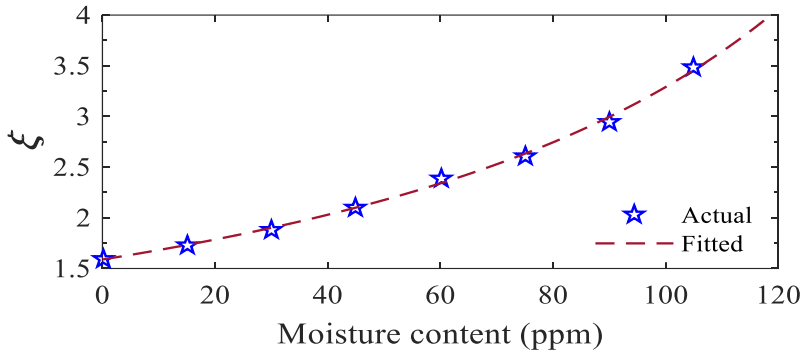

Figure 5.16 Variation of relaxation peak ratio (ξ) with moisture content.

From the relaxation frequency distribution spectra (as shown in Figure 5.12), the relaxation peak frequencies (frequencies at the position of M_{p2} and M_{p3} i.e. f_{p2} and f_{p3}, respectively) of different XLPE samples have been computed. The computed f_p values of the XLPE samples with different m.c. have represented in Table 5.13.

Table 5.13: Relaxation Frequency of XLPE cable insulation samples

Name	f_{p2} (mHz)	f_{p3} (mHz)
S_0	10.989	66.667
S_1	11.905	71.429
S_2	12.500	76.923
S_3	13.158	83.333
S_4	14.706	90.909
S_5	15.625	100.000
S_6	16.667	111.111
S_7	18.868	125.000

It can be observed from Table 5.13 that both f_{p2} and f_{p3} values increase with the inrush of the m.c. in the XLPE insulation. This fact can be described as the moisture increases, the relaxation rate of the insulation dielectrics increases and as a result the relaxation frequency get increased. Therefore, f_{p2} and f_{p3} values varies. As, the f_{p2} and f_{p3} vary with the m.c. in the XLPE

insulation, therefore, f_{p2} and f_{p3} has been used as m.c. estimating parameter. The variations of f_{p2} and f_{p3} (in Hz) with m.c. have been shown in Figures 5.17(a) and 5.17(b), respectively. From the variation nature of the f_{p2} and f_{p3} in Figure 5.17, an empirical relation has been derived using LSCF technique, stated as (5.19).

$$m.c.(ppm) = \frac{1}{\beta_2} \ln\left(\frac{f_p}{\beta_1}\right) \tag{5.19}$$

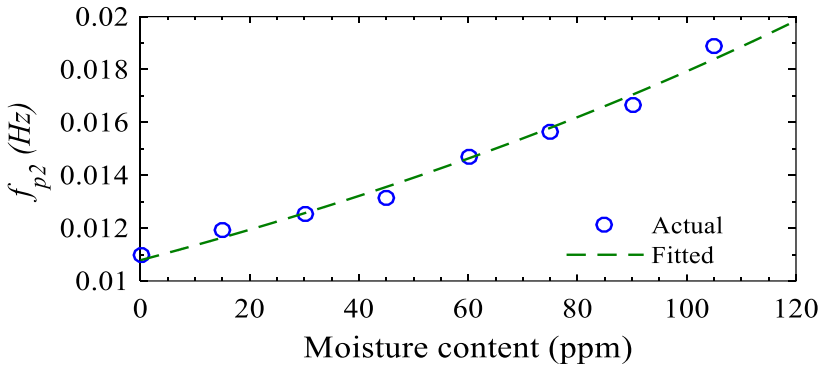

(a)

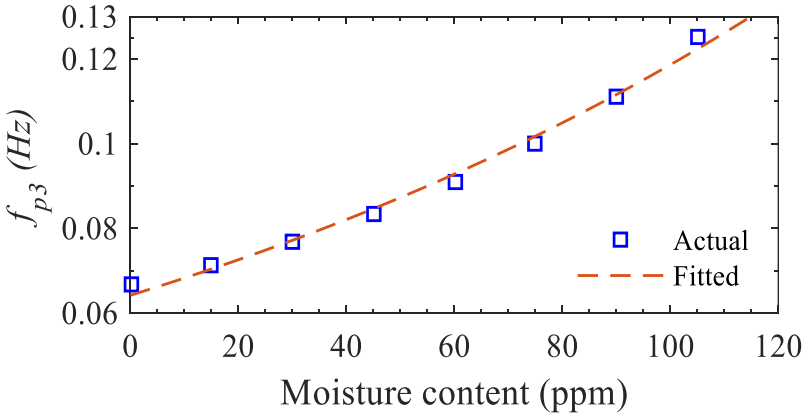

(b)

Figure 5.17 Variation of relaxation frequency with moisture content (a) f_{p2}, and (b) f_{p3}.

The estimated coefficients (i.e. β_1 and β_2) of equation (5.19) have been represented in Table 5.14.

Table 5.14: Fitted Coefficients of equation (5.19)

Parameters	Value	
	f_{p2}	f_{p3}
β_1	0.010790	0.064230
β_2	0.005082	0.006138
R^2	0.9864	0.9920

5.4.2.4 Validation of the Proposed Technique for XLPE Insulation

In this paper, a RFD based technique has been applied to estimate the m.c. in the XLPE insulation. For this investigation, five empirical relationships have been developed correlating the m.c. in the XLPE cable insulation. To validate the proposed scheme, three XLPE cable samples with known m.c. (i.e. 35, 65, and 80 ppm) were prepared. Thereafter, relaxation currents have been measured and the five different ageing sensitive parameters have been estimated as tabulated in Table 5.15. Based on those parameters, the m.c. of the test samples have been calculated through equations (5.17), (5.18) and (5.19) using the parameters have been stated in Tables 5.11, 5.12 and 5.14, respectively. The estimated m.c. and the error percentage with actual m.c. of the test XLPE cables have been tabulated in Table 5.15. Based on the estimated m.c., it may be observed that the proposed technique can closely predict the m.c. of the XLPE insulation with an acceptable deviation. From those predicted m.c. values, it has been identified that the estimated result using f_{p2} ensures closer estimation with lesser error compare to the estimated result using f_{p3}. Therefore, it can be inferred that the relaxation frequency zone of the second peak (i.e. near 10 mHz range) is more sensitive to the presence of water in the insulation. It was observed that the ξ parameter predicted the moisture content (m.c.) of the XLPE cable insulation with greater accuracy compared to the other parameters.

Table 5.15: Estimated Moisture Content Using Proposed Empirical Relationships

Actual Moisture Content (ppm)		35	65	80
Estimated Parameters	M_{p2} ($\times 10^{-9}$)	2.4265	3.964	5.2497
	M_{p3} ($\times 10^{-9}$)	1.2189	1.6558	1.8482
	ξ	1.9907	2.394	2.8404
	f_{p2} (mHz)	12.990	14.714	16.514
	f_{p3} (mHz)	81.043	98.535	108.596

Predicted Results	**Predicted Moisture Content (ppm)**	M_{p2}	32.82	60.29	83.26
		M_{p3}	39.43	72.55	87.14
		ξ	37.07	63.00	83.98
		f_{p2}	36.51	61.04	83.75
		f_{p3}	37.88	69.72	85.56
	Prediction Errors (%)	M_{p2}	06.23	07.25	04.08
		M_{p3}	12.67	11.62	08.93
		ξ	05.90	03.08	04.98
		f_{p2}	04.31	06.09	04.69
		f_{p3}	08.23	07.26	06.95

5.5 Conclusions

In this Chapter, a novel technique has been proposed to estimate the electro-thermal ageing state of epoxy nano-composites (EPNC) insulation and moisture content in XLPE insulation using dielectric relaxation current (DRC).

Primarily, this study focuses the effectiveness of relaxation peak frequency (f_p) and relaxation peak magnitude (M_p) for estimating the ageing state of epoxy nano-composites. In order to investigate the relaxation process, the RFD functions have been evaluated from the DRC response. At the major peak of RFD of the test samples, two ageing sensitive parameters (relaxation peak frequency (f_p) and peak value of the RFD function (M_p)) have been estimated. Table 5.4 shows that the f_p value decreases as the concentration of nano-filler (Al_2O_3) increases and rises with the progression of ageing. As seen in Table 5.6, the M_p value decreases with higher concentrations of nano-filler (Al_2O_3) and increases as ageing progresses. Based on the variation of f_p and M, two empirical relations have been derived (as shown by (5.15) and (5.16)). Three new test samples have been prepared for experimental validation of (5.15) and (5.16). The RFD functions of these test samples have been evaluated from their measured DRC and based on that, the corresponding f_p and M_p values have been estimated. Using the evaluated f_p and M_p values, the ageing state of these three test samples have been estimated using (5.15) and (5.16). Tables 5.8 and 5.9 demonstrate that the ageing state of the test samples can be accurately estimated using the derived empirical relations. However, the comparative analysis in Tables 5.8 and 5.9 indicates that f_p results in lower estimation errors than M_p when assessing the

ageing status of the insulation. Thus, the proposed technique can be used to investigate the relaxation characteristics as well as the ageing state of real life polymeric or composites insulations.

Similarly, an experimental investigation has been carried out on the several short section of the 11 kV XLPE cable samples having different m.c. (i.e. pristine, 15, 30, 45, 60, 75, 90, and 105ppm). Initially, the relaxation current of the test XLPE cable samples have been recorded at d.c. stress of 1kV. From the recorded relaxation current, the relaxation frequency distribution (RFD) function has been analyzed in the frequency range 1 mHz to 1 Hz to diagnosis the m.c. of the XLPE cable. Based on the distribution of the RFD function, the different relaxation zones have been explored which are correlated with the physical phenomenon of the XLPE insulation. Five m.c. sensitive parameters (i.e. M_{p2}, M_{p3}, ξ, f_{p2} and f_{p3}) are estimated from the RFD function. These five parameters are correlated with the m.c. in the XLPE cable insulation by empirical relations. These empirical relations are further verified with a new set of XLPE cable insulation with different m.c. From the observation of the validated results (as shown in Table 5.15), it has been identified that the relaxation frequency of the highest magnitude peak (i.e. f_{p2}) of the RFD function is more sensitive than the other relaxation frequency peak (i.e. f_{p3}). This investigation concludes that the proposed scheme can reliably estimate the moisture content of real-life XLPE cables, thereby enhancing the reliability of power system networks.

Chapter 6

Conclusions

In this dissertation, efforts have been made to establish different methodologies for condition assessment of dry-type insulation used in high voltage systems. The methodologies and investigation approaches for developing the condition assessment techniques are designed to be simple, straightforward, and easy to apply for ageing state estimation of dry-type insulation. In general, polymeric insulation is used as dry-type insulation in high-voltage equipment. In this dissertation work, different polymeric insulation such as LDPE, XLPE, Epoxy resin etc. are used for the experimental purpose. For the condition assessment, the dielectric response measurement methods are considered in this thesis work.

Nowadays, polymeric insulation and its nanocomposites have been a popular choice as dry-type insulation for high voltage applications (such as dry-type transformers, rotating machines, power cables, etc.). However, the dielectric response current measurement (i.e. polarization and depolarization current) of the polymeric insulation is quite challenging due to its low magnitude (in the range of few pA). In the ***Chapter 2*** of this thesis, an experimental setup has been developed for the measurement of polarization and depolarization current (PDC) suitable for the dry-type insulation. The developed experimental setup offers several advantages, such as capable to record low magnitude of current (in the range of pA), portability as well as low development cost. In addition, the experimental unit can able to distinguish different aged insulation samples as well as different ambient temperature measurement. Therefore, this developed model is suitable for onsite PDC measurement of the dry-type insulation.

During high voltage (HV) application, the polymeric insulations are influenced through multiplicative effects such as ionization collision and field emission etc. Result of that space charges are generated in the bulk of the polymeric insulation and further these charges are trapped or de-trapped during the charging and discharging phases. In addition, due to ageing of the insulation the bahaviour of the charge trapping characteristics are changed. So, the charge trapping and de-trapping characteristics are useful for the

condition assessment of the dry-type insulation. In the ***Chapter 3***, a methodology has been developed to investigate charge trapping characteristics by extracting the de-trapping current from the depolarization current. Further, the trapping parameters (i.e. trap depth and trap density) have also estimated from the detrapping current. For the experimental analysis, epoxy alumina nanocomposite insulation has been taken and the thermal ageing of the insulation has been performed. From the experimental results, it has been observed that with progress of thermal ageing generates deep traps. It can be justified as, with the thermal ageing due to material expansion generates new trapping sites as well as the scission reaction in the polymeric chain molecules creates new defects results in formation of new trapping sites. On the other hand, incorporation of alumina nanoparticles into the epoxy resin insulation creates new bonding with the base resin which further influences in reduction of deep traps. Overall, the proposed methodology is very straightforward for understanding the trapping characteristics from the depolarization current analysis.

From the methodology discussed in ***Chapter 3***, it is possible to extract the charge de-trapping current from the depolarization current measurements. However, obtaining detailed information about the charge de-trapping characteristics requires longer measurement durations (more than an hour) of charging under high voltage stress. Result of that, when the measurements are taken over an extended period, there may be a chance of occurrence of electrode polarization. Electrode polarization refers to the buildup of a charge layer on the surface of an electrode when it is in contact with the insulating material, which can alter the behavior of the insulation. This occurs as charges migrate within the insulation and accumulate on the electrode surface, leading to polarization. Consequently, the true relaxation behavior of the dielectric material is obscured by this effect. A similar issue can arise during frequency domain measurements, particularly at low frequencies (near to 1 mHz). Therefore, to accurately understand the dielectric material's relaxation behavior, the effect of electrode polarization must be eliminated. In ***Chapter 4***, a methodology has been developed to minimize the effect of electrode polarization and reveals the actual relaxation behavior of the insulation dielectric. In this work, electric modulus (i.e. inverse of the complex permittivity) has been utilized with the help of Cole-Cole relaxation model to reveal the relaxation process of the insulation material. For the experimental investigation, epoxy-alumina nanocomposite insulation has been used and its thermal ageing has been performed. Using the proposed methodology two ageing sensitive parameters (i.e relaxation frequency (f_p)

and Cole-Cole model shape parameter (β)) have been identified and two empirical relationships have been derived. From the experimental validation, it has been identified that the proposed methodology is able to estimate the ageing state of the epoxy nanocomposite with suitable accuracy.

The relaxation behavior of the polymeric insulation depends on its macromolecular structure. The macromolecular structure further related to the polymeric chain length as well as the concentration of the amorphous region and crystalline region in the polymer matrix. In addition, ageing of the insulation causes chain scissoring or stretching and create smaller polymeric chains. Depending on the chain length as well as the macromolecular structure, the relaxation behavior of the dipoles inside the polymeric insulation are different. Hence, for proper condition assessment of the polymeric insulation requires exact relaxation model which may reveals different relaxation processes. In this context, there are different relaxation models such as Debye model, Cole-Davidson model, and Havriliak-Negami (H-N) model, those models can able to model dielectric relaxation current based on multiple distinct relaxation times. Result of that, the modeling of relaxation currents using those models may sometimes deviate from the actual measured relaxation current, potentially obscuring crucial information about the insulation characteristics. In ***Chapter 5***, a methodology has been developed to address this problem. The proposed methodology named Relaxation Frequency Distribution (RFD) method is able to model the dielectric relaxation current by considering closely related relaxation times depending on the different relaxation process of the polymeric insulation. In this methodology, the RFD spectrum can reveal the distribution of the relaxation coefficient with respect to relaxation frequencies. For experimental investigation, i) epoxy-alumina nanocomposite insulation has been used and its electro-thermal ageing has been performed and ii) XLPE cable insulation has been used and its moisture ageing has been done. From the distribution of the RFD spectrum two ageing sensitive parameters such as relaxation peak frequency (f_p) and relaxation peak magnitude (M_p) has been identified and based on these parameters two empirical relationships has been developed for the estimation of the ageing state of the epoxy-alumina nanocomposite insulation. Similarly, for the moisture content (m.c.) estimation of the XLPE cable, five m.c. sensitive parameters (i.e. M_{p2}, M_{p3}, ξ, f_{p2} and f_{p3}) are identified and corresponding empirical relationships have been derived. Finally, from the experimental validation, it has been observed that the proposed methodology is able to estimate the ageing state of the epoxy nanocomposite as well as m.c. of the XLPE insulation with suitable accuracy.

From the overall analysis of the thesis it can be concluded that the proposed methodologies may able to estimate insulation condition (i.e. trap characteristics, ageing state of epoxy alumina nano composite, moisture content of the XLPE cable insulation). The overall findings can be helpful for the insulation diagnosis of the dry-type insulation for real life application in high voltage system.

6.1 Scope of Future Works

Future research can explore various directions, some of which are highlighted below.

In this thesis, a methodology has been established to estimate the de-trapping current from the depolarization current measurement. From the de-trapping current, the trapping parameters (i.e. trap density and trap depth) have been estimated. In future, it can be tried to evaluate more precisely the contribution of the hole charge carriers as well as electron charge carriers in the de-trapping current. There may be a scope to evaluate different other parameters such as the charge carrier mobility, trap cross section etc. from PDC analysis.

In this thesis, the proposed methodologies have been performed for a particular ambient temperature condition. However, in case of real-life application, the value of the ambient temperature is dependent on the environmental condition and it may vary from day to day, season to season. Result of that, it may provide dissimilarities in the insulation condition estimation even if the insulation condition is not changed. Considering this fact, there may be a future scope to improve those proposed methodologies and make it independent of temperature.

Finally, it is worthwhile to mention that this thesis has presented various empirical relationships derived through specific mathematical approaches for a particular type of dry-type insulating material, which can be used for different other materials with suitable modification in coefficients of the empirical relationships.

References

[1] W. S. Zaengl, "Dielectric spectroscopy in time and frequency domain for HV power equipment. I. Theoretical considerations", IEEE Electrical Insulation Magazine, Vol. 19, No. 5, pp. 5-19, 2003.

[2] S. Chakravorti, D. Dey and B. Chatterjee, "Recent Trends in the Condition Monitoring of Transformers-Theory, Implementation and Analysis", (1st Edition) Springer-Verlag London, 2013.

[3] Y. Wang, C. Feng, R. Fei and Y. Luo, "Thermal-ageing characteristics of dry-type transformer epoxy composite insulation", High Performance Polymers, Vol. 32, No. 7, pp. 741-752, 2020.

[4] M. Wen, J. Song, Y. Song, Y. Liu, C. Li and P. Wang, "Reliability assessment of insulation system for dry type transformers", IEEE Transactions on Dielectrics and Electrical Insulation, Vol. 20, No. 6, pp. 1998-2008, 2013.

[5] S. Asefi, S. Asefi, B. Asad, M. Leinakse, H. Manninen, J. Kilter, T. Vaimann, A. Kallaste, M. Tealane, and M. Landsberg, "Review of High Voltage Instrument Transformer Condition Monitoring", IEEE Transactions on Dielectrics and Electrical Insulation, 2024 (in Press).

[6] B. Biswas, B. X. Du, M. Florkowski, T. Hammarström, M. D. Judd, W. Kołtunowicz, B. Kordi, M. Kuniewski, G. Ma, C. Pan, C. Park, A. K. Pradhan, L. Satish and G. Stone, "Trends in Diagnostics and Monitoring of High-Voltage Insulation", IEEE Electrical Insulation Magazine, Vol. 40, No. 4, pp. 6-26, 2024.

[7] T. K. Saha, "Review of modern diagnostic techniques for assessing insulation condition in aged transformers", IEEE Transactions on Dielectrics and Electrical Insulation, Vol. 10, No. 5, pp. 903-917, 2003.

[8] M. Baranski, A. Decner and A. Polak, "Selected diagnostic methods of electrical machines operating in industrial conditions", IEEE Transactions on Dielectrics and Electrical Insulation, Vol. 21, No. 5, pp. 2047-2054, 2014.

[9] M. Erdogan and M. K. Eker, "A Comparative Analysis of Partial Discharge in 13 Combined Insulation Structures of 11 Materials Used in Cast-Resin Dry-Type Transformers", IEEE Transactions on Dielectrics and Electrical Insulation, Vol. 29, No. 6, pp. 2330-2339, 2022.

[10] Q. Ge, M. Wang, H. Jiang, Z. Lu, G. Yao and C. Sun, "Health Management of Dry-Type Transformer Based on Broad Learning System", IEEE Transactions on Industrial Electronics, Vol. 69, No. 3, pp. 3027-3036, 2022.

[11] Y. Li, A. Zhang, J. Huang and Z. Xu, "An Approach Based on Transfer Learning to Lifetime Degradation Rate Prediction of the Dry-Type Transformer", IEEE Transactions on Industrial Electronics, Vol. 70, No. 2, pp. 1811-1819, 2023.

[12] IS 335: 2018, Fifth Revision "New Insulating Oils-Specification", Indian Standard 2018.

[13] S. Chatterjee, "Studies on Measurement Time Reduction Techniques for Insulation Diagnostics in High Voltage Equipment", Phd Thesis, Jadavpur University, Kolkata, India, 2019.

[14] N. Lelekakis, J. Wijaya, D. Martin, and D. Susa, "The effect of acid accumulation in power-transformer oil on the aging rate of paper insulation", IEEE Electrical Insulation Magazine, Vol. 30, No. 3, pp. 19-26, 2014.

[15] T. V. Oommen and L. N. Arnold, "Cellulose Insulation Materials Evaluated by Degree of Polymerization Measurements", Proceedings of 15th IEEE Electrical and Electronics Insulation Conference (EIC), Chicago, IL, USA, pp. 257261, 1981.

[16] A. K. Pradhan, "Condition Monitoring of Transformer Insulation by Frequency Domain Spectroscopy using Non-sinusoidal Excitation", Phd Thesis, Jadavpur University, Kolkata, India, 2016.

[17] T. K. Saha and P. Purkait, "Transformer Ageing: Monitoring and Estimation Techniques", (1st Edition) John Wiley and Sons, 2017.

[18] D. J. T. Hill, T. T. Le, M. Darveniza and T.K. Saha, "A study of the degradation of cellulosic insulation materials in a power transformer. Part III: Degradation products of cellulose insulation paper", Polymer Degradation and Stability, vol. 51, no. 2, pp. 211-218, 1996.

[19] M. Schaible, "Electrical insulating papers–an overview", IEEE Electrical Insulation Magazine, Vol.3, No.1, pp. 8–12, 1987.

[20] G. C. Montanari, P. Seri, X. Lei, H. Ye, Q. Zhuang, P. Morshuis, G. Stevens and A. Vaughan, "Next generation polymeric high voltage direct

current cables—A quantum leap needed?", IEEE Electrical Insulation Magazine, vol. 34, no. 2, pp. 24-31, 2018.

[21] P. Chen, Y. Huang, F. Zeng, Y. Jin, X. Zhao and J. Wang, "Review On Insulation And Reliability Of Dry-type Transformer", Proceedings of the 2019 IEEE Sustainable Power and Energy Conference (iSPEC), Beijing, China, pp. 398-402, 2019.

[22] K. Xu, Q. Liang and K. Lee, "Outdoor, 3D wound core, VPI transformer", Proceedings of the CIRED 2021 - The 26th International Conference and Exhibition on Electricity Distribution, Online Conference, pp. 380-384, 2021.

[23] W. Li, Y. Zhang, X. Zhao, R. Liu, H. Liu, Z. Huang and G. Zhang, "Full-life-cycle eco-friendly polymeric insulating materials: research progress and future prospects", Journal of Physics D: Applied Physics, Vol. 56, No. 37, pp. 1-28, 2023.

[24] L. W. Pierce, "Thermal considerations in specifying dry-type transformers", IEEE Transactions on Industry Applications, Vol. 30, No. 4, pp. 1090-1098, 1994.

[25] I. Soltanbayev, M. Bagheri and T. Phung, "Real-time dry-type transformer aging evaluation", Proceedings of the 2017 International Symposium on Electrical Insulating Materials (ISEIM), Toyohashi, Japan, pp. 551-554, 2017.

[26] L. W. Pierce, "Predicting hottest spot temperatures in ventilated dry type transformer windings", IEEE Transactions on Power Delivery, Vol. 9, No. 2, pp. 1160-1172, 1994.

[27] C. Roy, R. Murillo, L. Cebrian, M. Berrogain, J. Brewer, and J. Williams, "Dry-type 145 kV transformers: safe indoor substations with improved environmental performance", Proceedings of the CIGRE A2-10864, Paris, 2022.

[28] M. Carlen, M. Berrogain, R. Camerroni, and M. Spiranelli, "Dry-type subtransmission transformer: compact and safe indoor substations", Proceedings of the CIGRE A2–304, Paris, 2014.

[29] P. Chen, Y. Huang, F. Zeng, Y. Jin, X. Zhao, and J. Wang, "Review on insulation and reliability of dry-type transformer", Proceedings of the 2019 IEEE Sustainable Power and Energy Conference (iSPEC), pp. 398-402, 2019.

[30] H. Xu, S. Matharage, Z. Wang, D. Squire, H. Syzwala and M. Fazakarley", Proceedings of the A Review of Thermal and Electrical Designs for Drytype Transformers and Future Perspectives", Proceedings of the 2024 IEEE Electrical Insulation Conference (EIC), Minneapolis, MN, USA, pp. 380-383, 2024.

[31] I. Pleşa, P.V. Noţingher, S. Schlögl, C. Sumereder and M.Muhr, Properties of Polymer Composites Used in High-Voltage Applications", Polymers, Vol. 8, No. 5, pp. 1-63, 2016.

[32] P. Preetha and M. J. Thomas, "Life estimation of electrothermally stressed epoxy nanocomposites", IEEE Trans. Dielectr. Electr. Insul., Vol. 21, No. 3, pp. 1154-1160, 2014.

[33] S. Dai T. Zhang, S. Mo, Y. Cai, W. Yuan, T. Ma, L. Hu and B. Wang, "Study on Preparation, Thermal Conductivity, and Electrical Insulation Properties of Epoxy/AlN", IEEE Transactions on Applied Superconductivity, vol. 29, no. 2, pp. 1-6, 2019.

[34] X. Xu, C. Huang, X. Qian and R. Yang, "Thermal Conductivity of Polymers and Their Nanocomposites", Materials Science and Engineering: R: Reports, Vol. 30, pp. 1705544, 2018.

[35] P. Preetha and M. J. Thomas, "AC breakdown characteristics of epoxy nanocomposites", IEEE Transactions on Dielectrics and Electrical Insulation, Vol. 18, No. 5, pp. 1526-1534, 2011.

[36] S. Singha and M. J. Thomas, "Dielectric properties of epoxy nanocomposites", IEEE Transactions on Dielectrics and Electrical Insulation, Vol. 15, No. 1, pp. 12-23, 2008.

[37] S. K. Paul, S. Maur, S. Biswas and A. K. Pradhan, "Review on Thermal and Electrical Properties for Condition Assessment of Epoxy Nano-Composites by Advanced Techniques", IEEE Transactions on Dielectrics and Electrical Insulation, Vol. 31, No. 1, pp. 230-245, 2024.

[38] P. Preetha and M. J. Thomas, "Partial discharge resistant characteristics of epoxy nanocomposites", IEEE Transactions on Dielectrics and Electrical Insulation, Vol. 18, No. 1, pp. 264-274, 2011.

[39] P. Preetha, M. J. Thomas and R. Ranjan, "Electrothermal ageing of epoxy nanocomposites", IEEE Transactions on Dielectrics and Electrical Insulation, Vol. 19, No. 6, pp. 2081-2089, 2012.

[40] N. Inoue, S. Sato, T. Yoshida, Y. Oida, A. Kumada and K. Hidaka, "Insulation properties of highly pressurized dry air-effects of anodic oxide coating and surface roughness of electrodes on breakdown voltage", IEEE Transactions on Dielectrics and Electrical Insulation, Vol. 21, No. 5, pp. 2081-2087, 2014.

[41] Y.K. Choi, K.I. Sugimoto, S.M. Song, Y. Gotoh, Y.Ohkoshi and M. Endo, "Mechanical and physical properties of epoxy composites reinforced by vapor grown carbon nanofibers", Carbon, Vol. 43, No. 10, pp. 2199-2208, 2005.

[42] G. C. Stone, "The statistics of aging models and practical reality", IEEE Transactions on Electrical Insulation, Vol. 28, No. 5, pp. 716-728, 1993.

[43] A. C. Gjerde, "Multifactor ageing models - origin and similarities", IEEE Electrical Insulation Magazine, Vol. 13, No. 1, pp. 6-13, 1997.

[44] E. L. Brancato, "A pathway to multifactor aging", IEEE Transactions on Electrical Insulation, Vol. 28, No. 5, pp. 820-825, 1993.

[45] J. Castellon, M. Suchitra, B. K. Vinay, S. Parameshwara, M. Umashankar, S. V. Panchami, "Electrical properties analysis of micro and nano composite epoxy resin materials", IEEE Transactions on Dielectrics and Electrical Insulation, Vol. 18, No. 3, pp. 651-658, June 2011.

[46] S. Zhang, H. Zhang, H. Feng, J. Yan, P. Liu and Z. Peng, "Relaxation processes and conduction mechanism of epoxy resin filled with graphene oxide," IEEE Transactions on Dielectrics and Electrical Insulation, Vol. 24, No. 1, pp. 519-527, 2017.

[47] C. Meichsner, T. Clark, P. Groeppel, B. Winter, B. Butz and E. Spiecker, "Formation of a protective layer during IEC(b) test of epoxy resin loaded with silica nanoparticles", IEEE Transactions on Dielectrics and Electrical Insulation, Vol. 19, No. 3, pp. 786-792, 2012.

[48] M. M. Bordeori and N. Gupta, "Electrochemical Changes in Epoxy Resin Due to Thermal Aging and Their Effect on Electrical Tree Growth", IEEE Transactions on Dielectrics and Electrical Insulation, Vol. 29, No. 5, pp. 1940-1947, 2022.

[49] R. Sarathi, V. S. Harsha, H. Griffiths and A. Haddad, "Understanding water droplet initiated discharges on epoxy nanocomposites under harmonic AC voltages adopting uhf technique", IEEE Transactions on Dielectrics and Electrical Insulation, Vol. 21, No. 2, pp. 918-925, 2014.

[50] M. Suchitra, N. M. Renukappa, C. Ranganathaiah and J. S. Rajan, "Correlation of free space length and surface energy of epoxy nanocomposites to surface tracking", IEEE Transactions on Dielectrics and Electrical Insulation, Vol. 25, No. 6, pp. 2129-2138, 2018.

[51] J. -J. Park and J. -Y. Lee, "Effect of Surface-Modified Nanosilicas on the Electrical Breakdown Strength in Epoxy Nanocomposites", IEEE Transactions on Dielectrics and Electrical Insulation, Vol. 30, No. 1, pp. 3-10, 2023.

[52] J. P. Varghese, N. Haque, R. Sunitha and P. Preetha, "Aging Characteristics of Epoxy Nanocomposites Doped With Silane-Functionalized Alumina Nanoparticles for High-Voltage Insulation Applications", IEEE Transactions on Dielectrics and Electrical Insulation, Vol. 30, No. 5, pp. 2334-2343, 2023.

[53] C. Li, J. He and J. Hu, "Surface morphology and electrical characteristics of direct fluorinated epoxy-resin/alumina composite", IEEE Transactions on Dielectrics and Electrical Insulation, Vol. 23, No. 5, pp. 3071-3077, 2016.

[54] R. Sarathi, S. Aravinth and K. Sethupathi, "Analysis of surface discharge activity in epoxy nanocomposites in liquid nitrogen under AC voltage", IEEE Transactions on Dielectrics and Electrical Insulation, Vol. 21, No. 2, pp. 452-459, 2014.

[55] H. Wen and X. Zhang, "Overheating decomposition characteristics of epoxy dielectrics in SF6 atmosphere", IEEE Transactions on Dielectrics and Electrical Insulation, Vol. 26, No. 5, pp. 1411-1417, 2019.

[56] A. Mohamad, G. Chen, Y. Zhang and Z. An, "Moisture effect on surface fluorinated epoxy resin for high-voltage DC applications", IEEE Transactions on Dielectrics and Electrical Insulation, Vol. 23, No. 2, pp. 1148-1155, 2016.

[57] Y. Gao, X. Liang, W. Bao, C. Wu and S. Li, "Degradation characteristics of epoxy resin of GFRP rod in the decay-like fracture of composite insulator", IEEE Transactions on Dielectrics and Electrical Insulation, Vol. 26, No. 1, pp. 107-114, 2019.

[58] U. J. Mahanta, J. P. Gogoi, D. Borah and N. S. Bhattacharyya, "Dielectric characterization and microwave absorption of expanded graphite integrated polyaniline multiphase nanocomposites in X-band",

IEEE Transactions on Dielectrics and Electrical Insulation, Vol. 26, No. 1, pp. 194-201, 2019.

[59] S. Paul and T. K. Sindhu, "Synthesis and characterization of epoxy-aluminum nanocomposites for energy storage applications", IEEE Transactions on Dielectrics and Electrical Insulation, Vol. 21, No. 5, pp. 2164-2171, 2014.

[60] A. Mohamad, G. Chen, Y. Zhang, and Z. An, "Surface fluorinated epoxy resin for high voltage DC application", IEEE Transactions on Dielectrics and Electrical Insulation, Vol. 22, No. 1, pp. 101-108, 2015.

[61] Z. Wu et al., "In- situ observation of electrical tree evolution in epoxy dielectrics with internal cracks", High Voltage, Vol. 6, No. 2, pp. 210–218, 2021.

[62] M. S. Babu, R. Sarathi, N. J. Vasa and T. Imai, "Understanding the influence of nano micro filler on electrical and mechanical behaviour of epoxy nanocomposites", IEEE Transactions on Dielectrics and Electrical Insulation, Vol. 26, No. 4, pp. 1098-1106, 2019.

[63] R. Sarathi, V. S. Harsha, N. J. Vasa, H. Griffiths and A. Haddad, "Water droplet initiated discharges on epoxy nanocomposites under DC voltages", IEEE Transactions on Dielectrics and Electrical Insulation, Vol. 23, No. 3, pp. 1743-1752, 2016.

[64] M. Suchitra, B. K. Vinay, S. Parameshwara, M. Umashankar and S. V. Panchami, "Effect of Combining Nano- and Microfillers for the Assessment of Thermal Class of Glass Fiber-Reinforced Epoxy Composites for Outdoor Insulation", IEEE Transactions on Dielectrics and Electrical Insulation, Vol. 30, No. 6, pp. 2896-2904, 2023.

[65] J. Manoj Dhivakar, R. Sarathi and S. Kornhuber, "Investigation on Electrical, Thermal, and Mechanical Properties of Silicone Rubber ATH Nanocomposites", IEEE Access, Vol. 10, pp. 94040-94050, 2022.

[66] G. Iyer, R. S. Gorur and A. Krivda, "Understanding electrical discharge endurance of epoxy micro- and nano-composites through thermal analysis", IEEE Transactions on Dielectrics and Electrical Insulation, Vol. 21, No. 1, pp. 225-229, 2014.

[67] C. Y. Shigue, R. G. S. dos Santos, C. A. Baldan and E. Ruppert-Filho, "Monitoring the epoxy curing by the dielectric thermal analysis method", IEEE Transactions on Applied Superconductivity, Vol. 14, No. 2, pp. 1173-1176, 2004.

[68] X. Chen, Q. Wang, X. Huang, M. Awais, A. Paramane and N. Ren, "Investigation of Electrical and Thermal Properties of Epoxy Resin/Silicon Carbide Whisker Composites for Electronic Packaging Materials", IEEE Transactions on Components, Packaging and Manufacturing Technology, Vol. 12, No. 7, pp. 1109-1121, 2022.

[69] L. Vouyovitch, N. D. Alberola, L. Flandin, A. Beroual and J.-L. Bessede, "Dielectric breakdown of epoxy-based composites: relative influence of physical and chemical aging", IEEE Transactions on Dielectrics and Electrical Insulation, Vol. 13, No. 2, pp. 282-292, 2006.

[70] Y. Chen and J. Wu, "Investigation on relationship between breakdown strength enhancement of composites and dielectric characteristics of nanoparticle", IEEE Transactions on Dielectrics and Electrical Insulation, Vol. 23, No. 2, pp. 927-934, 2016.

[71] C. Dai, Y. Tanaka, H. Miyake, K. Sato, X. Chen and A. Paramane, "Space-Charge Characteristics in Epoxy Composites Under Square Pulse Wave of Different Polarities With Various Frequencies at Various Temperatures", IEEE Transactions on Dielectrics and Electrical Insulation, Vol. 29, No. 1, pp. 137-144, 2022.

[72] J. Li, H. Liang, M. Xiao, B. Du and T. Takada, "Mechanism of deep trap sites in epoxy/graphene nanocomposite using quantum chemical calculation", IEEE Transactions on Dielectrics and Electrical Insulation, vol. 26, no. 5, pp. 1577-1580, 2019.

[73] S. B. Lang and R. Fleming, "A Comparison of Three Techniques for Solving the Fredholm Integral Equation of the Laser Intensity Modulation Method (LIMM)", IEEE Transactions on Dielectrics and Electrical Insulation, Vol. 16, No. 3, pp. 809-814, 2009.

[74] J. Lewiner, S. Hole and T. Ditchi, "Pressure wave propagation methods: a rich history and a bright future", IEEE Transactions on Dielectrics and Electrical Insulation, Vol. 12, No. 1, pp. 114-126, 2005.

[75] D. Saha, A. G. Anisimov, R. M. Groves, I. A. Tsekmes, P. H. F. Morshuis and R. Kochetov, "Epoxy-hBN nanocomposites: A study on space charge behavior and effects upon material", IEEE Transactions on Dielectrics and Electrical Insulation, Vol. 24, No. 3, pp. 1718-1725, 2017.

[76] M. Roy, J. K. Nelson, R. K. MacCrone, L. S. Schadler, C. W. Reed and R. Keefe, "Polymer nanocomposite dielectrics-the role of the interface",

IEEE Transactions on Dielectrics and Electrical Insulation, Vol. 12, No. 4, pp. 629-643, 2005.

[77] M. G. Veena, N. M. Renukappa, D. Meghala, C. Ranganathaiah and J. S. Rajan, "Influence of nanopores on molecular polarizability and polarization currents in epoxy nanocomposites", IEEE Transactions on Dielectrics and Electrical Insulation, Vol. 21, No. 3, pp. 1166-1174, 2014.

[78] N. Haque, "Investigation on Some Aspects of Charge Trapping in Dielectrics used in High Voltage Systems", Phd Thesis, Jadavpur University, Kolkata, India, 2019.

[79] S. Singha, M. J. Thomas and A. Kulkarni, "Complex permittivity characteristics of epoxy nanocomposites at low frequencies", IEEE Transactions on Dielectrics and Electrical Insulation, Vol. 17, No. 4, pp. 1249-1258, 2010.

[80] F. Tian and Y. Ohki, "Electric modulus powerful tool for analyzing dielectric behavior", IEEE Transactions on Dielectrics and Electrical Insulation, Vol. 21, No. 3, pp. 929-931, 2014.

[81] J. R. Macdonald, "Impedance Spectroscopy", John Wiley and Sons, New York, 1987.

[82] N. G. McCrum, B. E. Read and G. Williams, "Anelastic and Dielectric effects in polymeric Solids", John Wiley and Sons Ltd., London, 1967.

[83] M. Abramowitz and I. A. Stegun, "Handbook of Mathematical Functions", Dover publications Inc., New York, 1965.

[84] T. K. Saha and P. Purkait, "Investigation of Polarization and Depolarization Current Measurements for the Assessment of Oil-paper Insulation of Aged Transformers", IEEE Transactions on Dielectrics and Electrical Insulation, Vol. 11, No. 1, pp. 144-154, 2004.

[85] T. K. Saha, P. Purkait and F. Muller, "Deriving an equivalent circuit of transformers insulation for understanding the dielectric response measurements", IEEE Transactions on Power Delivery, Vol. 20, No. 1, pp. 149-157, 2005.

[86] T. K. Saha and P. Purkait, "Investigation of an expert system for the condition assessment of transformer insulation based on dielectric response measurements", IEEE Transactions on Power Delivery, Vol. 19, No. 3, pp. 1127-1134, 2004.

[87] P. R. Jota, S. M. Islam and F. G. Jota, "Modeling the Polarisation Spectrum in Composite Oil/Paper Insulation Systems", IEEE Transactions on Dielectrics and Electrical Insulation, Vol. 6, No. 2, pp. 145-151, 1999.

[88] N. Ando and F. Numajiri, "Experimental investigation of Space Charge in XLPE Cable using Dust Figure Method", IEEE Transactions on Electrical Insulation, Vol 14, No.2, pp. 36-42, 1979.

[89] T. R. Foord, "Measurement of the Distribution of Surface Electric Charge by Use of a Capacitive Probe", Journal of Phys. E: Sci. Instrum., Vol. 2, No. 5, pp. 411- 413, 1969.

[90] R. E. Collins, "Analysis of spatial distribution of charges and dipoles in electrets by a transient heating technique", Journal of Applied Physics, Vol. 47, No.11, pp. 4404-4408, 1976.

[91] S. B. Lang and D. K. Dasgupta, "Laser-intensity-modulation method: a technique for determination of spatial distributions of polarization and space charge in polymer electrets", Journal of Applied Physics, Vol. 59, No. 6, pp. 2151-2160, 1986.

[92] J.G. Simmons and M. C. Tam, "Theory of isothermal currents and the direct determination of trap parameters in semiconductors and insulators containing arbitrary trap distributions", Physical Review B, Vol. 7, No. 8, pp. 3706-3713, 1973.

[93] M. Fu, G. Chen, A.E. Davies and J.G. Head, "Space charge measurements in power cables using PEA system", Proceedings of Eighth International Conference on Dielectric Materials, Measurements and Applications, Edinburgh, UK, 2000.

[94] T W Dakin, "Electrical Insulation Deterioration Treated as a Chemical Rate Phenomenon", AlEE Transactions, Vol. 67, No. 1, pp. 113-122, 1948.

[95] S. Glasstone, K. J. Laidler and H. Eyring, The Theory of Rate Processes, New York: McGraw Hill, 1941.

[96] T. Tanaka and A. Greenwood, "Effects of Charge Injection and Extraction on Tree Initiation in Polyethylene", IEEE Transactions on PAS, Vol. 97, pp. 1749-1759, 1978.

[97] L. A. Dissado, G. Mazzanti and G.C. Montenary, "The incorporation of space charge degradation in the life model for electrical insulating

materials", IEEE Transactions on Dielectrics and Electrical Insulation, Vol. 2. No. 6, pp. 1147-1158, 1995.

[98] H. Torkaman and F. Karimi, "Influence of ambient and test conditions on insulation resistance/polarization index in hv electrical machines - a survey", IEEE Transactions on Dielectrics and Electrical Insulation, Vol. 22, No. 1, pp. 241-250, 2015.

[99] M. A. Talib, N. A. M. Ghazali, M. Christie and W. Zakaria, "Diagnosis of transformer Insulation condition using recovery voltage measurements", Proceedings of National Conference on Power Engineering (PECon), Malaysia, 2003.

[100] G. Williams, "Dielectric Relaxation Behavior of Amorphous Polymers and Related Materials", IEEE Transactions on Electrical Insulation, Vol. 20, No. 5, pp. 843-857, 1985.

[101] C. T. Moynihan, L. P. Boesch and N. L. Laberge, "Decay function for the electric Field relaxation in vitreous ionic conductors", Physics and Chemistry of Glasses, Vol. 14, No. 6, 1973.

[102] S. K. Ojha, "Studies on Dielectric Relaxation Phenomena for Condition Monitoring of Oil-Paper Insulation in Transformer", Phd Thesis, Jadavpur University, Kolkata, India, 2021.

[103] A. K. Jonscher, "The Universal' dielectric response II", IEEE Electrical Insulation Magazine, Vol. 6, No. 3, pp. 24-28, 1990.

[104] H. Bao, P. Wu, B. Bao, M. Chen and H. Wu, "Sallen–Key low-pass filter based inductor-free simplified Chua's circuit", The Journal of Engineering, Vol. 2017, No. 12, pp. 653–655, 2017.

[105] Y. Cao, P. C. Irwin and K. Younsi, "The future of nanodielectrics in the electrical power industry", IEEE Transactions on Dielectrics and Electrical Insulation, Vol. 11, No. 5, pp. 797-807, 2004.

[106] T. Tanaka, "Dielectric nanocomposites with insulating properties", in IEEE Transactions on Dielectrics and Electrical Insulation, Vol. 12, No. 5, pp. 914-928, 2005.

[107] Y. N. Wang, et al., "Research progress on space charge measurement and space charge characteristics of nanodielectrics", IET Nanodielectrics, Vol. 1, No. 3, pp. 114–121, 2018.

[108] S. Zhong, et al, "Past and future on nanodielectrics", IET Nanodielectrics, Vol. 1, No. 1, pp. 41–47, 2018.

[109] J. A. Anta, G. Marcelli, M. Meunier, and N. Quirke, "Models of electron trapping and transport in polyethylene: Current–voltage characteristics", Journal of Applied Physics, Vol. 92, No. 2, pp. 1002–1008, 2002.

[110] S. Li, D. Min, W. Wang and G. Chen, "Linking traps to dielectric breakdown through charge dynamics for polymer nanocomposites", IEEE Transactions on Dielectrics and Electrical Insulation, Vol. 23, No. 5, pp. 2777-2785, 2016.

[111] J. C. Pandey and N. Gupta, "Study of treeing in epoxy-alumina nanocomposites using electroluminescence", IEEE Transactions on Dielectrics and Electrical Insulation, Vol. 26, No. 2, pp. 648-654, 2019.

[112] T. Andritsch, R. Kochetov, B. Lennon, P. H. F. Morshuis and J. J. Smit, "Space charge behavior of magnesium oxide filled epoxy nanocomposites at different temperatures and electric field strengths," 2011 Electrical Insulation Conference (EIC)., Annapolis, MD, USA, pp. 136-140, 2011.

[113] J. Dong et. al., "Effect of temperature gradient on space charge behavior in epoxy resin and its nanocomposites", IEEE Transactions on Dielectrics and Electrical Insulation, Vol. 24, No. 3, pp. 1537–1546, 2017.

[114] J. C. Pandey and N. Gupta, "Charge behavior at interfaces involving nanocomposites", IEEE Transactions on Dielectrics and Electrical Insulation, Vol. 25, No. 1, pp. 73-83, 2018.

[115] D. Saha, A. G. Anisimov, R. M. Groves, I. A. Tsekmes, P. H. F. Morshuis and R. Kochetov, "Epoxy-hBN nanocomposites: A study on space charge behavior and effects upon material", IEEE Transactions on Dielectrics and Electrical Insulation, Vol. 24, No. 3, pp. 1718-1725, 2017.

[116] M. S. Babu et. al, "Investigation on space charge and charge trap characteristics of gamma-irradiated epoxy micro–nano composites", High Voltage, Vol. 5, No. 2, pp. 191-201, 2020.

[117] S. Zhang et. al, "Experimental and simulation study on space charge characteristics of epoxy resin filled with graphene oxide", IET Science, Measurement & Technology, Vol. 13, No. 3, pp. 426-434, 2011.

[118] N. Haque, S. Dalai, B. Chatterjee, and S. Chakravorti, "Studies on the effects of moisture and ageing on charge de-trapping properties of

oil-impregnated pressboard based on IRC measurement", High Voltage, Vol. 4, No. 2, pp. 151–157, 2019.

[119] Y. Wang, J. Wu and Y. Yin, "Investigation of surface trap distribution in LDPE/SiO2 nanocomposite based on simultaneous observation of space charge and relaxation current", IEEE Transactions on Dielectrics and Electrical Insulation, Vol. 23, No. 6, pp. 3486-3493, 2016.

[120] J. Li, F. Zhou, D. Min, S. Li and R. Xia, "The energy distribution of trapped charges in polymers based on isothermal surface potential decay model", IEEE Transactions on Dielectrics and Electrical Insulation, vol. 22, no. 3, pp. 1723-1732, 2015.

[121] S. Singha and M. J. Thomas, "Dielectric properties of epoxy nanocomposites", IEEE Transactions on Dielectrics and Electrical Insulation, Vol. 15, No. 1, pp. 12-23, 2008.

[122] N. Mondal, N. Haque, S. Dalai, B. Chatterjee, and S. Chakravorti, "A Method for Identifying Ageing in Epoxy-mica Composite Insulation used in Rotational machines through Modelling of Dielectric Relaxation", High Voltage, Vol. 5, No. 2, pp. 184-190, 2019.

[123] L. C. Castro, J. L. Oslinger, N. Taylor and M. Wahlander, "Dielectric and physico-chemical properties of epoxy-mica insulation during thermoelectric aging", IEEE Transactions on Dielectrics and Electrical Insulation, Vol. 22, No. 6, pp. 3107-3117, 2015.

[124] R. Su et al., "Carrier transport in LDPE and its nanocomposites", IEEE Transactions on Dielectrics and Electrical Insulation, Vol. 27, No. 2, pp. 368-376, 2020.

[125] P. Maity, S. Basu, V. Parameswaran and N. Gupta, "Degradation of polymer dielectrics with nanometric metal-oxide fillers due to surface discharges", IEEE Transactions on Dielectrics and Electrical Insulation, Vol. 15, No. 1, pp. 52-62, 2008.

[126] F. N. Alhabil et. al., "Introducing particle interphase model for describing the electrical behaviour of nanodielectrics", Materials and Design, Vol. 158, pp. 62-73, 2018.

[127] A. Sharma, S. Basu and N. Gupta, "Detection of charge around a nanoparticle in a nanocomposite using electrostatic force microscopy", IEEE Transactions on Dielectrics and Electrical Insulation, Vol. 27, No. 3, pp. 866-872, 2020.

[128] F. Tian, J. Yao, P. Li, Y. Wang, M. Wu and Q. Lei, "Stepwise electric field induced charging current and its correlation with space charge formation in LDPE/ZnO nanocomposite", IEEE Transactions on Dielectrics and Electrical Insulation, Vol. 22, No. 2, pp. 1232-1239, 2015.

[129] S. Neelmani, et.al, "Investigation on Space charge dynamics and Mechanical Properties of Epoxy Alumina nanocomposites", Materials Research Express, Vol. 7, No. 2, pp. 025-037, 2020.

[130] R. Mi et al., "Effect of morphology and traps on DC conductivity and breakdown of polyethylene nanocomposites", IEEE Transactions on Dielectrics and Electrical Insulation, Vol. 27, No. 2, pp. 489-497, 2020.

[131] Y. Gao, J. Wang, F. Liu and B. Du, "Surface Potential Decay of Negative Corona Charged Epoxy/Al2O3 Nanocomposites Degraded by 7.5-MeV Electron Beam", IEEE Transactions on Plasma Science, Vol. 46, No. 7, pp. 2721-2729, 2018.

[132] S. Yu et. al., "Surface trap effects on flashover voltages of epoxy/Al2O3 nanocomposites for high voltage insulation", Journal of Materials Science: Materials in Electronics, Vol. 20, No. 19, pp. 18135-18143, 2019.

[133] D. Min, S. Li, N. Hirai and Y. Ohki, "Dielectric spectroscopic analysis of degradation in ethylene-propylene-diene copolymer," IEEE Transactions on Dielectrics and Electrical Insulation, Vol. 23, No. 6, pp. 3620-3630, 2016.

[134] J. Liu, X. Fan, Y, Zhang, H. Zheng and M. Zhu, "Quantitative evaluation for moisture content of cellulose insulation material in paper/oil system based on frequency dielectric modulus technique," Cellulose, Vol. 27, pp. 2343-2356, 2020.

[135] J. Liu, X. Fan, Y. Zhang, H. Zheng and J. Jiao, "Temperature correction to dielectric modulus and activation energy prediction of oil-immersed cellulose insulation", IEEE Transactions on Dielectrics and Electrical Insulation, Vol. 27, No. 3, pp. 956-963, 2020.

[136] J. Li et. al., "Interfacial Characteristics of Boron Nitride Nanosheet/Epoxy Resin Nanocomposites: A Molecular Dynamics Simulation", Applied Sciences, Vol. 9, No. 14, pp. 28-32, 2019.

[137] T.J. Lewis, "A Model for Nano-composite Polymer Dielectrics under Electrical Stress", Proc. of the IEEE International Conference on Solid Dielectrics (ICSD) ,Winchester, UK, pp. 11–14, 8–13 July, 2007.

[138] S. Morsalin and B. T. Phung, "Modeling of dielectric dissipation factor measurement for XLPE cable based on Davidson-Cole model", IEEE Transactions on Dielectrics and Electrical Insulation, Vol. 26, No. 3, pp. 1018-1026, 2019.

[139] S. K. Ojha et al., "Application of Cole–Cole model to transformer oil-paper insulation considering distributed dielectric relaxation", High Voltage, Vol. 4, No. 1, pp. 72–79, 2019.

[140] E. Tuncer, Y. V. Serdyuk and S. M. Gubanski, "Dielectric Mixtures: Electrical Properties and Modeling", IEEE Transactions on Dielectrics and Electrical Insulation, Vol. 9, No. 5, pp. 809-828, 2002.

[141] T. Tanaka, "Ageing of polymeric and composite insulating materials-aspects of interfacial performance in ageing", IEEE Transactions on Dielectrics and Electrical Insulation, Vol. 9, No. 5, pp. 704-716, 2002.

[142] H. Yan et al., "Aging behaviour of encapsulated assemblies of epoxy resin under accelerated thermal cycling", International Journal of Polymer Analysis and Characteristics, Vol. 27, No. 3, pp. 180-194, 2022.

[143] Y. Zhang et al., "Analysis of Polarization Information of XLPE Cables Based on Distribution of Relaxation Time IEEE Transactions on Dielectrics and Electrical Insulation, Vol. 30, No. 3, pp. 946-954, 2023.

[144] M. Florkowski et al., "Metal migration at conductor / XLPE interface subjected to partial discharges at different electrical stresses", IEEE Transactions on Dielectrics and Electrical Insulation, Vol. 22, No. 1, pp. 456-462, 2015.

[145] J. C. Fothergill et al., "Electrical, microstructural, physical and chemical characterization of HV XLPE cable peelings for an electrical ageing diagnostic data base", IEEE Transactions on Dielectrics and Electrical Insulation, Vol. 10, No. 3, pp. 514–527, 2003.

[146] K. Li et al., "Understanding the Crystalline Region Damage Mechanism of XLPE in Water Tree Propagation by Erosion Method", IEEE Transactions on Dielectrics and Electrical Insulation, Vol. 28, No. 6, pp. 2074-2082, 2021.

[147] A. K. Das et al., "Estimation of Moisture Content in XLPE Cable Insulation Using Electric Modulus", IEEE Transactions on Dielectrics and Electrical Insulation, Vol. 29, No. 3, pp. 1030-1037, 2022.

[148] J. Liu et al., "Fast Detection Method on Water Tree Aging of MV Cable Based on Nonsinusoidal Response Measurement", IEEE Transactions on Power Delivery, Vol. 38, No. 1, pp. 146-153, 2023.

[149] P. Werelius et al., "Dielectric spectroscopy for diagnosis of water tree deterioration in XLPE cables", IEEE Transactions on Dielectrics and Electrical Insulation, Vol. 8, No. 1, pp. 27-42, 2001.

[150] K. Zhou et al., "Assessing Aging Status and Type of XLPE Cable Insulation With a Graphic Approach Based on PDC Measurement", IEEE Transactions on Power Delivery, Vol. 37, No. 6, pp. 5114-5123, 2022.

[151] Cigre Working Group B1.09, "Remaining life management of existing AC underground lines", 2008.

[152] T. Zhang et al., "Analysis of Transformer Oil-Paper Insulation State Using Fractional Poynting–Thomson Model", IEEE Transactions on Dielectrics and Electrical Insulation, Vol. 29, No. 2, pp. 583-590, 2022.

[153] E. Tuncer and S. M. Gubanski, "On dielectric data analysis using the monte carlo method to obtain relaxation time distribution and comparing non-linear spectral function fits", IEEE Transactions on Dielectrics and Electrical Insulation, Vol. 8, No. 3, pp. 310-320, 2001.

[154] N. Farag et al., "Numerical transformations of widerange time and frequency domain relaxational spectra", Technol M.,(Ed.), IEE Proc. Science, Sarrbruecken, Germany, Vol. 150, No. 2, pp. 65–74, 2003.

[155] H. Kliem, P. Fuhrmann and G. Arlt, "A numerical method for the determination of first-order kinetics relaxation time spectra", IEEE Transactions on Electrical Insulation, Vol. 23, No. 6, pp. 919-927, 1988.

[156] Electrical Insulation- Thermal Evaluation and Designation, IEC Standard 60085 3rd edition, 2004.

[157] S. Helleso et al, "Water tree initiation and growth in XLPE cables under static and dynamic mechanical stress", IEEE International Symposium on Electrical Insulation (ISEI), pp. 623–627, 2012.

[158] General construction and test methods of power, control and instrumentation cables for shipboard and offshore applications, IEC 60092-350, 2008.

[159] Power cables with extruded insulation and their accessories for rated voltages above 30 kV (Um = 36 kV) up to 150 kV (Um = 170 kV) – Test methods and requirements, IEC 60840, 2020.

[160] M. Dong et al., "Explanation and analysis of oil-paper insulation based on frequency-domain dielectric spectroscopy", IEEE Transactions on Electrical Insulation, Vol. 22, No. 5, pp. 2684-2693, 2015.

[161] R. M. Hill and L. A. Dissado, "A cluster approach to the structure of imperfect materials and their relaxation spectroscopy," Royal Society London. A. Math. Phys. Sci., vol. 390, no. 1798, pp. 131–180, 1983.

[162] S. Morsalin and B. T. Phung, "Dielectric response study of service-aged XLPE cable based on polarisation and depolarisation current method", IEEE Transactions on Electrical Insulation, Vol. 27, No. 1, pp. 58-66, 2020.

[163] Y. Zhang et al., "Study on Nonuniform Thermal Aging State of XLPE Based on Dissado–Hill Model", IEEE Transactions on Plasma Science, Vol. 50, No. 11, pp. 4566-4575, 2022.

[164] Y. Q. Zhang et al., "Water-Tree Resistant Characteristics of Crosslinker-Modified-SiO2/XLPE Nanocomposites", Materials, MDPI, Vol. 14, pp. 1-13, 2021.

Subhajit Maiz.
30.10.2024